Presentation and Accessibility of Surface Bound Ligands on Amphiphilic Graft Copolymer Films

by

William A. Kuhlman

B.S. Chemistry
New York University, 2000

B.E. Materials Science
Stevens Institute of Technology, 2000

Submitted to the Department of Materials Science and Engineering in Partial Fulfillment of the Requirements for the Degree of

Doctor of Philosophy in Materials Science and Engineering

at the

Massachusetts Institute of Technology

June 2007

Signature of Author: _____
Department of Materials Science and Engineering
March 28, 2007

Certified by: _____
Anne M. Mayes
Toyota Professor of Materials Science and Engineering
Thesis Supervisor

Certified by: _____
Linda G. Griffith
Professor of Biological Engineering and Mechanical Engineering
Thesis Supervisor

Accepted by: _____
Samuel M. Allen
POSCO Professor of Physical Metallurgy
Chair, Departmental Committee on Graduate Students

Presentation and Accessibility of Surface Bound Ligands on Amphiphilic Graft Copolymer Films

by

William A. Kuhlman

Submitted to the Department of Materials Science and Engineering on March 28. 2007 in partial fulfillment of the requirements for the Degree of Doctor of Philosophy in Materials Engineering

Abstract:

Amphiphilic comb-type graft copolymers comprising a poly(methyl methacrylate) (PMMA) backbone and short, polyethylene oxide (PEO) side chains, PMMA-*g*-PEO, are proposed to self-organize at the polymer/water interface, resulting in quasi-2D confinement of the backbone at the immediate surface. The branched architecture and amphiphilic chemistry of these polymers results in a dense PEO brush that resists cell adhesion. To facilitate specific cell-surface interactions, small biological molecules such as adhesion peptides can be selectively tethered to PEO chain ends. Quasi-2D confinement of the polymer backbone results in clustering of tethered epitopes on a length scale dictated by the backbone. The present work investigates two aspects of this polymer architecture on organization of tethered ligands: nanometer length-scale clustering through backbone 2D confinement, and tether length effects on the availability of tethered peptides for cell adhesion.

To directly probe 2D confined polymer conformations, combs at the film/water interface were labeled with gold nanoparticles and observed by transmission electron microscopy. A 2D radius of gyration (R_g) was calculated by reconstructing nanoparticle-decorated chain trajectories, and compared with Monte Carlo simulations of a 2D melt of similarly broad length distribution. The 2D R_g calculated from observed conformations scaled with the number of backbone segments (N) as $R_g \sim N^{0.69\pm0.02}$ Monte Carlo simulations yielded a scaling exponent $\nu = 0.67 \pm 0.03$, suggesting that the deviation from classical 2D melt behavior ($\nu = 0.5$) arose from polydispersity.

Tether length effects on cell adhesion to comb copolymer films functionalized with the adhesion peptide PHSRNGGGK(GGC)GGRGDSPY were further investigated by observing cell attachment and spreading on combs with long (22 EO unit) and short (10 EO unit) tethers. Longer tethers increased the rate of spreading and reduced the time required to form focal adhesions. Fluorescence resonance energy transfer (FRET) measurements suggest that the added mobility afforded by longer tethers allowed cells to reorganize tethered peptides. In addition, adhesion peptides were selectively coupled to short or long PEO tethers within a bimodal brush. Short peptide tethers in a bed of long inert chains did not promote cell attachment. Long peptide tethers with short inert chains resulted in cell attachment comparable to a monomodal brush of long chains. These findings may be of value in designing protein-resistant bioactive surfaces, where nanometer length-scale organization of ligands plays an important role in cell-surface interactions.

Thesis Supervisor: Anne M. Mayes
Title: Toyota Professor of Materials Science and Engineering

Thesis Supervisor: Linda G. Griffith
Title: Professor of Biological Engineering and Mechanical Engineering

Table of Contents:

List of Figures

List of Tables

Acknowledgements

This thesis is dedicated to Professor Anne M. Mayes, who has been essential to my development as a scientist. Her commitment to the highest standards of technical evidence, her scientific curiosity, her seemingly endless knowledge and her dedication to her students have earned my deepest admiration and respect. As a teacher, an advisor and a mentor she has both inspired me and guided me through years of research. I have learned a lot from her, and am forever indebted to her for her patience, guidance and insight.

I also wish to offer my deepest thanks to Professor Linda G. Griffith, who has provided me with so many opportunities for scientific and personal growth. Much of what I have learned during my research, I owe to her ideas and to the many collaborations she has engineered. Her encouragement and enthusiasm led to many of the most interesting and rewarding discoveries of my research. I am deeply grateful for her dedication, interest, patience and support.

Several other researchers at MIT have also contributed to this work, and I would like to express my appreciation their assistance. TEM imaging for the 2D quasi-confinement work was performed by Elsa Olivetti, without whose meticulous microscopy, cautious sample preparation and thoughtful discussions, none of this would have been possible. Ikuo Taniguchi was instrumental in developing methods for PEO_{22} macromonomer synthesis, and in devising approaches to producing soluble polymers. I am grateful to Ikuo for his clear teaching of synthesis, boundless expertise and general camaraderie. Metin H. Acar first introduced me to the delicate art of synthesis, and is

among the finest teachers I have had the pleasure to work with. I wish to thank him especially for his enthusiasm and support during my first years at MIT and for the creativity and scientific rigor of our late night discussions. Metin guided me towards the path that led to much of this research. I also wish to extend my gratitude to Maria L. Ufret for teaching me peptide chemistry, protein conjugation and for her critical review of my experimental design. Her leadership united our group, consolidating our research methods into a series of concise, robust protocols. In addition, I thank Lily Koo for teaching me cell culture and for helping me find my way when I first joined the group.

I would like to thank Mr. Mike Frongillo for assistance in obtaining the TEM images, Christina Lewis and Stacey Pawson for keeping the labs running smoothly, and Mr. Daniel Pregibon for his work in scaling-up polymer synthesis, Juan Gonzalez for his companionship, indefatigable love of research and preternatural understanding of thermodynamics, and Ayse Asatekin for her imperturbable cheer and numerous clever suggestions. I am also grateful for the support of my labmates, Nick Marcantonio, Ada Au, Ley Richardson, John Wright, Jane Park, Nathan Lovell, Ariya Akthakul, Ozge Akbulut, and Stella Park for their friendship, ideas and many useful discussions.

Finally, I would like to acknowledge the support of my friends and family, especially my parents, for sparking my interest in science and for encouraging me to pursue research, and Colleen Butler for all of her talks about science.

This work was funded by NIH grants #1R0GM59870-01 and U54-GM064346, and made use of the Shared Experimental Facilities supported by the MRSEC Program of the National Science Foundation under award number DMR 02-13282. This work also used facilities supported by NIH grant 1S10RR13886-01.

Chapter 1: Introduction

1.1 The Need for Tissue Engineering Materials

As life expectancy in the United States continues to rise, an increasing number of people live to an age where individual organs become damaged in an otherwise healthy body. As a consequence, there is an increasing demand for therapies that can restore damaged organ function. Nearly twenty percent of the population age 65 and older will require some form of organ replacement. World-wide, nearly 20 million people benefit from organ replacement therapies [1]. Improved therapies could result in dramatic improvements in the quality of life for millions of people still in need of organ replacement.

There are three major strategies for organ and tissue replacement: transplant, synthetic replacement and tissue engineering [2, 3]. Currently, transplantation is arguably the most successful, with respect to replacing native organ function. Donor tissues, extracted from other sites on the patient (autograft), from another human donor (allograft) or from an animal (xenograft), are used to replace damaged tissue or organs. Of these three, autograft is the most common. Autograft replaces the damaged tissue using tissue harvested from another site on the patient. Burn patients, for example, are frequently treated using grafts of skin removed from elsewhere on the body. Similarly, veins removed from the leg or other sites are commonly used to repair damaged arteries during heart surgery. Though this method poses few problems in terms of organ rejection, it involves removal of tissue from an undamaged site, resulting in further injury to the

patient. As a result, it can only be applied to a few relatively abundant tissues, such as skin.

Allograft increases the pool of available tissues, as numerous organs have been successfully transplanted. These transplants, however, run a risk of rejection by the immune system or transmission of disease from donor to recipient. Furthermore, the supply of donor organs is far smaller than demand. An American Heart Association survey from 1997, for example, found that only 2,300 of 40,000 patients in need of a heart transplant received one [4]. Xenografts, while relatively abundant, pose a greater risk of organ rejection.

The second clinical approach towards organ replacement involves permanent implantation of a synthetic device whose function replicates that of the native organ. Each year, nearly 300,000 damaged hip joints are replaced with titanium implants [5]. While this approach provides immeasurable relief from the pain associated with deterioration of the hip joint, full native organ function is not restored, and nearly 25% require further surgical intervention. Though titanium implants may provide a replacement, the resulting physical and biological properties are an inferior substitute for native tissue. For example, these implants do not grow with the recipient or heal in response to wear as a result of ordinary use and typically must be replaced after ten years. Discrepancies between the synthetic material and the body can lead to additional complications. In the case of hip implants, mismatch in the mechanical properties of titanium and bone can cause resorption of the surrounding bone, which may ultimately lead to failure of the implant [6]. While advances in design and materials will most likely improve these devices, they are never expected to equal native biological tissue. Ideally

an organ replacement therapy would replace the damaged tissue with new tissue that is indistinguishable from the native material.

Tissue engineering presents an alternative to transplant or total synthetic replacement. This approach seeks to guide the body's natural healing response, re-directing it to create new tissue [2, 3, 7, 8]. Tissue engineering is perhaps best understood in terms of the body's innate response to tissue damage. In the absence of any external agents, the body responds to tissue damage through a cascade of biological signals that ultimately lead to contraction and formation of scar tissue, a form of repair that isolates the damaged tissue without restoring native function [3]. The essential idea behind tissue engineering is to redirect these responses, inhibiting contraction and scar formation and guiding regeneration of native tissue. In contrast to synthetic replacement, this approach ideally leaves no foreign materials once the tissue has fully regenerated. Because it does not require extensive tissue donation, this approach significantly reduces risk of rejection and eliminates shortages associated with transplantation.

Though there is no universal path for regeneration of organs, all tissue engineering techniques employ some combination of three essential components: cells, soluble cell-regulators (cytokines) and an insoluble matrix that provides the structural support and chemical cues required to guide cell regeneration. Cells can be extracted from the patient, derived from other human sources or induced to migrate from the surrounding tissue. Cytokines, likewise, may be explicitly added, or produced through incorporation of DNA plasmids into the matrix to induce cytokine production by cells on the scaffold [9, 10]. Of these three, the matrix is possibly the most important element. The matrix serves as a surrogate for the extracellular matrix (ECM), a network of

insoluble molecules that supports cells and plays a key role in guiding cell proliferation and differentiation. A tissue engineering matrix can be made from natural materials, as in the case of collagen matrices, [3] or synthetic materials, such as the poly(lactic–co-glycolic acid) matrices used for skin regeneration [11]. Ideally, this device should degrade as the tissue matures, supporting the growing tissue through its development, but ultimately leaving only regenerated tissue [8].

The three essential properties of all tissue scaffolds, then, are that they (1) inhibit undesired biological responses, (2) guide specific cell functions and (3) biodegrade or resorb.

1.2 Producing Bioinert Surfaces

Possibly the most critical of these features is their ability to inhibit undesired biological responses. For example, scaffolds that exacerbate the inflammatory response, induce clot formation or provoke an immune response are usually undesirable. These and numerous other biological responses occur as a consequence of interactions between cells and adsorbed proteins. Upon contact with the blood, proteins adsorb on most synthetic surfaces. Cellular reactions to this protein adsorption then trigger a cascade of biological responses that can lead to adverse physiological outcomes [12]. Thrombus formation on artificial blood vessels, for example, occurs after platelets adhere to adsorbed proteins, releasing additional proteins that ultimately lead to formation of an insoluble clot [13].

It is crucial, therefore, that any device that is to have a controlled biological response *in vivo* must either resist protein adsorption, or mediate it in some way to ensure that only a benign response is observed. Understanding and preventing uncontrolled

protein adsorption, then, is essential in designing biomaterials for applications such as tissue scaffolds. Though the process of protein adsorption is still not fully understood, several general principles have emerged [14]. One of the most direct correlations between materials properties and protein adsorption is interfacial energy [15]. This correlation can be understood in terms of protein structure: proteins have both hydrophilic and hydrophobic domains. In an aqueous environment, proteins take on a globular structure, with hydrophobic domains buried in the center and hydrophilic groups exposed to the surrounding fluid. The resulting structure minimizes unfavorable hydrophobic interactions. Substantial reductions in interfacial energy can therefore be realized if a protein adsorbs and denatures on a hydrophobic surface. When the protein adsorbs, hydrophobic domains orient toward the hydrophobic surface, while hydrophilic domains orient towards the protein/water interface, resulting in an overall decrease in interfacial energy [16, 17].

Interfacial energy alone, however, is not the only factor dictating whether proteins will adsorb. A survey of materials that resist protein adsorption sought to determine what properties made a surface protein resistant [18]. This study found that, though nearly all protein resistant materials were hydrophilic, protein resistant surfaces included hydrogen bond acceptors but not hydrogen bond donors. In addition, it was observed that most protein resistant surfaces had an overall neutral charge. These findings suggest that the interaction of functional groups with water is key in determining resistance to protein adsorption.

Further driving forces for protein adsorption arise from entropic gains resulting from protein denaturing. Proteins in solution typically adopt a single conformation. A

protein that has adsorbed onto a surface and denatured, however, can adopt many conformations on the surface, resulting in a large increase in entropy when the protein adsorbs. As a result, even in the absence of a strong enthalpic driving force, proteins can adsorb due to the resulting increase in entropy [19]. Significant increases in entropy also arise from changes in water structure associated with hydrophobic interactions as the protein is denatured [17, 20].

This suggests a twofold approach to creating protein resistant surfaces: create a hydrophilic surface and reduce the entropy gained through protein adsorption. Both strategies are realized in the polyethylene oxide (PEO)[†] brush. PEO is uncharged, strongly hydrophilic, and possesses no hydrogen bond donors, making it highly resistant to protein adhesion. This material is considered the "gold standard" for protein adhesion resistance, and has found its way into numerous biomedical applications [21]. In a brush configuration, wherein PEO chains are densely tethered to a surface, protein adsorption requires an entropically unfavorable compression of PEO chains and expulsion of water.

A number of approaches towards producing protein-resistant PEO surfaces have been investigated. Among the most common approaches in research is the use of self-assembled monolayers (SAMs) [18, 22, 23]. These surfaces consist of a layer of metal (typically gold), onto which a monolayer of alkane thiols are coupled. Because of the high affinity of the gold-thiol bond, and the nearly perfect molecular registration of the alkane groups, these surfaces are able to produce high density PEO brushes that offer

[†] Polyethylene oxide (PEO) and polyethylene glycol (PEG) share the same chemical structure and physical properties. Their names are often used interchangeably. To avoid confusion, this work refers to all such polymers as PEO.

exceptional protein resistance. The chemistry required to couple alkane thiols to a gold surface is mild, and a wide variety of functionally modifiable alkane thiols are commercially available, making this an attractive approach for lab-scale studies [24-26]. SAMs have been used in a wide variety of applications, from creating biologically active micro-patterned surfaces [27-30], to commercial sensors [31]. This approach, however, has several disadvantages. SAMs degrade over time [32-35], such that protein resistance diminishes over the course of several weeks. In addition, a pristine metal surface is required for assembly of the SAM. Both factors have limited applicability in tissue engineering applications.

Similar approaches towards grafting PEO chains that are applicable to a wider range of surfaces have also been investigated. For example, a number of researchers have investigated formation of PEO brushes using reactive silane-terminated PEO chains [36]. Additional approaches employ isocyanate chemistry [37-39], amide chemistry [40], adsorption of block copolymers [41-43] and polymerization from initiators chemically immobilized on a surface [44, 45]. The essential problem in each of these approaches is achieving a sufficiently high grafting density to resist protein adhesion. Because the specificity and registration between grafted molecules is not as great as what is found in SAMs, these materials frequently do not perform as well.

Another approach towards producing a dense polymer brush involves formation of the brush in solution as a comb-shaped graft copolymer, followed by subsequent immobilization on a surface through chemical or physical means. In solution, it is possible to achieve high grafting densities in copolymers, making it possible to generate PEO brushes sufficient to resist protein adsorption. Winblade and coworkers, for

example, used electrostatic interactions to adsorb poly(L-lysine)-*graft*-poly(ethylene glycol) onto titanium surfaces, rendering them bioinert [46-50]. Similarly, Snellings and coworkers synthesized PEO graft copolymers bearing a small number of pendant thiol groups along the backbone, poly(poly (ethylene glycol) methacrylate -*co*-methylmethacrylate -*co* -2- (methylthio) ethylmethacrylate), that can be used to anchor these polymers to a gold surface, thereby generating a protein resistant PEO brush [51]. In situations where the copolymer is not water soluble, it is sometimes possible to create protein resistant surfaces through solvent casting [52] or through surface segregation of a branched polymer in a blend with linear polymers [53-55]. These latter approaches exploit self-organization of hydrophilic PEO side chains at the polymer/water interface to produce brushes sufficiently dense to provide protein resistant surfaces.

1.3 Engineering Cell-Materials Interactions

A protein resistant surface in and of itself, however, is not sufficient for tissue scaffolds. Though the absence of adsorbed proteins would reduce the possibility of undesired biological responses, it would eliminate all interactions with cells, thereby inhibiting tissue regeneration. Where it is necessary to control cell-surface interactions, modifications must be made to place appropriate cell-signaling molecules on these otherwise inert backgrounds. In systems that employ a PEO brush, incorporation of biologically active molecules can be accomplished by chemically attaching them to the free ends of some fraction of the PEO molecules [12, 53, 54, 56-58]. This approach has been investigated using a wide variety of small biological molecules, including growth factors [59], DNA [60], sugars [61] and adhesion peptides [42, 47, 53, 58, 62-65].

1.4 Controlling Cell Adhesion

Cell adhesion is a key behavior to regulate in tissue engineering. For most normal cells, adhesion is necessary for survival and function, and other behaviors including migration and proliferation. Cell adhesion can be induced through the adsorption of adhesion proteins such as fibronectin, found in the extracellular matrix (ECM). Researchers have found, however, that small peptides can mimic some properties of these adhesive proteins. The tri-peptide sequence arg-gly-asp (RGD), for example, is sufficient enable integrin-mediated adhesion [66]. Tethering peptides to PEO offers many potential advantages over use of the full proteins in that it may be less expensive, easier to process, and can direct responses related to specific adhesion sites [62]. Furthermore, use of a short peptide sequence rather than an entire protein reduces the possibility that the protein will denature either during processing or through interactions with the substrate [67]. This strategy has been employed in numerous approaches to engineering cell-adhesive surfaces for both medical and academic purposes [62]. Because of its small size, this peptide also makes it possible to obtain greater surface densities of adhesive domains than could occur naturally. Mougin and coworkers, for example, investigated the effects of peptide density on cell adhesion kinetics by creating gradients of RGD on SAMs [68]. Because of its large size, comparable adhesion site densities would not be accessible through adsorption of fibronectin.

Further enhancements in cell adhesion can be realized by using both RGD and the synergy peptide sequence PHSRN [69] presented in a branched conformation. Co-localization of these epitopes has been shown to greatly improve cell adhesion over linear

RGD peptides [70-73]. Benoit and Anseth, for example, observed an enhancement in osteoblast proliferation and metabolic activity when PHSRN was added to adhesive peptides in RGD-modified hydrogels [72]. Ochsenhirt and coworkers demonstrated that this improvement in adhesion is a function of both the peptides used and the spatial organization of these peptides. By varying the amount of RGD and PHSRN in Langmuir-Blodgett films, they observed maximum cell spreading when the spacing between PHSRN and RGD was comparable to that found in fibronectin (~11 Å) [64].

1.5 The Biological Importance of Ligand Presentation

Biological recognition of a specific moiety is not only a function of its available chemical groups; spatial organization also plays a key role. Proteins, for example, contain many levels of structure. Apart from the sequence of amino acids that determines their primary structure, proteins fold into spatially complicated secondary and tertiary structures [74]. These additional levels of structure selectively expose or mask some chemical functionality, while bringing others into closer proximity, or defining a specific spatial organization necessary for biological activity. In the absence of these higher levels of structure, such as in a denatured protein, biological function is often lost. Because the higher-order structure plays such an important role in the function of natural materials such as proteins, similar improvements in biological function may be produced through creation of biomaterials with higher-order structure. Though there are numerous approaches towards producing higher order structures that might be investigated, two are readily accessible using PEO-based polymer systems: spatial clustering of tethered ligands and variation of the tether length governing ligand mobility.

1.5.1 Clustering and Cluster Size

Biological systems often require the formation of multiple ligand-receptor bonds within a sub-micron area to produce a particular cellular response. This can come about either through the formation of multiple bonds with a single receptor, or through the formation of multiple independent ligand-receptor bonds, followed by aggregation of these bound ligands [75]. In either instance, ligand spatial organization plays a key role in bioactivity. In these systems, sub-micron length scale structures with multiple available ligands facilitate multivalent interactions and receptor clustering, enhancing bioactivity relative to individual ligands. Macrophage recognition of an infecting particle, for example, requires formation of multiple simultaneous contacts between the macrophage and antibodies bound to the infecting particle. Macrophages will not bind un-complexed antibodies in solution, or an individual bound antibody. Instead, the macrophage requires the presence of multiple antibodies, localized on a length scale dictated by the size of receptors on the surface of the macrophage [76, 77]. What signals the macrophage to the presence of a foreign body, therefore, is not merely the presence of antibodies, but their spatial organization.

Of more immediate relevance to tissue engineering is the impact of spatial organization of adhesion peptides on cell adhesion. Following binding of an individual integrin to its ligand, integrins re-organize within the cell membrane forming spatial aggregates that are a prerequisite for formation of higher-order cell structures such as contacts in focal adhesions [78, 79]. When aggregation is prevented through mutations to the integrin, cell adhesion is impaired [80]. In order to obtain strong cell adhesion, it must

be possible not only for integrins to bind, but also for bound integrins to cluster [78, 80-82].

Multivalent synthetic analogues for adhesion proteins, based on RGD have been produced in a number of ways. By coupling different numbers of RGD-containing peptides to bovine serum albumin (BSA), Danilov and coworkers demonstrated that clustering RGD peptides enhances cell adhesion. Clusters of RGD peptides have also been produced using synthetic polymers [83]. Maheshwari and coworkers, for example, created RGD clusters using PEO star polymers radiation grafted to a solid substrate [84]. They observed a strong enhancement in cell adhesion and proliferation to RGD clustered substrates when compared with non-clustered substrates of comparable peptide density. Other researchers using chemically similar systems have made similar findings [85]. Similar synthetically well-defined systems employing branched [86] and linear [87] peptides have also been investigated. Spatial clusters of adhesion peptides can also be produced using through self-organization of comb-shaped graft copolymers [53, 54, 58].

1.5.2 Effects of Tether Length on Ligand Availability

The effects of tether length on ligand-receptor binding have been studied previously both experimentally [88, 89] and theoretically [90, 91]. Jeppesen and coworkers studied avidin binding to PEO-tethered biotin using a surface force apparatus. They found that tethering enhanced the activity of biotin by extending the minimum distance required to bind avidin, from a natural distance of a few angstroms to a distance of several nanometers, corresponding to the fully-extended length of the polymer tether [88, 89]. These findings were further supported by numerical simulations [90, 91].

As with biotin-avidin interactions, integrin-peptide interactions occur over a short range, typically on the order of a nanometer [81]. Consequently, extension of active chains used to tether adhesion peptides may result in enhanced cell attachment to cell-adhesive polymer brushes. Beer and coworkers studied interaction of platelets with RGD bound to a surface by a short poly(glycine) tether [92]. They observed that platelets did not interact with the surface when RGD was bound by a single glycine. As the number of glycines increased, however, platelet adhesion increased, plateauing at a value of 9-10 glycine repeat units. They attributed this increase in interactions to the size of an integrin: binding was possible only when the glycine spacer was sufficiently long to permit the RGD to access its binding site on the integrin. Other researchers, however, have observed cell adhesion to RGD bound to surfaces with effectively no tether [93], implying that other factors such as surface roughness may also play a role in accessibility.

Tether length may also govern cell responses subsequent to binding by influencing the ability of bound integrins to spatially reorganize and cluster in the cell membrane. In the previously described protein, star- and graft-copolymer systems, multimeric ligand-receptor interactions are facilitated by the spatial organization of the substrate [53, 54, 83, 84]. The need for spatial organization on the substrate, however, may be alleviated through use of longer tethers. Previous research by Griffith and coworkers, for example, demonstrated that longer spacers allow re-arrangement of carbohydrates into clusters, thereby enhancing hepatocyte spreading [94]. For ligands bound to the surface through PEO tethers, therefore, longer tethers may enhance cell attachment by promoting integrin cluster formation through the larger number of available chain conformations.

Further increases in bioactivity may also be possible through use of a bimodal polymer brush. When a polymer brush is composed of chains with two different lengths, short chains force the ends of long chains to the top of the brush layer, resulting in stratification of chain ends [95-99]. Functional groups attached to the ends of short active chains should thus be masked by long inert chains, reducing their bioactivity. This was demonstrated experimentally by Houseman and Mrksich [57] who observed a decrease in cell adhesion to tethered RGD in oligoethylene glycol (OEG) self-assembled monolayers when inert OEG chains were of equal or greater length than the RGD tethers. Similar effects were observed in cell adhesion to peptide-modified polymer brushes formed using Langmuir-Blodgett films [56] and in model avidin-biotin systems [100, 101]. By inference, the use of long active chains in a sea of short inert chains should enhance ligand presentation by forcing tethered active groups to the surface. In Monte Carlo simulations of receptor binding to tethered ligands, Chen and Dormidontova [102] observed an increase in binding efficiency when active chains were longer than inert chains.

1.6 Amphiphilic Graft Copolymers for Tissue Engineering

One approach towards creating surfaces that resist protein adsorption and can be functionalized with cell-signaling molecules uses amphiphilic comb copolymers having a hydrophobic backbone such as poly(methylmethacrylate) (PMMA) with poly(ethylene oxide) (PEO) side chains, as shown in Figure 1.1.

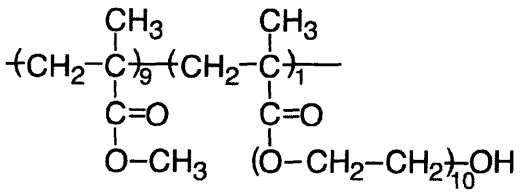

Figure 1.1 Structure of PMMA-*g*-PEO copolymers

These polymers are of interest because they can be induced to preferentially segregate to the surface of polymer blends, forming a stable PEO brush that resists protein adhesion [53]. This surface segregation is driven by entropy gained when polymer chain ends are localized at a surface [103]. In water, additional driving forces for segregation arise from energetic gains obtained through a reduction in surface enthalpy associated with exposing the PEO chains to water [55, 104]. Irvine et al. showed that spin-coated thin films of this polymer exhibited good protein resistance as determined by ellipsometry and radiolabeling [53]. Walton et al. studies similarly demonstrated that these surfaces were resistant to cell attachment, even in the presence of serum-containing media [55], while Guo et al. demonstrated their blood compatibility [52].

Functionalization of the side-chain ends of these combs can be accomplished using standard protein coupling chemistry [53]. When functionalized with the adhesion peptide GRGDSP, this polymer showed good cell attachment, suggesting that it is suitable for guiding specific cell-surface interactions on an otherwise protein resistant background [53]. An added advantage of this approach is its ability to cluster ligands, which has been shown to improve cell attachment: attachment and spreading were observed even at very low surface concentrations of GRGDSP when the ligands were clustered as a consequence of comb architecture [53, 58, 84]. This approach is not unique

to polymers having a PMMA backbone, and can be generally applied to other engineering polymers, such as polylysine [47, 48], PVDF [105] or polysulfone [106]. Similar approaches have also been successfully employed using biodegradable polymers [107].

1.7 Overview and Outline of Thesis

The present work is concerned with application of PMMA-*g*-PEO comb copolymers to control nanometer length-scale organization and accessibility of tethered ligands. Two aspects of polymer architecture can be varied to provide this control: cluster size can be controlled through variation in backbone molecular weight, and ligand accessibility can be controlled by varying the length of PEO side chains. To correlate biological function with polymer architecture, both parameters are investigated using a combination of materials characterization and *in vitro* cell-based assays. Direct measurements of spatial organization of ligands are made for the first time using transmission electron microscopy (TEM) and FRET measurements. Evaluation of bioactivity is accomplished through cell attachment and spreading assays, in addition to observations of cell morphology and structure through immunochemical staining.

To facilitate discussion of these subjects, this thesis is divided as follows: In the second chapter, we define the system under investigation and describe synthetic approaches used, particularly methods for polymer activation and methods for preparation of PEO macromonomers with varying PEO length. The third chapter provides direct observation of ligand clusters formed using these polymers, and establishes a scaling relationship between cluster size and polymer backbone molecular

weight. The fourth chapter examines the effects of PEO tether length on cell adhesion, and suggests that longer PEO tethers enhance cell adhesion by allowing cells to re-organize bound ligands. Finally, the thesis concludes with a summary and outlook in chapter 5.

1.8 References

1. Lysaght, M.J. and Reyes, J. "The growth of tissue engineering." *Tissue Engineering*, **2001**, 7(5): p. 485-493.
2. Lanza, R.P.; Langer, R. and Chick, W.L. "Principles of tissue engineering." Academic Press; San Diego 1996.
3. Yannas, I.V. "Tissue and organ regeneration in adults." Springer-Verlag; New York 2001.
4. Mooney, D.J. and Mikos, A.G. "Growing new organs." *Scientific American*, **1999**, 280(4): p. 60.
5. Citron, P. and Nerem, R.M. "Bioengineering: 25 years of progress — but still only a beginning." *Technology in Society*, **2004**, 26(2-3): p. 415.
6. Windler, M. and Kaldburne, R. "Titanium for hip and knee prostheses." Springer; Berlin 2001.
7. Langer, R. "Tissue engineering." *Molecular Therapy*, **2000**, 1(1): p. 12.
8. Langer, R. and Vacanti, J.P. "Tissue engineering." *Science*, **1993**, 260(5110): p. 920-926.
9. Bonadio, J.; Smiley, E.; Patil, P. and Goldstein, S. "Localized, direct plasmid gene delivery in vivo: Prolonged therapy results in reproducible tissue regeneration." *Nature Medicine*, **1999**, 5: p. 753-759.
10. Shea, L.D.; Smiley, E.; Bonadio, J. and Mooney, D.J. "DNA delivery from polymer matrices for tissue engineering." *Nature Biotechnology*, **1999**, 17: p. 551 - 554.

11. Rotter, N., Aigner, J., Naumann, A., *et al.* "Cartilage reconstruction in head and neck surgery: Comparison of resorbable polymer scaffolds for tissue engineering of human septal cartilage." *Journal of Biomedical Materials Research*, **1998**, 42(3): p. 347-356.

12. Tirrell, M.; Kokkoli, E. and Biesalski, M. "The role of surface science in bioengineered materials." *Surface Science*, **2002**, 500: p. 61-83.

13. Anderson, J.M. "Biological responses to materials." *Annu. Rev. Mater. Res.*, **2001**, 31: p. 81-110.

14. Robert, A.L. "Thermodynamic perspectives on the molecular mechanisms providing protein adsorption resistance that include protein-surface interactions." *Journal of Biomedical Materials Research Part A*, **2006**, 78A(4): p. 843-854.

15. Rapoza, R.J. and Horbett, T.A. "Postadsorptive transitions in fibrinogen: Influence of polymer properties." *Journal of Biomedical Materials Research*, **1990**, 24(10): p. 1263-1287.

16. Norde, W. "Adsorption of proteins from solution at the solid-liquid interface." *Advances in Colloid and Interface Science*, **1986**, 25: p. 267.

17. Claesson, P.M.; Blomberg, E.; Froberg, J.C.; Nylander, T. and Arnebrant, T. "Protein interactions at solid surfaces." *Advances in Colloid and Interface Science*, **1995**, 57: p. 161-227.

18. Ostuni, E.; Chapman, R.G.; Holmlin, R.E.; Takayama, S. and Whitesides, G.M. "A survey of structure-property relationships of surfaces that resist the adsorption of protein." *Langmuir*, **2001**, 17: p. 5605-5620.

19. Haynes, C.A. and Norde, W. "Globular proteins at solid/liquid interfaces." *Colloids and Surfaces B: Biointerfaces*, **1994**, 2(6): p. 517.

20. Vogler, E.A. "Water and the acute biological response to surfaces." *J. Biomater. Sci. Polymer Edn.*, **1999**, 10(10): p. 1015-1045.

21. Harris, J.M. "Poly(ethylene glycol) chemistry: Biotechnical and biomedical applications." Plenum Press; New York 1992.

22. Bain, C.D.; Troughton, E.B.; Tao, Y.T., *et al.* "Formation of monolayer films by the spontaneous assembly of organic thiols from solution onto gold." *Journal of the American Chemical Society*, **1989**, 111(1): p. 321 - 335.

23. Prime, K.L. and Whitesides, G.M. "Self-assembled organic monolayers: Model systems for studying adsorption of proteins at surfaces." *Science*, **1991**, 252(5009): p. 1164-1167.

24. Senaratne, W.; Andruzzi, L. and Ober, C.K. "Self-assembled monolayers and polymer brushes in biotechnology: Current applications and future perspectives." *Biomacromolecules*, **2005**, 6(5): p. 2427.

25. Love, J.C.; Estroff, L.A.; Kriebel, J.K.; Nuzzo, R.G. and Whitesides, G.M. "Self-assembled monolayers of thiolates on metals as a form of nanotechnology." *Chemical Reviews*, **2005**, 105(4): p. 1103.

26. Schreiber, F. "Self-assembled monolayers: From "Simple" Model systems to biofunctionalized interfaces." *Journal of Physics: Condensed Matter*, **2004**, 16(28): p. R881.

27. Smith, R.K.; Lewis, P.A. and Weiss, P.S. "Patterning self-assembled monolayers." *Progress in Surface Science*, **2004**, 75(1-2): p. 1.

28. Lopez, G.P.; Albers, M.W.; Schreiber, S.L., *et al.* "Convenient methods for patterning the adhesion of mammalian cells to surfaces using self-assembled monolayers of alkanethiolates on gold." *J. Am. Chem. Soc.*, **1993**, 115: p. 5877-5878.

29. Zhang, S., Yan, L., Altman, M., *et al.* "Biological surface engineering: A simple system for cell pattern formation." *Biomaterials*, **1999**, 20: p. 1213-1220.

30. Chen, C.S.; Mrksich, M.; Huang, S.; Whitesides, G.M. and Ingber, D.E. "Micropatterned surfaces for control of cell shape, position, and function." *Biotechnol. Prog.*, **1998**, 14: p. 356-363.

31. Manz, A. and Becker, H. "Microsystem technology in chemistry and life sciences." Springer-Verlag; Berlin 1998.

32. Willey, T.M.; Vance, A.L.; van Buuren, T., *et al.* "Rapid degradation of alkanethiol-based self-assembled monolayers on gold in ambient laboratory conditions." *Surface Science*, **2005**, 576(1-3): p. 188.

33. Noh, J. and Hara, M. "Molecular-scale desorption processes and the alternating missing-row phase of alkanethiol self-assembled monolayers on au(111)." *Langmuir*, **2001**, 17(23): p. 7280-7285.

34. Scott, J.R.; Baker, L.S.; Everett, W.R.; Wilkins, C.L. and Fritsch, I. "Laser desorption fourier transform mass spectrometry exchange studies of air-oxidized alkanethiol self-assembled monolayers on gold." *Anal. Chem.*, **1997**, 69(14): p. 2636-2639.

35. Schoenfisch, M.H. and Pemberton, J.E. "Air stability of alkanethiol self-assembled monolayers on silver and gold surfaces." *J. Am. Chem. Soc.*, **1998**, 120(18): p. 4502-4513.

36. Jo, S. and Park, K. "Surface modification using silanated poly(ethylene glycol)s." *Biomaterials*, **2000**, 21(6): p. 605.

37. Zhao-Xia, G.; Wen-Fang, L.; Ying, L. and Jian, Y. "Grafting of poly(ethylene glycol)s onto nanometer silica surface by a one-step procedure." *Journal of Macromolecular Science, Part A: Pure and Applied Chemistry*, **2005**, V42(2): p. 221.

38. Archambault, J.G. and Brash, J.L. "Protein resistant polyurethane surfaces by chemical grafting of PEO: Amino-terminated PEO as grafting reagent." *Colloids and Surfaces B: Biointerfaces*, **2004**, 39(1-2): p. 9.

39. Wang, W.-P. and Pan, C.-Y. "Synthesis and characterizations of poly(ethylene oxide) methyl ether grafted on the expanded graphite with isocyanate groups." *European Polymer Journal*, **2004**, 40(3): p. 543.

40. Patel, S., Thakar, R.G., Wongd, J., *et al.* "Control of cell adhesion on poly(methylmethacrylate)." *Biomaterials*, **2006**, 27: p. 2890-2897.

41. Lee, J.H.; Kopecek, J. and Andrade, J.D. "Protein-resistant surfaces prepared by PEO-containing block copolymer surfactant." *J. Biomed Mater Res*, **1989**, 23: p. 351-368.

42. Otsuka, H.; Nagasaki, Y. and Kataoka, K. "Self-assembly of poly(ethylene glycol)-based block copolymers for biomedical applications." *Current Opinion in Colloid & Interface Science*, **2001**, 6: p. 3-10.

43. Elbert, D.L. and Hubbell, J.A. "Self-assembly and steric stabilization at heterogeneous, biological surfaces using adsorbing block copolymers." *Chemistry & Biology*, **1998**, 5(3): p. 177.

44. Fan, X.; Lin, L. and Messersmith, P.B. "Cell fouling resistance of polymer brushes grafted from ti substrates by surface-initiated polymerization: Effect of ethylene glycol side chain length." *Biomacromolecules*, **2006**, 7(8): p. 2443-2448.

45. Singh, N.; Cui, X.; Boland, T. and Husson, S.M. "The role of independently variable grafting density and layer thickness of polymer nanolayers on peptide adsorption and cell adhesion." *Biomaterials*, **2007**, 28(5): p. 763.

46. Tosatti, S., Paul, S.M.D., Askendal, A., *et al.* "Peptide functionalized poly(L-lysine)-*g*-poly(ethylene glycol) on titanium: Resistance to protein adsorption in full heparinized human blood plasma." *Biomaterials*, **2003**, 24: p. 4949-4958.

47. VandeVondele, S.; Vörös, J. and Hubbell, J.A. "RGD-grafted poly-L-lysine-graft-(polyethylene glycol) copolymers block non-specific protein adsorption while promoting cell adhesion." *Biotechnol. Bioeng.*, **2003**, 82: p. 784-790.

48. Winblade, N.D.; Nikolic, I.D.; Hoffman, A.S. and Hubbell, J.A. "Blocking adhesion to cell and tissue surfaces by the chemisorption of a poly-L-lysine-graft-(poly(ethylene glycol); phenylboronic acid) copolymer." *Biomacromolecules*, **2000**, 1(4): p. 523-533.

49. Winblade, N.D.; Schmökel, H.; Baumann, M.; Hoffman, A.S. and Hubbell, J.A. "Sterically blocking adhesion of cells to biological surfaces with a surface-active copolymer containing poly(ethylene glycol) and phenylboronic acid." *Journal of Biomedical Materials Research*, **2002**, 59(4): p. 618-631.

50. Huang, N.P., Michel, R., Voros, J., *et al.* "Poly(L-lysine)-*g*-poly(ethylene glycol) layers on metal oxide surfaces: Surface-analytical characterization and resistance to serum and fibrinogen adsorption." *Langmuir*, **2001**, 17(2): p. 489-498.

51. Snellings, G.M.B.F.; Vansteenkiste, S.O.; Corneillie, S.I.; Davies, M.C. and Schacht, E.H. "Protein adhesion at poly(ethylene glycol) modified surfaces." *Advanced Materials*, **2000**, 12(24): p. 1959-1962.

52. Guo, S.; Shen, L. and Feng, L. "Surface characterization of blood compatible amphiphilic graft copolymers having uniform poly(ethylene oxide) side chains." *Polymer*, **2001**, 42(3): p. 1017.

53. Irvine, D.J.; Mayes, A.M. and Griffith, L.G. "Nanoscale clustering of RGD peptides at surfaces using comb polymers. 1. Synthesis and characterization of comb thin films." *Biomacromolecules*, **2001**, 2: p. 85-94.

54. Irvine, D.J.; Ruzette, A.-V.G.; Mayes, A.M. and Griffith, L.G. "Nanoscale clustering of RGD peptides at surfaces using comb polymers. 2. Surface segregation of comb polymers in polylactide." *Biomacromolecules*, **2001**, 2: p. 545-556.

55. Walton, D.G., Soo, P.P., Mayes, A.M., *et al.* "Creation of stable poly(ethylene oxide) surfaces on poly(methyl methacrylate) using blends of branched and linear polymers." *Macromolecules*, **1997**, 30: p. 6947-6956.

56. Dori, Y.; Bianco–Peled, H.; Satija, S.K., *et al.* "Ligand accessibility as means to control cell response to bioactive bilayer membranes." *Langmuir*, **2000**, 50: p. 75-81.

57. Houseman, B.T. and Mrksich, M. "The microenvironment of immobilized Arg-Gly-Asp peptides is an important determinant of cell adhesion." *Biomaterials*, **2001**, 22: p. 943-955.

58. Koo, L.Y.; Irvine, D.J.; Mayes, A.M.; Lauffenburger, D.A. and Griffith, L.G. "Co-regulation of cell adhesion by nanoscale RGD organization and mechanical stimulus." *Journal of Cell Science*, **2002**, 115(7): p. 1424-1433.

59. Kuhl, P.R. and Griffith-Cima, L.G. "Tethered epidermal growth factor as a paradigm for growth factor-induced stimulation from the solid phase." *Nat Med*, **1996**, 2(9): p. 1022-1027.

60. Segura, T. and Shea, L.D. "Surface-tethered DNA complexes for enhanced gene delivery." *Bioconjugate Chem.*, **2002**, 13(3): p. 621-629.

61. Otsuka, H.; Nagasaki, Y. and Kataoka, K. "Characterization of aldehyde-PEG tethered surfaces: Influence of PEG chain length on the specific biorecognition." *Langmuir*, **2004**, 20(26): p. 11285-11287.

62. Hersel, U.; Dahmen, C. and Kessler, H. "RGD modified polymers: Biomaterials for stimulated cell adhesion and beyond." *Biomaterials*, **2003**, 24: p. 4385-4415.

63. Neff, J.A.; Tresco, P.A. and Caldwell, K.D. "Surface modifcation for controlled studies of cell-ligand interactions." *Biomaterials*, **1999**, 20: p. 2377-2393.

64. Ochsenhirt, S.E.; Kokkoli, E.; McCarthy, J.B. and Tirrell, M. "Effect of RGD secondary structure and the synergy site PHSRN on cell adhesion, spreading and specific integrin engagement." *Biomaterials*, **2006**, 27: p. 3863-3874.

65. Zhu, J.; Beamish, J.A.; Tang, C.; Kottke-Marchant, K. and Marchant, R.E. "Extracellular matrix-like cell-adhesive hydrogels from RGD-containing poly(ethylene glycol) diacrylate." *Macromolecules*, **2006**, 39(4): p. 1305-1307.

66. Pierschbacher, M.D. and Ruoslahti, E. "Cell attachment activity of fibronectin can be duplicated by small synthetic fragments of the molecule." *Nature*, **1984**, 309(5963): p. 30.

67. Elbert, D.L. and Hubbell, J.A. "Surface treatments of polymers for biocompatibility." *Annual Review of Materials Science*, **1996**, 26: p. 365-294.

68. Mougin, K.; Ham, A.S.; Lawrence, M.B.; Fernandez, E.J. and Hillier, A.C. "Construction of a tethered poly(ethylene glycol) surface gradient for studies of cell adhesion kinetics." *Langmuir*, **2005**, 21: p. 4809-4812.

69. Buck, C.A. and Horwitz, A.F. "Cell surface receptors for extracellular matrix molecules." *Ann Rev Cell Biol*, **1987**, 3: p. 179-205.

70. Kao, W.J.; D., L.; Schense, J.C. and Hubbell, T.A. "Fibronectin modulates macrophage adhesion and FBGC formation." *J Biomed Mater Res*, **2001**, 55: p. 79-88.

71. Kao, W.J. and Lee, D. "In vivo modulation of host response and macrophage behavior by polymer networks grafted with fibronectin-derived biomimetic oligopeptides: The role of RGD and PHSRN domains." *Biomaterials*, **2001**, 22: p. 2901-2909.

72. Benoit, D.S.W. and Anseth, K.S. "The effect on osteoblast function of colocalized RGD and PHSRN epitopes on PEG surfaces." *Biomaterials*, **2005**, 26: p. 5209-5220.

73. Ufret, M.L. and Griffith, L.G. *in preparation.*

74. Branden, C. and Tooze, J. "Introduction to protein structure." Garland Publishing; New York 1999.

75. Mammen, M.; Choi, S.-K. and Whitesides, G.M. "Polyvalent interactions in biological systems: Implications for design and use of multivalent ligands and inhibitors." *Angewandte Chemie International Edition*, **1998**, 37(20): p. 2754-2794.

76. Engelhardt, W.; Gorczytza, H.; Butterweck, A.; Minkemann, H. and Frey, J. "Structural requirements of the cytoplasmic domains of the human macrophage Fcγ Receptor IIa and b cell Fcγ Receptor IIb2 for the endocytosis of immune complexes." *European Journal of Immunology*, **1991**, 21(9): p. 2227-2238.

77. Dower, S.K.; DeLisi, C.; Titus, J.A. and Segal, D.M. "Mechanism of binding of multivalent immune complexes to fc receptors. 1. Equilibrium binding." *Biochemistry*, **1981**, 20(22): p. 6326-6334.

78. Miyamoto, S.; Akiyama, S.K. and Yamada, K.M. "Synergistic roles for receptor occupancy and aggregation in integrin transmembrane function." *Science*, **1995**, 267(5199): p. 883-885.

79. Miyamoto, S., Teramoto, H., Coso, O.A., *et al.* "Integrin function: Molecular hierarchies of cytoskeletal and signaling molecules." *J. Cell Biol.*, **1995**, 131(3): p. 791-805.

80. Yauch, R.L.; Felsenfeld, D.P.; Kraeft, S.-K., *et al.* "Mutational evidence for control of cell adhesion through integrin diffusion/clustering, independent of ligand binding." *J. Exp. Med.*, **1997**, 186: p. 1347-1355.

81. Hynes, R.O. "Integrins: Bidirectional, allosteric signaling machines." *Cell*, **2002**, 110: p. 673-687.

82. Laplantine, E., Maurer, P., Vallar, L., *et al.* "The integrin β1 subunit cytoplasmic tail forms oligomers: A potential role in b1 integrin clustering." *Biology of the Cell*, **2002**, 94(6): p. 375-387.

83. Danilov, Y.N. and Juliano, R.L. "$(Arg\text{-}Gly\text{-}Asp)_n$-albumin conjugates as a model substratum for integrin-mediated cell adhesion." *Experimental Cell Research*, **1989**, 182: p. 186-196.

84. Maheshwari, G.; Brown, G.; Lauffenburger, D.A.; Wells, A. and Griffith, L.G. "Cell adhesion and motility depend on nanoscale RGD clustering." *Journal of Cell Science*, **2000**, 113: p. 1677-1686.

85. Groll, J., Fiedler, J., Engelhard, E., *et al.* "A novel star PEG– derived surface coating for specific cell adhesion." *Journal of Biomedical Materials Research*, **2005**, 74A: p. 607-617.

86. Thumshirn, G.; Hersel, U.; Goodman, S.L. and Kessler, H. "Multimeric cyclic RGD peptides as potential tools for tumor targeting: Solid-phase peptide synthesis and chemoselective oxime ligation." *Chem. Eur. J.*, **2003**, 9: p. 2717-2725.

87. Murata, J.; Saiki, I.; Ogawa, R., *et al.* "Molecular properties of poly(RGD) and its binding capacities to metastatic melanoma cells." *Int J Pept Prot Res*, **1991**, 38: p. 212-217.

88. Wong, J.Y.; Kuhl, T.L.; Israelachvili, J.N.; Mullah, N. and Zalipsky, S. "Direct measurement of a tethered ligand-receptor interaction potential." *Science*, **1997**, 275: p. 820-822.

89. Jeppesen, C., Wong, J.Y., Kuhl, T.L., *et al.* "Impact of polymer tether length on multiple ligand-receptor bond formation." *Science*, **2001**, 293: p. 465-468.

90. Longo, G. and Szleifer, I. "Ligand-receptor interactions in tethered polymer layers." *Langmuir*, **2005**, 21: p. 11342-11351.

91. Moreira, A.G. and Marques, C.M. "The role of polymer spacers in specific adhesion." *Journal of Chemical Physics*, **2004**, 120(13): p. 6229-6237.

92. Beer, J.H.; Springer, K.T. and Coller, B.S. "Immobilized Arg-Gly-Asp (RGD) peptides of varying lengths as structural probes of the platelet glycoprotein iib/iiia receptor." *Blood*, **1992**, 79(1): p. 117-128.

93. Massia, S.P. and Hubbell, J.A. "An RGD spacing of 440 nm is sufficient for integrin $\alpha_v\beta_3$- mediated fibroblast spreading and 140 nm for focal contact and stress fiber formation." *J. Cell Biol.*, **1991**, 114(5): p. 1089-1100.

94. Griffith, L.G. and Lopina, S. "Microdistribution of substratum-bound ligands affects cell function: Hepatocyte spreading on PEO-tethered galactose." *Biomaterials*, **1998**, 19(11-12): p. 979.

95. Milner, S.T.; Witten, T.A. and Cates, M.E. "Effects of polydispersity in the end-grafted polymer brush." *Macromolecules*, **1989**, 22: p. 853-861.

96. Dan, N. and Tirrell, M. "Effects of bimodal molecular weight distribution on the polymer brush." *Macromolecules*, **1993**, 26: p. 6467-6473.

97. Chakrabarti, A. and Toral, R. "Density profile of terminally anchored polymer chains: A monte carlo study " *Macromolecules*, **1990**, 23(7): p. 2016-2021.

98. Kent, M.S.; Factor, B.J.; Satija, S.; Gallagher, P. and Smith, G.S. "Structure of bimodal polymer brushes in a good solvent by neutron reflectivity." *Macromolecules*, **1996**, 29: p. 2843-2849.

99. Levicky, R.; Koneripalli, N.; Tirrell, M. and Satija, S.K. "Stratification in bidisperse polymer brushes from neutron reflectivity." *Macromolecules*, **1998**, 31(8): p. 2616-2621.

100. Lin, J.J.; Silas, J.A.; Bermudez, H., *et al.* "The effect of polymer chain length and surface density on the adhesiveness of functionalized polymersomes." *Langmuir*, **2004**, 20(13): p. 5493-5500.

101. Kim, D.H.; Klibanov, A.L. and Needham, D. "The influence of tiered layers of surface-grafted poly(ethylene glycol) on receptor-ligand-mediated adhesion between phospholipid monolayer-stabilized microbubbles and coated glass beads." *Langmuir*, **2000**, 16(6): p. 2808-2817.

102. Chen, C.-C. and Dormidontova, E.E. "Architectural and structural optimization of the protective polymer layer for enhanced targeting." *Langmuir*, **2005**, 21: p. 5605-5615.

103. Walton, D.G. and Mayes, A.M. "Entropically driven segregation in blends of branched and linear polymers." *Physical Review E*, **1996**, 54(3): p. 2018-2021.

104. Hiemenez, P.C. and Rajagopalan, R. "Principles of colloid and surface chemistry." Marcel Dekker; New York 1997.

105. Hester, J.F.; Banerjee, P. and Mayes, A.M. "Preparation of protein-resistant surfaces on poly(vinylidene fluoride) membranes via surface segregation." *Macromolecules*, **1999**, 32(5): p. 1643-1650.

106. Park, J.Y.; Acar, M.H.; Akthakul, A.; Kuhlman, W. and Mayes, A.M. "Polysulfone-graft-poly(ethylene glycol) graft copolymers for surface modification of polysulfone membranes." *Biomaterials*, **2006**, 27: p. 856-865.

107. Taniguchi, I.; Mayes, A.M.; Chan, E.W.L. and Griffith, L.G. "A chemoselective approach to grafting biodegradable polyesters." *Macromolecules*, **2005**, 38: p. 216-219.

Chapter 2: Experimental Methods

2.1 Introduction

The synthetic methods employed in the present work are similar to those employed by Irvine et al. [1]. Several notable modifications have been made, however, to accommodate variations in tether length and to improve peptide coupling efficiency. As the length of PEO tethers is increased, the number of PEO side chains must decrease to prevent the polymer from becoming water soluble. To ensure the presence of a sufficient number of active chain ends on each polymer, all PEO chain ends were terminated with hydroxyl groups. In addition, owing to the scarcity of active groups, an alternate high-yield coupling chemistry was employed.

2.1.1 Strategies for Comb Polymer Synthesis

There are three general approaches to making comb-like graft copolymers: grafting-from, grafting-to and macromonomer copolymerization (Figure 2.1) [2]. In grafting-from (Figure 2.1a), the polymer backbone is first synthesized with some fraction of segments possessing a functional group that can act as an initiator from which a second monomer can be polymerized. In grafting-to schemes (Figure 1b), a backbone bearing chemically derivitizable groups is first synthesized, and the copolymer is then formed through addition of a second polymer with a terminal functional group that will react with the backbone. Finally, macromonomer polymerization (Figure 1c) routes

involve copolymerization of the backbone monomer with a telechelic polymer of the desired side chain monomer.

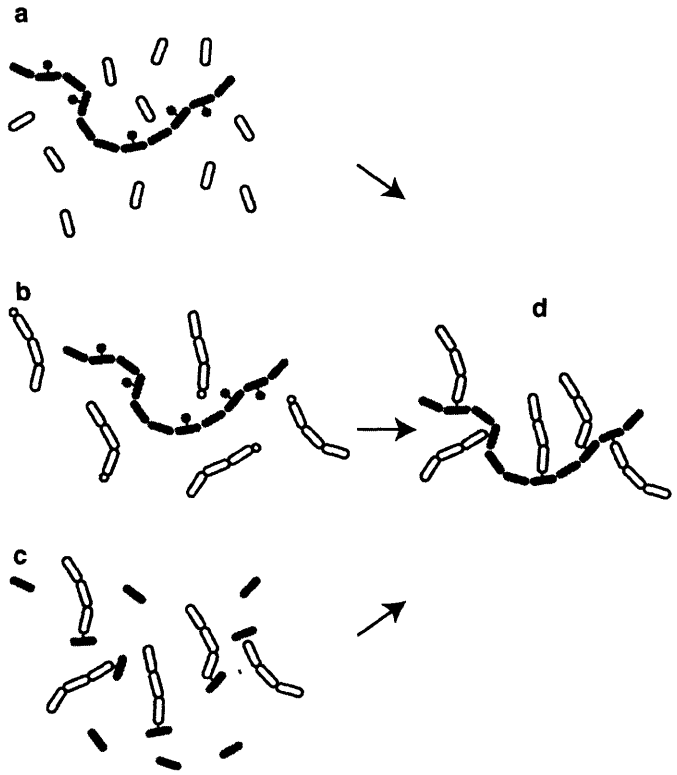

Figure 2.1 Schemes for producing a comb copolymer: (a) grafting-from, (b) grafting-to and (c) macromonomer copolymerization.

With respect to PEO-based chemistry, each of these general approaches has been employed [3]. Polyethylene-*graft*-poly(ethylene oxide) graft copolymers have been produced directly through polymerization of ethylene oxide from poly(ethylene-*co*-*p*-methyl styrene) that was first modified using *sec*-butyl lithium and ethylene oxide [4]. Park and coworkers grafted PEO directly onto a polysulfone backbone using Williamson ether synthesis [5]. A similar technique that joins the side chain to a chloromethylated

polystyrene backbone through an amide linkage using Schiff's base has also been reported [6]. While these methods produced brushes that were sufficiently dense to make the polymers resistant to cell attachment, these processes require the use of strong bases, making them unsuitable for use with biodegradable polymers and biologically active molecules.

A less chemically aggressive approach was employed by Hubbell and coworkers who synthesized poly(lysine)-*g*-PEO by grafting *n*-hydroxy succinimide- (NHS-) terminated PEO onto poly(lysine) backbones [7]. This chemistry was mild enough to permit further chemical modification of these polymers with peptides using NHS-based heterobifunctional linkers [8]. Other approaches that employ chemistry suitable for biological applications have also been investigated; including Diels-Alder based click chemistry [9] dicyclohexyl carbodiimide-mediated esterification [10] and chemoselective ligation [11, 12]. The latter approach is mild enough to be suitable for use with biodegradable polymers.

Several macromonomer routes to production of graft copolymer architectures with PEO side chains have also been investigated. Rieger and coworkers synthesized polycaprolactone-*graft*-poly (ethylene oxide) (PCL-*g*-PEO) by polymerizing ε-caprolactone with γ-poly(ethylene oxide) caprolactone macromonomer [13]. Ikeda and coworkers prepared a similar PCL-*g*-PEO copolymer through copolymerization of epoxy-terminated poly(ethylene oxide) with ε-caprolactone [14]. A more common approach involves use of PEO terminated in an acrylate or methacrylate group [1, 15-19]. This approach is especially attractive because monomers are commercially available, and there are a wealth of polymerization techniques that are compatible with the PEO

methacrylate macromonomer [20]. In addition, both PMMA and PEO have found use in commercial medical devices, increasing the likelihood that new devices made from materials based on these polymers will be viewed favorably for FDA approval.

2.1.2 Macromonomer Synthesis and Purification

PMMA-*g*-PEO copolymer is readily synthesized through a macromonomer route, where methyl methacrylate (MMA) is copolymerized with polyethylene glycol methacrylate. Only two lengths of polyethylene glycol methacrylate (6 and 10), however, are commercially available. Several approaches towards synthesis of PEO macromonomer have been reported in the literature, including anionic polymerization of ethylene oxide [21-23] and reaction of α,ω–hydroxy PEO with metyhacryloyl chloride [24] The former approach offers greater control over molecular weight, while the latter approach employs milder reaction conditions and can therefore be applied to a broader range of molecules.

Both approaches require separation of unreacted PEO from mono- and bi-functional PEO. For the cases where the number of EO segments is small (<6), this separation can be readily accomplished through distillation or column chromatography. For longer chain lengths, however, the polarity of the polymer dominates over the end groups, and separation by simple physical means becomes impossible. Taniguchi et al. recently demonstrated a method of purification using a solid phase resin [25] that extends the length of chain the can be separated to 10 EO segments. This approach, however, suffers from poor yields when the number of EO segments increases beyond 20. Consequently, the present work uses an alternate approach. Because of the difficulty in

separation of mono-, bi- and non-functionalized PEO, reaction conditions were chosen that minimize the amount of bi-functional PEO formed, and this crude product was used without further purification in copolymerization with MMA. Provided that the fraction of bi-functional PEO chains is sufficiently small, negligible cross-linking will occur during polymerization, and the remaining non-functionalized PEO can be separated during polymer purification using preparative size exclusion chromatography.

2.1.3 Methods for Coupling Peptides to Synthetic Polymers

Numerous approaches are available for conjugation of biomolecules to synthetic polymers [26-29]. These approaches can be broadly categorized by the functional groups they employ. For PMMA-*g*-PEO, the most readily available chemical group is the terminal hydroxyl end of the PEO chains. Two major approaches exist to chemically link a biomolecule to this functional group (Figure 2.2): coupling through a leaving group, such as NHS, or formation of a thioether through reaction with an active group such as a maleimide.

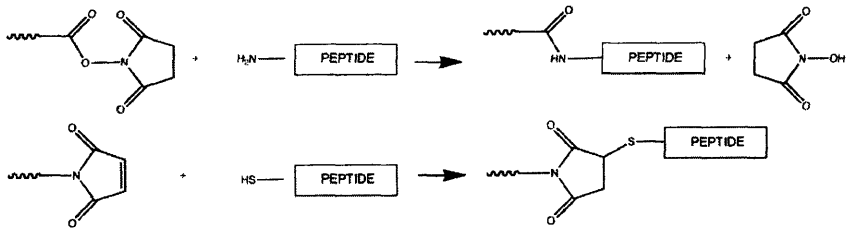

Figure 2.2 Two general schemes for coupling a peptide to a synthetic molecule.

Approaches employing leaving groups have the advantage that they are applicable to any biomolecule containing a primary amine. Most proteins terminate in an amine, and many

common biologically active small molecules are available in aminated forms, making this approach attractive for general coupling purposes. This approach, however, has several drawbacks. Most chemically active leaving groups (including NHS) are susceptible to hydrolysis, limiting yields when reactions must be performed in an aqueous environment. Furthermore, these reactions often have poor specificity. A given biomolecule, such as a protein, may have several available primary amines, any of which can react with the active group.

An alternate approach is to use an active group that reacts with a functional species that has been specifically engineered into the biomolecule. Maleimides, for example, react only with sulfhydryl groups, such that they bind only with thiol-bearing amino acids. In certain cases, such amino acids can be readily engineered into the protein or peptide of interest, making it possible to dictate the position at which the maleimide will bind. Maleimides do not readily hydrolyze at physiological pH and react rapidly with thiols to form a stable thioether. It should be noted, however, that at high pH's (>8.5) maleimides lose their specificity towards thiols and may also react with amines [30, 31]. Care should therefore be used when co-tethering different epitopes using orthogonal coupling chemistries.

Several methods can be used to convert primary alcohols to maleimides [32, 33]. The Mitsonobu reaction (Figure 2.3), for example, has been employed successfully on many small molecules [34]. In this reaction, a primary alcohol is converted into an amide through reaction with an amine, mediated using triphenyl phosphine (Ph_3P) and diisopropylazo dicarboxylate (DIAD).

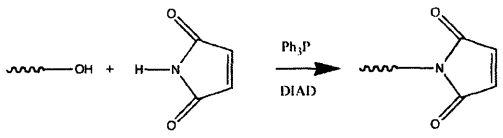

Figure 2.3 The Mitsonobu reaction

This reaction, however, involves an intermediate that is susceptible to formation of cross-links, making it inappropriate for polymer functionalization. An alternative method employs the heterobifunctional linker *p*-maleimidophenyl isocyanate [35]. This linker contains both a maleimide and an isocyanate that reacts readily with available alcohols or amines in a one-step reaction. An added advantage of this approach is that it produces no side products, simplifying purification. In addition, PMPI produces a number of characteristic peaks that are distinct from other peaks associated with PMMA-*g*-PEO, facilitating characterization. This method was chosen over the alternatives because of its high yield and specificity.

2.2 Experimental Methods

2.2.1 Materials

Methyl methacrylate (MMA), polyethylene oxide (PEO, M_n 1,000), methacryloyl chloride, polyethylene oxide methacrylate (M_n = 526), poly(methyl methacrylate) (PMMA) and 2,2'-azobis(2-methylpropionitrile) (AIBN) were obtained from Aldrich Chemical Co. N-(*p*-maleimidophenyl) isocyanate (PMPI) and bovine serum albumin (BSA) were obtained from VWR Scientific. BioBeads were purchased from Bio-Rad.

Biacore chips were purchased from Biacore. All chemicals were reagent grade and used as supplied unless otherwise noted.

2.2.2 Macromonomer Synthesis

PEO_{22} methacrylate macromonomer was synthesized by adding 0.15 equivalents of methacryloyl chloride dropwise to a 30 wt% solution of PEO (1,000 Da) and a two-fold excess of triethylamine (TEA) in dichloromethane, chilled in an ice bath (Figure 2.4).

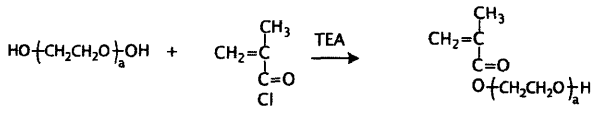

Figure 2.4 Synthetic scheme for macromonomer production.

The reaction was allowed to proceed overnight with stirring. The crude product was extracted once with 0.01 M hydrochloric acid, twice with brine and finally once with deionized water. The product was dried over magnesium sulfate and the solvent removed by rotary evaporation. ^{1}H NMR (Bruker, DPX-400) showed the appearance of a new peak at δ=*4.29* ppm, corresponding to the methylene protons of PEO adjacent to the methacrylate ester. ^{1}H NMR (400 MHz in $CDCl_3$), δ (ppm): 1.96 (s, 3H, CH_3), 3.44-3.82 (m, 86H, CH_2CH_2O), 4.29 (t, 2H, $COOCH_2$), 5.59 (s, 1H, CH=C), and 6.15 (s, 1H, CH=C) (Figure 2.5).

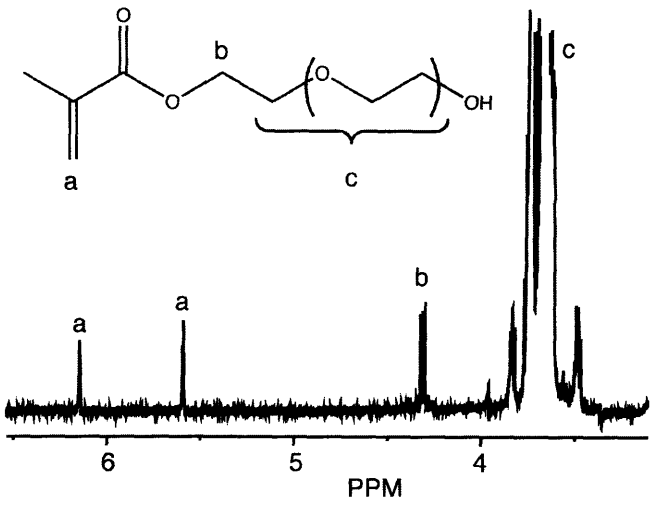

Figure 2.5 NMR of PEO-methacrylate macromonomer.

2.2.3 Polymer Synthesis

PMMA-*g*-PEO comb copolymers with 10 EO segments per side chain (PMMA-*g*-PEO_{10}) were synthesized by free radical polymerization in toluene through a macromonomer route using AIBN as reported elsewhere [1]. PMMA-*g*-PEO_{22} was prepared by copolymerizing 17.6 g the crude PEO derivative containing 4 mmol PEO_{22} methacrylate macromonomer (22 % purity) with 6.35 g of MMA (6.35 mmol) in 100 mL ethanol using 30 mg AIBN as an initiator at 65°C overnight. The reaction mixture was precipitated in hexane, and the polymer purified by size exclusion chromatography (BioBeads) using tetrahydrofuran as an eluent. Purity was verified by gel permeation chromatography (Waters Styragel HR4, HR5), which found complete removal of residual PEO in the purified product as indicated by the disappearance of the PEO peak at ~21 mL (Figure 2.6). The yield was approximately 14%.

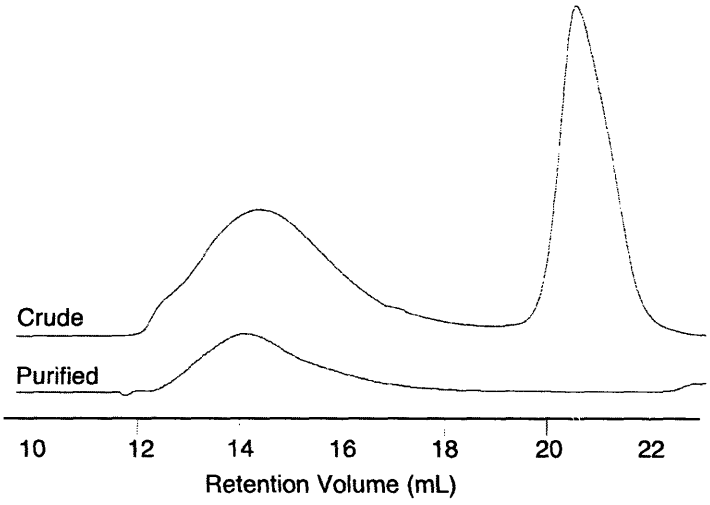

Figure 2.6 GPC chromatograms of PMMA-*g*-PEO_{22} purification, showing complete removal of residual PEO_{22} macromonomer in the purified polymer.

Molecular weights were determined using gel-permeation chromatography (Waters Styragel HR3, HR4, HR5) with in-line light scattering (Wyatt MiniDawn) [36]. Number-average molecular weight and polydispersity were M_n = 510 kDa and PDI = 3.7 for PMMA-*g*-PEO_{22} (Figure 2.7a), and M_n=142 kDa and PDI = 3.2 for PMMA-*g*-PEO_{10} (Figure 2.7b).

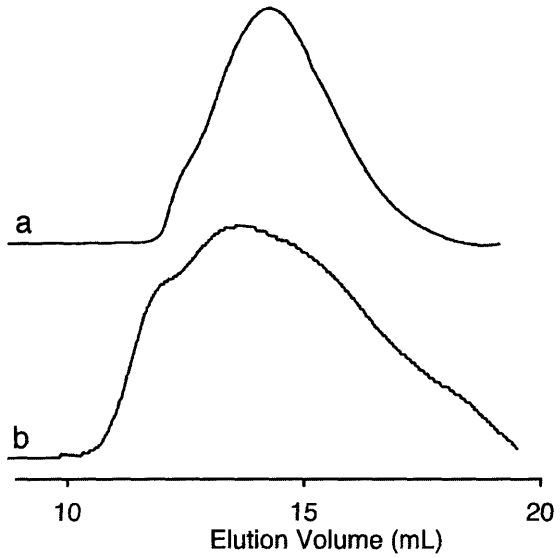

Figure 2.7 GPC chromatograms of PMMA-*g*-PEO_{22} (*a*) and PMMA-*g*-PEO_{10} (*b*).

Polymer composition was determined by proton NMR (Bruker DPX, 400 MHz) in deuterated chloroform using previously reported peak assignments (Figure 2.8) [1]. PMMA-*g*-PEO_{10} and PMMA-*g*-PEO_{22} contained 32 and 29 wt% PEO, respectively. This corresponds to 1 PEO chain per 11 backbone units for PMMA-*g*-PEO_{10}, and 1 PEO chain per 23 backbone units for PMMA-*g*-PEO_{22}. Based on previous studies by Irvine et al. [1], and Au et al. [37] these PEO contents are sufficiently high to resist cell adhesion yet low enough to render the polymers water insoluble.

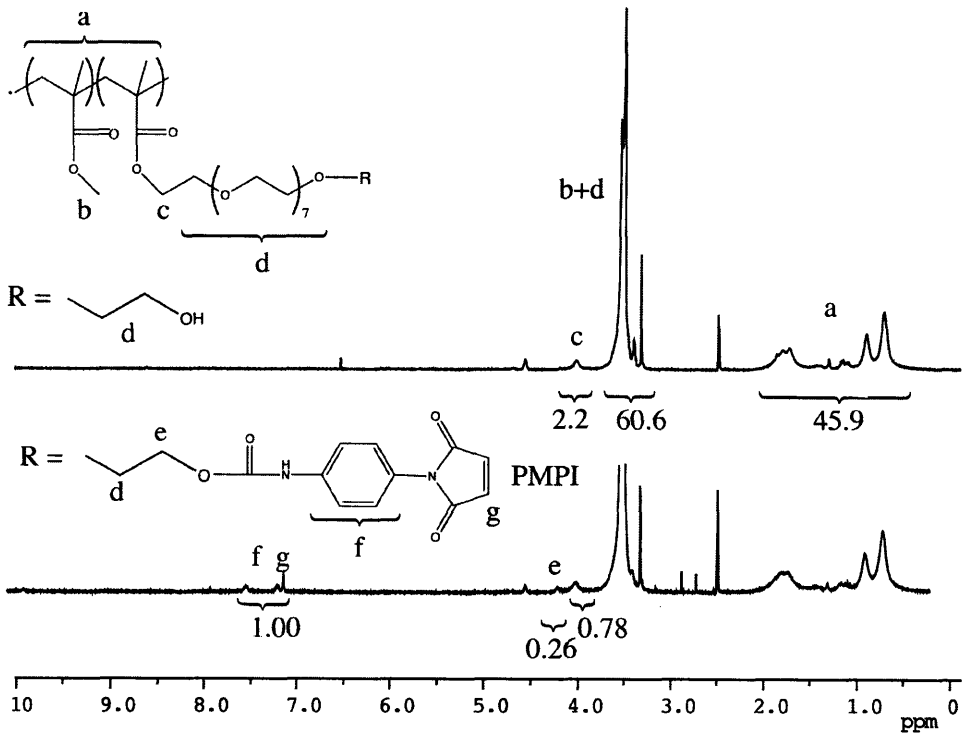

Figure 2.8 NMR spectra of PMMA-*g*-PEO_{10} (top) and PMPI activated PMMA-*g*-PEO_{10} (bottom)

Differential scanning calorimetry (TA Q-100 DSC) was performed on PMMA-*g*-PEO_{10} to determine a glass transition temperature, used in sample annealing (Figure 2.9). DSC was performed in a sealed aluminum crucible under a helium atmosphere. Temperature was scanned from -100 to 150 at a scan rate of 10°C/min. The sample was first heated to 140°C, then cooled to -100 and then re-heated to 150°C (Figure 2.9, second heating cycle shown). A single mixed-state glass transition temperature (T_g) was found at 42.7°C, in close agreement with the T_g of 43°C estimated by group contribution methods by Irvine et al. [38, 39].

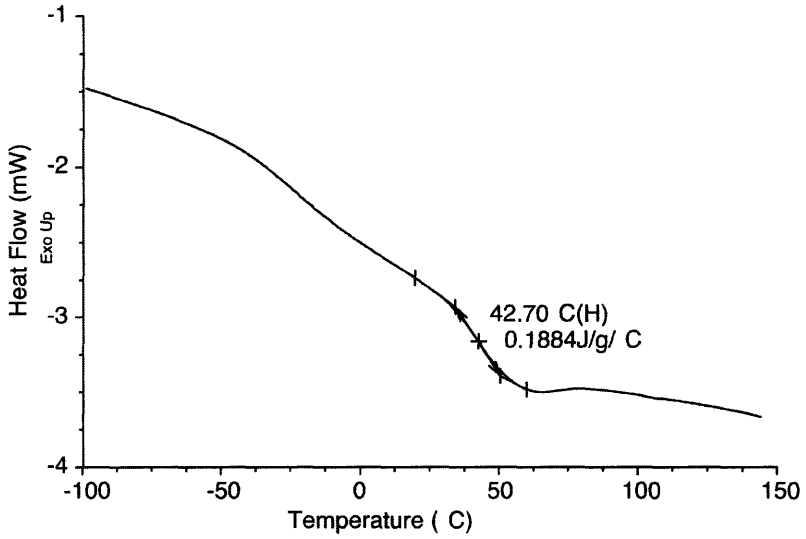

Figure 2.9 DSC of PMMA-*g*-PEO_{10} showing a single T_g at 42.7°C

2.2.4 PMPI Activation

Desired fractions of PEO chain ends were functionalized with maleimide groups using PMPI, following the method of Annunziato et al. (Figure 2.10) [35].

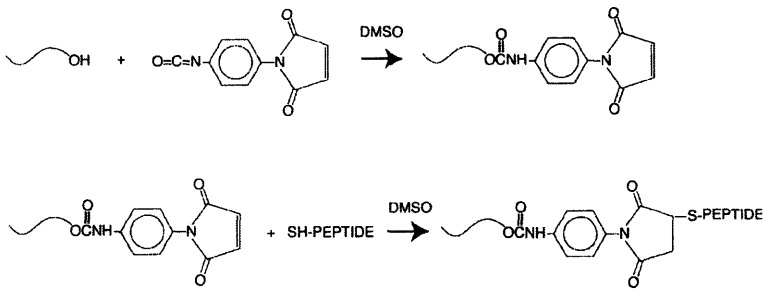

Figure 2.10 Scheme for coupling peptides to PMMA-*g*-PEO_{10} using PMPI

The polymer was first dissolved in benzene to a concentration of ~10 mg/ml in a round bottom flask fitted with a 3-way stopcock. The flask was then immersed in liquid nitrogen and gently rotated such that the polymer solution froze in a thin (~2 mm) shell around the inside of the flask. Once the polymer was fully frozen, the flask was attached

to a vacuum line equipped with a liquid nitrogen trap and the benzene was allowed to sublimate until the flask reached room temperature and the polymer readily crumbled into a fine white powder. The flask was purged with nitrogen and anhydrous DMSO was introduced via syringe to produce a ~40 mg/ml solution. Two equivalents of PMPI relative to hydroxyl groups were added under nitrogen, and the reaction was allowed to proceed with mixing overnight at room temperature. Afterward, purification of the product was accomplished through repeated precipitation in diethyl ether. The product was characterized by proton NMR in deuterated DMSO. Degree of functionalization was determined by measuring the ratio of the peak at δ =7.2 ppm (s, 2H, maleimide) to the peak at 4.2 ppm (t, 2H, ester methylene). The fraction of activated PEO chain ends on PMMA-*g*-PEO_{10} and PMMA-*g*-PEO_{22} was 60±10% and 80±10%, respectively. Availability of the maleimide groups and their reactivity towards thiols was verified by adding a small amount of peptide to an NMR tube containing PMPI-activated polymer dissolved in deuterated DMSO. A color change from amber to clear was observed after a few minutes. Complete disappearance of the maleimide peak (δ~7.2) was observed by 1H NMR (Figure 2.11).

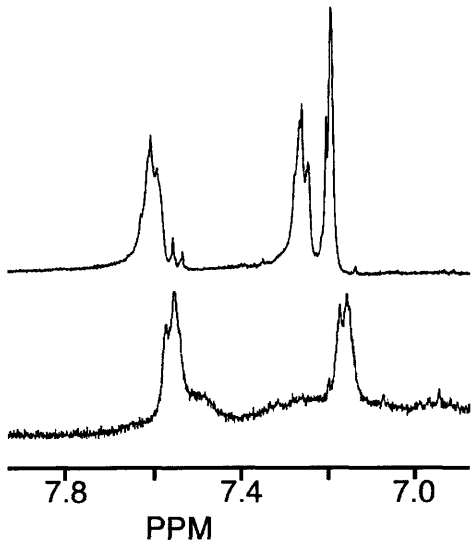

Figure 2.11 NMR spectra showing PMPI activated (top) and peptide-coupled polymer (bottom).

2.2.5 Protein Adsorption Resistance

Protein adsorption resistance of PMMA-*g*-PEO_{10} was verified using surface plasmon resonance (Biacore BIA2000). Surfaces were spin-coated from a 10 mg/ml solution of PMMA or PMMA-*g*-PEO_{10} in toluene onto gold Biacore chips that were then mounted as per the manufacturer's instructions. Chips were loaded into the Biacore, warmed to 37°C and allowed to equilibrate for 30 minutes. Each surface was then exposed to a 1mg/ml solution of BSA, for 60 seconds, followed by a 5 minute PBS rinse. The flow rate for all steps in this procedure was 10 µl/min. Protein adsorption was taken to be the difference between the detector signal immediately before exposure to BSA and the detector signal following the 5 minute PBS rinse. This approach found a 40-fold reduction in non-specific protein adsorption on PMMA-*g*-PEO_{10} coated surfaces relative to PMMA following exposure to a 1 mg/ml solution of BSA (Figure 2.12). Additional

evidence of protein adsorption resistance is given in Chapter 4, where no cell attachment is observed on surfaces prepared from PMMA-*g*-PEO_{10} or PMMA-*g*-PEO_{22}.

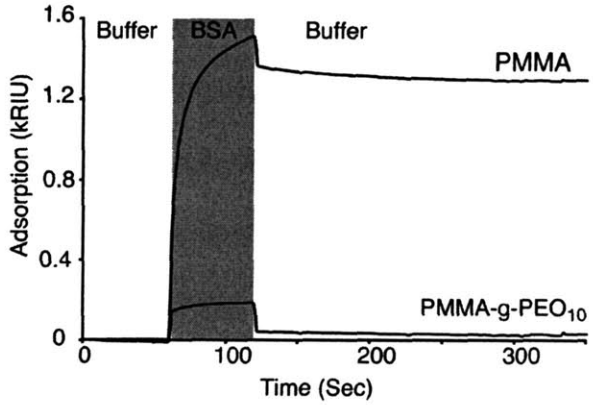

Figure 2.12 SPR flowgram of BSA adsorption to PMMA and PMMA-*g*-PEO_{10}

2.3 Discussion

Previous research used a blend of hydroxy- and methoxy-terminated PEO to ensure that the resulting polymer was both insoluble in water and yet resistant to nonspecific protein adsorption [1]. Polymers synthesized for this study contain only hydroxy groups, but are low enough in PEO content that they remain insoluble in water. Despite their lower PEO content, however, these polymers remain protein resistant. For both polymers employed in this work, the molecular weight is large enough to produce clusters on a length scale observable by TEM. The broad polydispersity (PDI = 3.2) observed can be attributed to the intrinsically high PDI associated with free-radical copolymerization, coupled with a small degree of cross-linking caused by residual bi-functional PEO in the macromonomer. The number of PMPI-activated side chains is enough to provide up to 100,000 ligands/μm^2, which is sufficient for the studies conducted in Chapter 4. More detailed discussion of choice of polymer composition is provided in the discussion section of later chapters.

2.4 Conclusions

The synthetic approach outlined above provides a facile route to production of PMMA-*g*-PEO polymers with side chains of different lengths. Two polymers were produced, PMMA-g-PEO_{10} having a number-average molecular weight of M_n=142 kDa and PDI = 3.2, containing 32 wt% PEO, and PMMA-g-PEO_{22} having a number-average molecular weight of M_n = 510 kDa and PDI = 3.7, containing 29 wt% PEO. PMPI was readily coupled to both polymers, resulting in functionalization of more than half of all end groups on both polymers.

The polymerization chemistry employed is mild enough that it can be generalized to other systems, possibly facilitating future adaptation of more complicated chemical or biological species. The coupling chemistry, similarly, requires only the presence of a hydroxyl group, making it suitable for a broad range of applications. Two areas for further study remain, however: improved methods for purification of PEO macromonomers and control over molecular weight. Given the low efficiency of separation with increasing molecular weight by conventional means, the best approach towards obtaining higher macromonomer purity may be through alternative synthetic approaches, such as those described by Ito et al. [24]. In the absence of bi-functional macromonomer, molecular weight control may be achieved using controlled radical or anionic polymerization methods. For the purposes of this study, however, the techniques described above offer a robust route to producing large quantities of suitable polymers.

2.5 References

1. Irvine, D.J.; Mayes, A.M. and Griffith, L.G. "Nanoscale clustering of RGD peptides at surfaces using comb polymers. 1. Synthesis and characterization of comb thin films" *Biomacromolecules* **2001**, *2*: p. 85-94.
2. Odian, G. "Principles of polymerization" Wiley; New York 1991.
3. Xie, H.-Q. and Xie, D. "Molecular design, synthesis and properties of block and graft copolymers containing polyoxyethylene segments" *Progress in Polymer Science* **1999**, *24* (2): p. 275.
4. Lu, Y.; Chen, S.; Hu, Y. and Chung, T.C. "Synthesis of graft copolymer polyethylene-graft-poly(ethylene oxide) by a new anionic graft-from polymerization" *Polymer International* **2004**, *53* (12): p. 1963-1967.
5. Park, J.Y.; Acar, M.H.; Akthakul, A.; Kuhlman, W. and Mayes, A.M. "Polysulfone-graft-poly(ethylene glycol) graft copolymers for surface modification of polysulfone membranes" *Biomaterials* **2006**, *27*: p. 856-865.
6. Wang, Y.; Du, Q. and Huang, J. "Grafting of poly(ethylene oxide) with Schiff's base end group onto chloromethylated polystyrene via decker-forster reaction" *Macromolecular Rapid Communications* **1998**, *19* (5): p. 247-250.
7. Winblade, N.D.; Nikolic, I.D.; Hoffman, A.S. and Hubbell, J.A. "Blocking adhesion to cell and tissue surfaces by the chemisorption of a poly-L-lysine-graft-(poly(ethylene glycol); phenylboronic acid) copolymer" *Biomacromolecules* **2000**, *1* (4): p. 523-533.

8. Vandevondele, S.; Vörös, J. and Hubbell, J.A. "RGD-grafted poly-L-lysine-graft-(polyethylene glycol) copolymers block non-specific protein adsorption while promoting cell adhesion" *Biotechnol. Bioeng.* **2003**, *82*: p. 784-790.

9. Gacal, B.; Durmaz, H.; Tasdelen, M.A., et al. "Anthracene-maleimide-based Diels-Alder "Click chemistry" As a novel route to graft copolymers" *Macromolecules* **2006**, *39* (16): p. 5330-5336.

10. Parrish, B. and Emrick, T. "Aliphatic polyesters with pendant cyclopentene groups: Controlled synthesis and conversion to polyester-graft-PEG copolymers" *Macromolecules* **2004**, *37* (16): p. 5863-5865.

11. Taniguchi, I.; Mayes, A.M.; Chan, E.W.L. and Griffith, L.G. "A chemoselective approach to grafting biodegradable polyesters" *Macromolecules* **2005**, *38*: p. 216-219.

12. Taniguchi, I.; Kuhlman, W.A.; Mayes, A.M. and Griffith, L.G. "Functional modification of biodegradable polyesters through a chemoselective approach: Application to biomaterial surfaces" *Polymer International* **2006**, *55*: p. 1385-1397.

13. Rieger, J.; Dubois, P.; Jerome, R. and Jerome, C. "Controlled synthesis and interface properties of new amphiphilic PCL-*g*-PEO copolymers" *Langmuir* **2006**, *22* (18): p. 7471-7479.

14. Ikeda, I.; Horie, N. and Suzuki, K. "Synthesis of graft poly(ester ether) by ring-opening copolymerization of epoxy-terminated poly(ethylene glycol) with lactones" *Journal of Applied Polymer Science* **1994**, *54*: p. 1123-1126.

15. Ali, M.M. and Stover, H.D.H. "Well-defined amphiphilic thermosensitive copolymers based on poly(ethylene glycol monomethacrylate) and methyl methacrylate prepared by atom transfer radical polymerization" *Macromolecules* **2004**, *37*: p. 5219-5227.

16. Walton, D.G.; Soo, P.P.; Mayes, A.M., et al. "Creation of stable poly(ethylene oxide) surfaces on poly(methyl methacrylate) using blends of branched and linear polymers" *Macromolecules* **1997**, *30*: p. 6947-6956.

17. Brown, A.A.; Khan, N.S.; Steinbock, L. and Huck, W.T.S. "Synthesis of oligo(ethylene glycol) methacrylate polymer brushes" *European Polymer Journal* **2005**, *41* (8): p. 1757.

18. Nath, N.; Hyun, J.; Ma, H. and Chilkoti, A. "Surface engineering strategies for control of protein and cell interactions" *Surface Science* **2004**, *570* (1-2): p. 98-110.

19. Hyun, J.H.; Ma, H.W.; Zhang, Z.P.; Beebe, T.P. and Chilkoti, A. "Universal route to cell micropatterning using an amphiphilic comb polymer" *Advanced Materials* **2003**, *15* (7-8): p. 576-579.

20. Hawker, C.J.; Mecerreyes, D.; Elce, E., et al. ""Living" Free radical polymerization of macromonomers: Preparation of well defined graft copolymers" *Macromolecular Chemistry and Physics* **1997**, *198* (1): p. 155-166.

21. Ito, K.; Hashimura, K.; Itsuno, S. and Yamada, E. "Poly(ethylene oxide) macromonomers. 8. Preparation and polymerization of ω-hydroxypoly(ethylene oxide) macromonomers" *Macromolecules* **1991**, *24* (14): p. 3977-3981.

22. Nagasaki, Y.; Ogawa, R.; Yamamoto, S.; Kato, M. and Kataoka, K. "Synthesis of heterotelechelic poly(ethylene glycol) macromonomers. Preparation of poly(ethylene glycol) possessing a methacryloyl group at one end and a formyl group at the other end" *Macromolecules* **1997**, *30* (21): p. 6489-6493.

23. Xie, H.-Q.; Liu, J. and Li, H. "An improved synthetic method for preparing polyoxyethylene macromers and a study of their copolymerization with alkyl acrylates" *J. Macromol. Sci-Chem* **1990**, *A27* (6): p. 725-741.

24. Ito, K.; Tsuchida, H.; Hayashi, A., et al. "Reactivity of poly(ethylene oxide) macromonomers in radical copolymerization" *Polymer Journal* **1985**, *17* (7): p. 827-839.

25. Taniguchi, I.; Kuhlman, W.A.; Griffith, L.G. and Mayes, A.M. "Macromonomer purification strategy for well-defined polymer amphiphiles incorporating poly(ethylene glycol) monomethacrylate" *Macromol. Rapid Commun.* **2006**, *27*: p. 631 – 636.

26. Veronese, F.M. "Peptide and protein PEGylation: A review of problems and solutions" *Biomaterials* **2001**, *22*: p. 405-417.

27. Roberts, M.J.; Bentley, M.D. and Harris, J.M. "Chemistry for peptide and protein PEGylation" *Advanced Drug Delivery Reviews* **2002**, *54*: p. 459-476.

28. Hermanson, G.T. "Bioconjugate techniques" Academic Press; San Diego 1996.

29. Li, J. and Kao, W.J. "Synthesis of polyethylene glycol (PEG) derivatives and PEGylated-peptide biopolymer conjugates" *Biomacromolecules* **2003**, *4* (4): p. 1055-1067.

30. Chang, C.-D. "Coupling method using selective amination of maleimide." US Patent 5,283,334,

31. Shen, G.; Horgan, A. and Levicky, R. "Reaction of *n*-phenyl maleimide with aminosilane monolayers" *Colloids and Surfaces B: Biointerfaces* **2004**, *32*: p. 59-65.

32. Tournier, E.J.M.; Wallach, J. and Blond, P. "Sulfosuccinimidyl 4-(n-maleimidomethyl)-1-cyclohexane carboxylate as a bifunctional immobilization agent. Optimization of the coupling conditions" *Analytica Chimica Acta* **1998**, *361*: p. 33-44.

33. King, H.D.; Dubowchik, G.M. and Walker, M.A. "Facile synthesis of maleimide bifunctional linkers" *Tetrahedron Letters* **2002**, *43*: p. 1987-1990.

34. Walker, M.A. "The Mitsunobu reaction: A novel method for the synthesis of bifunctional maleimide linkers" *Tetrahedron Letters* **1994**, *35* (5): p. 665-668.

35. Annunziato, M.; Patel, U.; M., R. and Palumbo, P. "*p*-Maleimidophenyl isocyanate: A novel heterobifunctional linker for hydroxyl to thiol coupling" *Bioconjugate Chem.* **1993**, *4*: p. 212-218.

36. Podzimek, S. "The use of GPC coupled with a multiangle laser light scattering photometer for the characterization of polymers" *Journal of Applied Polymer Science* **1994**, *54*: p. 91-103.

37. Au, A.; Boehm, C.A.; Mayes, A.M.; Muschler, G.F. and Griffith, L.G. "Formation of osteogenic colonies on well-defined adhesion peptides by freshly isolated human marrow cells" *Biomaterials* **2007**, *28* (10): p. 1847-1861.

38. Irvine, D.J.; Ruzette, A.-V.G.; Mayes, A.M. and Griffith, L.G. "Nanoscale clustering of RGD peptides at surfaces using comb polymers. 2. Surface segregation of comb polymers in polylactide" *Biomacromolecules* **2001**, *2*: p. 545-556.

39. Krevelen, D.W.V. "Properties of polymers: Correlations with chemical structure" Elsevier; New York 1972.

Chapter 3: Observation of Ligand Clustering and Two-Dimensional Scaling of R_g

3.1 Introduction

Interactions requiring sub-micron sized clusters of ligand-receptor bonds are ubiquitous in biology [1]. Examples include recognition of antibody coated infectious particles by macrophages [2], viral [3, 4] and bacterial [5] infection of mammalian cells, and cell adhesion to extracellular matrix [6-9]. In these processes, bioactivity is dictated not only by the presence of specific functional groups, but also on their spatial organization. Surfaces that prevent formation of clusters of bound receptors through insufficient local ligand density may produce little or no biological response in comparison to systems where receptor aggregation is facilitated through the presence of sub-micron clusters of ligands within the substrate [10-13]. Control over spatial organization of substrate-bound ligands, therefore, is of value in designing bioactive surfaces with controlled cell-surface interactions. The ability to control the size and spacing of clusters in addition to the number of ligands per cluster can be used to create surfaces that are more effective in eliciting a desired cellular response with fewer peptides. One such approach of interest involves application of amphiphilic comb copolymers. This chapter provides direct observation of ligand clusters formed using PMMA-*g*-PEO and analyzes the relationship between molecular weight and cluster size.

PMMA-*g*-PEO comb copolymers have been proposed to self-organize at the polymer/water interface, resulting in the effective confinement of the backbone to two dimensions [10, 14, 15] for chains at the immediate surface of a PMMA-*g*-PEO film

(Figure 3.1). Under these circumstances, the conformations [16] and dynamics [17] of individual polymer chains may differ greatly from their bulk state. Polymers confined in a 2D melt are expected to form non-interpenetrating disks. Ligands bound to the backbone of these polymers will follow the spatial organization of the backbone, resulting in clustering of ligands within the dimensions of the 2D confined polymer.

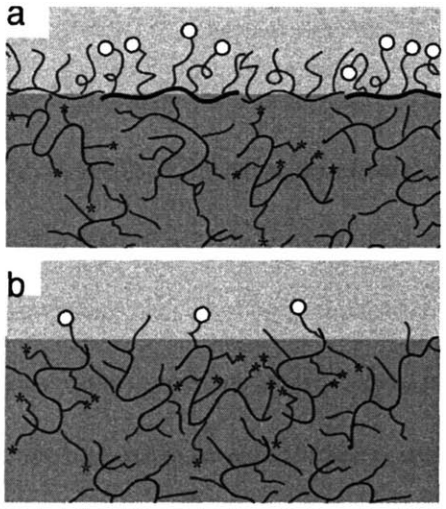

Figure 3.1 (a) Schematic illustration of amphiphilic comb copolymers confined in two dimensions at the polymer film/water interface. Nanoparticles attached to side chains of maleimide-modified comb polymers create nanoparticle clusters at the surface. By contrast, nanoparticles attached to surface maleimide groups on 3D comb polymer chains (b) will be scattered uniformly across the surface.

Understanding the behavior of PMMA-*g*-PEO polymers at the water/polymer interface, therefore, can be of value in designing bioactive substrates where nanometer length-scale organization of ligands is important. This chapter describes the use of gold nanoparticle labeling to observe the conformations of PMMA-*g*-PEO molecules at the water/polymer interface and reports the effects of molecular weight distribution on cluster size.

Conformations of polymer chains confined to two dimensions are predicted to depend strongly on polymer chain concentration. Swollen polymer coils in two dimensions have been modeled as self-avoiding random walks, for which the radius of gyration (R_g) scales with the number of segments (N) as $R_g \sim N^{\nu}$ where ν=0.75 [18]. With increasing chain concentration, screening effects cause a reduction in chain dimensions such that for a 2D monodisperse melt, chains exhibit ideal behavior with ν=0.5 [16, 19-21]. These scaling predictions have been verified through Monte Carlo (MC) simulations [19, 21]. Three-dimensional chains exhibit identical scaling in the melt (ν=0.5), while ν=0.6 in dilute solution [16].

There have been few experimental reports of the determination of ν for polymers in 2D confinement [22-29]. Jones et al. [22, 23] performed small-angle neutron scattering studies on thin polystyrene films incorporating a deuterated polystyrene fraction and found that the scattering intensity scaled with wavevector as $I(k) \sim k^{-2}$ for films of sub-R_g thickness, consistent with ideal chain statistics (ν=0.5). Maier and Rädler investigated the conformations of micron-length strands of fluorescently labeled DNA confined in 2D via adsorption to mobile cationic lipid bilayers. For isolated chains they found that R_g scaled with number of DNA base pairs as $R_g \sim N^{0.79}$, while for concentrated systems chain collapse was observed, consistent with theoretical predictions, though no scaling exponent was reported [24, 25]. Wang and Foltz [26] conducted atomic force microscopy (AFM) studies on dense 2D films of nanoropes (worm-like micelles) formed from polystyrene-*block*-polybutadiene copolymers and found that the lateral dimension scaled with contour length as $R \sim L^{0.63}$. For dilute surface concentrations, however, surface tension effects resulted in more collapsed configurations with $R \sim L^{0.51}$. Sukhishvili et al.

[27] performed fluctuation correlation spectroscopy on isolated fluorescently-labeled polyethylene oxide (PEO) chains adsorbed onto a self-assembled monolayer on silica and obtained a diffusion coefficient scaling of $D \sim N^{3/2}$, implying $R_g \sim N^{3/4}$. From Langmuir trough experiments on polymers confined at the air/water interface, Vilanove and Rondelez [28] extracted ν values of 0.56 and 0.79 for poly(methyl methacrylate) and poly(vinyl acetate), respectively, using the semidilute scaling relation $\Pi \sim c^{2\nu/(2\nu-1)}$, where Π and c denote the surface pressure and concentration, respectively. More recently, a similar analysis by Gavranovic et al. [29] on poly(*tert*-butyl methacrylate) yielded ν=0.53.

To directly probe the conformations of PMMA-*g*-PEO in this study, combs modified with maleimide groups on the PEO chain ends were blended at 0.5-10 wt% with unmodified PMMA-*g*-PEO and cast into films of thickness ~$3R_g$. Films were immersed in aqueous solution to induce orientation of surface molecules, and maleimide-functionalized chains at the film/water interface were labeled with 1.4 nm dia. Au nanoparticles. Transmission electron microscopy (TEM) was then used to trace the trajectories of individual nanoparticle-decorated chains. The distribution of observed 2D chain lengths was compared to the molecular weight distribution obtained by gel permeation chromatography. The scaling exponent ν for the 2D radius of gyration was calculated, and compared to that obtained from Monte Carlo simulation of a 2D melt having a chain length distribution fitted to that of our experimental system. The results suggest that polydispersity significantly influences 2D melt conformations.

3.2 Experimental Methods

3.2.1 Materials

The PMMA-*g*-PEO_{10} polymers used for this study is described in Chapter 2 (M_n=142 kDa and PDI = 3.2, 32 wt% PEO). Tris(2-carboxyethyl)phosphine was purchased from Aldrich Chemical Co. Toluene, hexane, (*p*-maleimidophenyl) isocyanate (PMPI), ethyl ether, 1,2-ethane dithiol, dimethyl sulfoxide (DMSO), Chromerge, and phosphate buffered saline (PBS) were purchased from VWR Scientific. Siliclad was purchased from Gelest. Deionized (DI) water was produced using a Millipore Milli-Q unit. All materials were reagent grade and used without further purification.

3.2.2 Anticipated Cluster Size

The PMMA-*g*-PEO_{10} polymer used for this study has a number-average molecular weight of 142 kDa. Proton NMR showed that 60% of the PEO chain ends were functionalized, translating to one maleimide per every 19 MMA backbone segments. Using this composition and the model by Irvine et al. [10] a theoretical density of $\rho_M \approx$ 88,000 maleimides/μm^2 at the film/water interface can be estimated for a film of 100% malemide-modified comb:

$$\rho_M \approx \frac{\phi_M s_M}{\pi R_{g,2D}^2} \qquad (3.1)$$

where ϕ_M is the mass fraction of maleimide-modified polymer in the blend, s_M is the average number of malimide-modified side chains per comb molecule (s_M = 64), and

$R_{g,2D}$ is the average in-plane R_g for chains confined at the comb/water interface. Assuming the polymer backbone is confined at the interface, $R_{g,2D}$ can be calculated [10]:

$$R_{g,2D}^2 \approx aC\sqrt{\frac{N}{\phi_{bb}^s}} \qquad (3.2)$$

In this expression, a is the backbone segment size (6.4Å), C is a constant (~1.45 [30]) and ϕ_{bb}^s is the volume fraction of backbone segments at the surface (ϕ_{bb}^s=0.67) determined from the self-consistent field calculations of Irvine et al.[10]. For the system observed, N = 960, resulting in $R_{g,2D}$ = 18.6 nm.

3.2.3 Surface Preparation

2.5 cm square pieces of silicon wafer (University Wafers) were cleaned overnight in Chromerge, thoroughly rinsed in DI water, treated with a 1% aqueous solution of Gelest Siliclad for 30 seconds and cured at 100°C for 5 minutes. Blends of PMPI-modified and unmodified comb polymers were spin cast from 1 wt% solution in toluene onto Siliclad-treated wafers. To enable detection of individual maleimide-bearing chains, blends used in this study contained 0.5-10% PMPI-modified comb. After spin casting, films were annealed under vacuum at 65°C (20 degrees above the glass transition) overnight. Dry film thickness was determined by ellipsometry (Gartner L125A) to be ~35 nm (~3R_g). This thickness was chosen so as to be thin enough for TEM observation, but thicker than the coil diameter, to avoid film thickness effects on chain conformation [22, 23].

3.2.4 Nanoparticle Coupling

Nanoparticle coupling was performed with films immersed in aqueous solution. In a water-based environment, PMMA-*g*-PEO molecules at the film surface are expected to exhibit quasi-2D conformations, with the insoluble PMMA backbone pinned at the interface and PEO side chains extending into solution [10, 14, 15], thus becoming fully accessible to react with nanoparticles. Maleimide end groups of PMPI-modified chains will be present both at the surface and within the film; however, only those at the surface appear accessible for nanoparticle coupling, as described below. PMPI-modified chain ends were first reacted with 1,2 ethane dithiol (10 μM in buffer solution) for two hours at ambient temperature to produce thiol end groups. Monomaleimido gold nanoparticles (1.4 nm diameter, Nanoprobes) were subsequently coupled to thiol chain ends in a 10 μM aqueous buffer solution for 4 hours (Figure 3.2). A 10-fold excess of tris(2-carboxyethyl)phosphine was added to minimize formation of disulfide bonds.

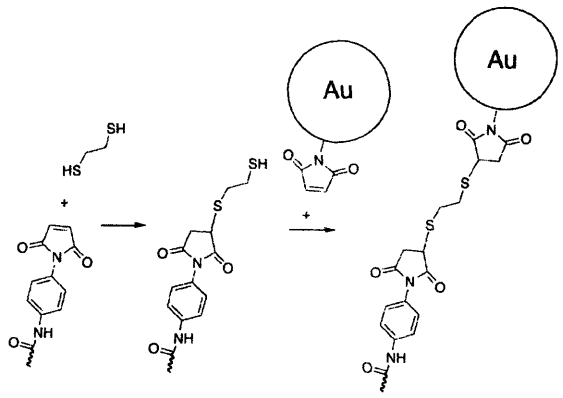

Figure 3.2 Schematic illustration of coupling chemistry employed to covalently link PMPI-modified comb copolymers to maleimide-bearing nanoparticles using 1,2 ethane dithiol as a linker.

Because each Au nanoparticle is stabilized by a shell of tris (aryl) phosphine ligands, it can react with thiols only through its single maleimide. Consequently, each gold nanoparticle covalently binds to only one thiol-terminated PEO side chain, tracing the backbone contours of the surface-confined PMMA-*g*-PEO chains modified with PMPI. While changes to backbone conformations due to nanoparticle coupling cannot be ruled out, similar methods to label proteins for TEM imaging did not affect their biological function [31, 32], suggesting minimal disturbance of native chain conformations for the small nanoparticle sizes and mild reaction conditions employed here.

Nanoparticle-coupled surfaces were dried under vacuum, coated with a thin layer of carbon, removed from the silicon using polyacrylic acid [33] and mounted on TEM grids.

3.2.5 TEM Imaging of Polymer Chains

Transmission electron microscopy was performed by graduate researcher Elsa Olivetti. All imaging was performed on a JEOL 2010 TEM at 200 kV and 400kx magnification. TEM images were recorded on Kodak film, and then scanned at high resolution (Figure 3.3).

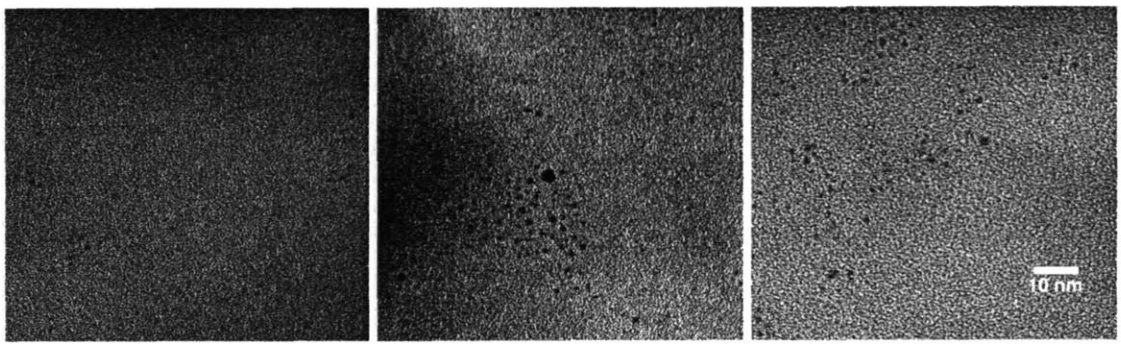

Figure 3.3 Sample TEM images showing gold nanoparticle clusters on blends of 10% active PMMA-*g*-PEO_{10}

Particles on the scanned images were identified using Scion Image software and their positions converted to *x,y* coordinate pairs (Figure 3.4).

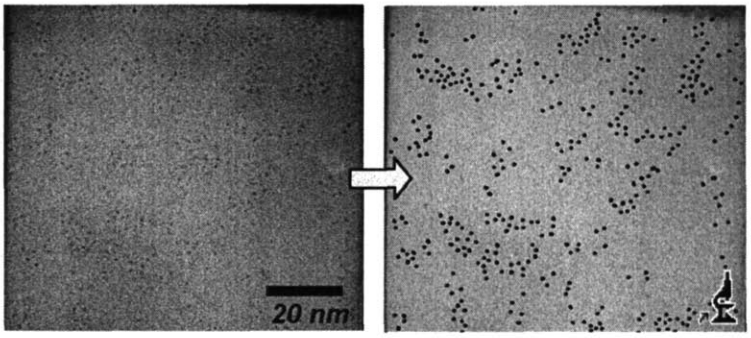

Figure 3.4 Particles on TEM images (left) are identified by Scion Image (right).

3.2.6 Stereoimaging

Stereoimaging was used to verify that particles observed by TEM were located on the same plane. Each surface was imaged first with no tilt; the sample holder was then rotated 7° and the sample was imaged again. The position of each particle in the image was recorded for each image, and a z height relative to an arbitrary point was calculated using elementary geometry shown in Figure 3.5.

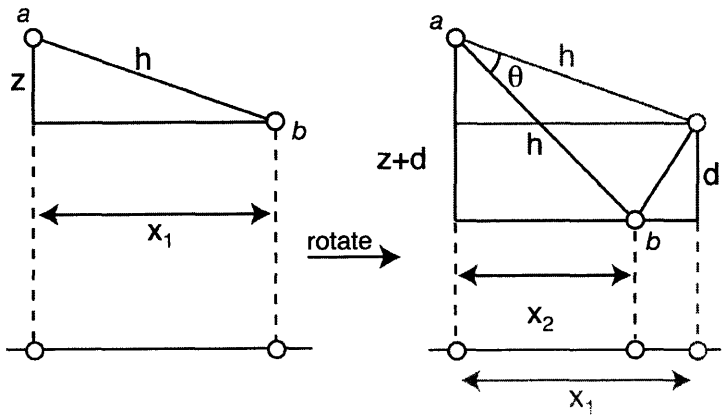

Figure 3.5 Geometry of images used in stereoimaging.

Here, x_1 and x_2 are the observed distances between the particle (*a*) and a reference point (*b*), *z* is the vertical position of the particle relative to the reference point, *d* is the vertical displacement of the particle following rotation and *h* is the 3D distance between *a* and *b*. For this geometry, three right-triangles can be formed, resulting in the equations:

$$\begin{aligned} z^2 + x_1^2 &= h^2 \\ (z+d)^2 + x_2^2 &= h^2 \\ (x_1 - x_2)^2 + d^2 &= 4h^2 \sin^2 \tfrac{\theta}{2} \end{aligned} \qquad (3.3)$$

Solving these equations yields the distance along the *z* axis from the reference point to the particle in question. To determine co-planarity, the resulting data was fit to a plane $z=ax+by+c$. Deviations from this plane were calculated and used to determine a root-mean square (RMS) deviation for each sample (Figure 3.6).

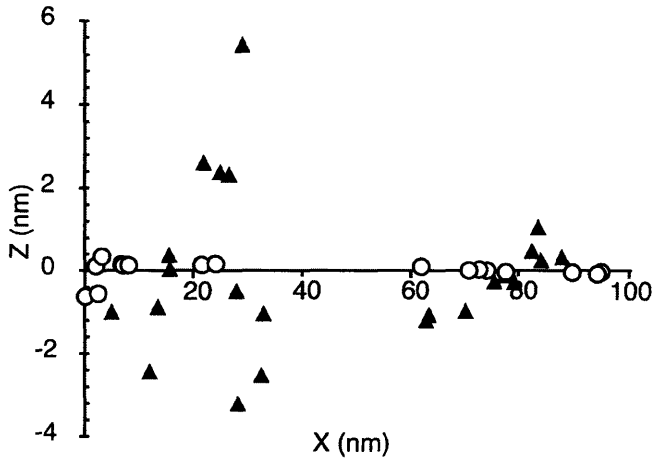

Figure 3.6 Distribution of observed nanoparticle heights (Z) as determined by stereoimaging for 2D (open circles) and 3D (triangles) samples.

As a control, a sample was prepared in which gold nanoparticles were coupled to the polymer in solution prior to spin coating. Because coupling was performed in solution, gold particles in the resulting film sample should be distributed three-dimensionally throughout the sample, rather than confined to the polymer surface.

Surfaces made using both approaches were imaged. Calculated cross-sections showing the spatial distribution of particles for surface-coupled (2D) and solution-coupled (3D) samples are given in Figure 3.6. Following this approach, an RMS deviation of 0.2 nm was found for the surface-coupled sample, and 3.0 nm for the solution-coupled sample, indicating that gold nanoparticles coupled to the film surface are located within a single plane.

3.2.7 Monte Carlo Simulation

Monte Carlo lattice simulations of polymers confined to two dimensions were conducted to better understand the effects of molecular weight on chain behavior. The simulation employed a 100x100 2D square lattice, filled entirely with polymer chains, following the methods of Reiter [19] and Mansfield [34]. One simulated segment was taken to be 23 backbone segments, in keeping with the estimated number of segments between successive gold nanoparticles, as described below. At each time step, a chain end was chosen at random and joined with a neighboring chain. The superchain thus formed was then broken in two at a randomly chosen segment, subject to the constraint that two linear chains were created (Figure 3.7). Because the number of chain ends is preserved, the probability of rearrangement for any given chain end is approximately constant.

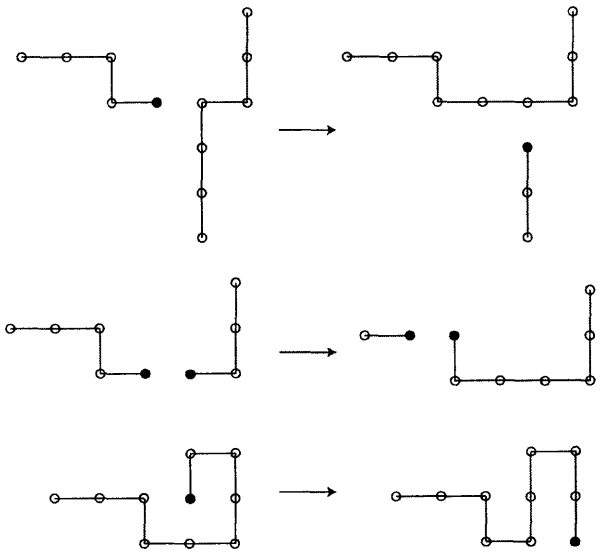

Figure 3.7 Sample Monte Carlo steps.

Following each attempted chain rearrangement, the distribution of chain lengths was calculated and compared with that determined for our polymer by GPC-LS. A

metropolis-like procedure was then used to direct the simulated distribution towards the measured distribution. If rearrangement brought the two distributions into closer agreement, it was accepted. Otherwise, it was accepted with a probability determined by their difference:

$$P = e^{-\beta \sum_N \left(\phi_N - \hat{\phi}_N\right)^2} \qquad (3.4)$$

where $\hat{\phi}_N$ is the observed fraction of chains of length N and ϕ_N is the simulated fraction of chains of the same length. For each simulation, β was initially set small enough that all rearrangements were accepted. The system was allowed to equilibrate until $<R_g^2>$ reached a steady value, β was then doubled and the system was again allowed to equilibrate. This procedure was repeated until suitable agreement between distributions was achieved. Results of several simulations were pooled to compute the value of ν from the R_g^2 values of individual chains.

3.3 Results and Discussion

3.3.1 TEM Observation of Ligand Clusters

Figure 3.3 shows characteristic TEM images of gold nanoparticles coupled to a 10 wt% blend film of PMPI-modified comb with unmodified comb. Individual nanoparticles are clearly observed at this magnification and appear to be arranged into clusters. No close-packed or overlapping particle formations are present. Moreover, the number of coupled particles scales monotonically with the fraction of PMPI-modified comb

copolymer in the blend film (Figure 3.8), indicating that clustering of particles is caused by attachment to individual polymer chains, rather than by aggregation of adsorbed nanoparticles.

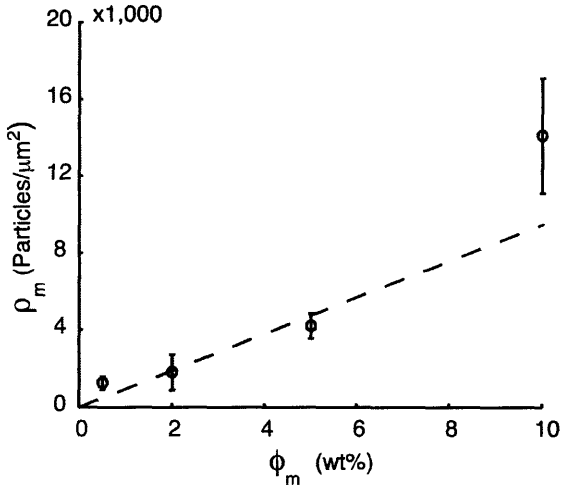

Figure 3.8 Number of gold nanoparticles observed per field as a function of weight percent PMPI-modified comb in blend film. The dashed line indicates the theoretical number of particles based on the polymer composition from equation 3.1. Error bars represent one standard deviation.

Several findings support the premise that nanoparticle coupling is confined to surface-localized molecules. First, the observed nanoparticle densities are consistent with theoretical predictions for surface densities from equation 3.1 based on film composition (dashed line in Figure 3.8) [10]. Particle densities on the order of $\sim 10^4/\mu m^2$ are obtained for a 10% blend film. By comparison, the total number of reactive groups for a 35 nm thick, 10% blend is $\sim 10^6/\mu m^2$, two orders of magnitude larger than the observed number, suggesting that little nanoparticle coupling occurred in the film interior. Secondly, the absence of overlapping particles in the TEM images (> 100 images taken) is consistent

with nanoparticles binding only at the surface. Finally, stereoimaging of a representative blend film showed particles to lie in the same plane to within ±0.2 nm (section 3.2.5).

3.3.2 Statistical Analysis of Clustering

Because of the relatively small number of particles available on each TEM micrograph, pair-correlation functions calculated directly from the TEM data produced broad, diffuse rings that made it difficult to obtain length scale data. To obtain a statistical measurement of clustering, we employ a method similar to that described by Diggle [35]. For each sample, the distance y_i from each of m measured particles to their nearest neighbor was measured and their values were tabulated (Figure 3.9).

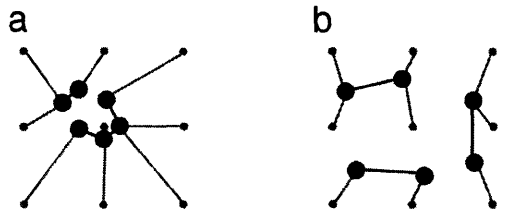

Figure 3.9 Statistical analysis of spatial clustering. On a clustered surface (a) the distance between nearest neighbor particles (black) will be smaller than the distance from a randomly selected point (grey) to the nearest particle. In a non-clustered system (b), by contrast, these distances will be similar.

An equal number (m) of points was then selected at random and the distance x_i from each of these points to the nearest observed particle was also tabulated. The ratio h of the sum of squares of each of these values provides a measure of the degree to which a system of particles is clustered:

$$h = \frac{\sum_{i=1}^{m} x_i^2}{\sum_{i=1}^{m} y_i^2} \sim F_{2m,2m} \tag{3.5}$$

x_i = Distance from each of m random points the nearest particle

y_i = Distance from each particle to its nearest neighbor

The ratio of these values is distributed according to an F distribution. In an unclustered system, the distance from nearest neighbor measurements will be indistinguishable from the distance to a random point, and we can expect that h will approach unity. As the system becomes increasingly clustered, however, this value will become large: the average distance between neighboring particles gets small, while the average distance to an arbitrarily chosen point remains unchanged. Comparing this value to an F distribution then provides a means of statistically distinguishing between clustered and non-clustered surfaces.

A summary of h values determined for each set of observational conditions is provided in Table 3.1. Periodic boundary conditions were employed to reduce edge effects when calculating nearest neighbor distances. Similar measurements using only particles near the center of the image produced nearly identical results, suggesting that edge effects did not play a significant role in the overall calculation. In almost all of the observed fields, substantial deviations from randomness were observed at the $p \leq 0.05$ level. These results provide strong evidence of clustering.

Table 3.1 Statistical analysis of gold nanoparticle clustering:

	Wt% Active Polymer			
	10	5	2	0.5
Fields Observed	8	10	15	24
Number Statistically Clustered	8	7	15	21

The length scale of clustering can be quantified following the quadrant count method [36]. This method determines the length scale of clustering by sub-dividing each TEM field into progressively smaller and smaller portions, determining at each step whether the number of particles in each sub-divided field deviates statistically from the number expected based on the overall particle density (Figure 3.10).

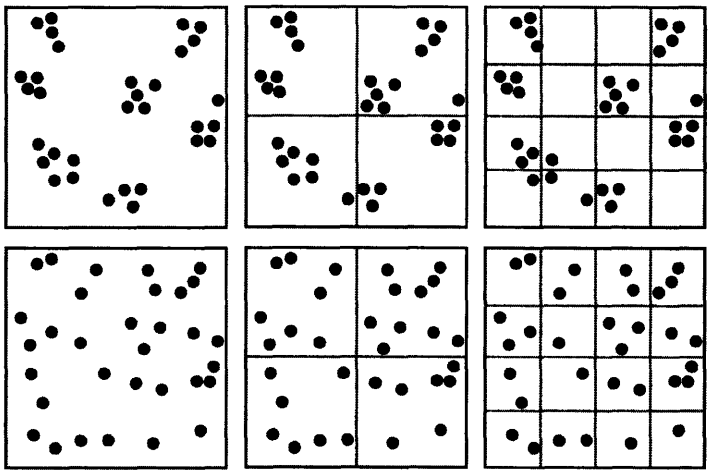

Figure 3.10 The quadrant count method: if particles are clustered (top), as the field is increasingly sub-divided, the number density of particles per division deviates more significantly from the mean particle density of the image as a whole. The same does not hold true for non-clustered particles (bottom).

A calculation proceeds as follows: the number of particles in an image is first calculated and used to determine an average number density of particles for the entire field ($\bar{n}$). The image is then divided into m equal parts, and the number density of particles (n) is

determined for each part. The sum of the squares of their normalized deviations (X^2) from the original field can be determined. Because this is the sum of m squared standardized normal random variables, a χ^2 distribution can be used to determine the degree to which the observed number of particles deviates from that expected from the average observed particle density.

$$X^2 = \sum_{i=1}^{m} \frac{(n_i - \overline{n})^2}{\overline{n}} \sim \chi^2_{m-1} \tag{3.6}$$

This calculation is then repeated, increasing the number of times each image is sub-divided, and the X statistic is calculated for each until a maximum deviation is observed. The size of sub-division where this deviation is a maximum corresponds to the length scale on which the particles are least randomly distributed, which approximately corresponds to the cluster size. While this method does not provide a strict cluster radius, it provides a quantitative length scale at which the particles are most clustered.

A plot of X^2 -χ^2 for $p=0.01$ on 2 wt% active polymer surfaces is provided in Figure 3.11. Data from each image has been normalized such that the maximum value from each image is 1. This plot shows cumulative data for all fields observed. As the observed length scale (l) approaches the size of a whole image, deviation from the average particle density becomes small. As l becomes smaller, however, deviation increases, approaching a maximum around what we assume to be the average cluster size and then diminishing once the sampled area becomes smaller than a single cluster. Statistically significant deviations are observed on lengths ranging from 10-40 nm, with a few scattered points as high as 60 nm. No systematic spatial correlations on a length scale larger than these average chain dimensions are observed, suggesting that nanoparticle-decorated chains are randomly distributed.

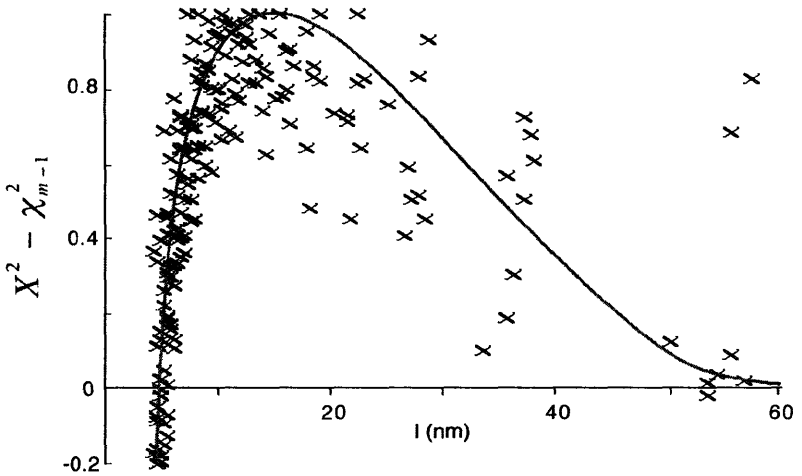

Figure 3.11 Statistical deviation from average observed number of particles for 2 wt% active polymer surfaces using the standard quadrant count method. Higher values of $X^2 - \chi^2_{m-1}$ indicate an increasing degree of clustering.

By this method, we find an average cluster size of 14.0±3.6 nm. This is consistent with qualitative observations, where some clusters appear to be only a few nm in size, while others are many tens of nanometers. The broadness of the distribution reflects the broadness of the distribution of the underlying polymer. With a PDI of 3.2 the smallest chains will contain only a few ligands and be several nm in diameter, while the largest chains will contain hundreds of ligands and may be nearly a hundred nanometers in diameter. Furthermore, the breadth of the distribution would result in broad peaks in an observed pair-correlation function, which is also consistent with our observations.

To demonstrate that the measured values are not an artifact of the chosen geometry, a similar analytical method was employed using a different geometry: a circle of a given diameter was chosen arbitrarily on the field such that it did not touch the edges, and the number density of observed particles within that circle was tabulated (3.12).

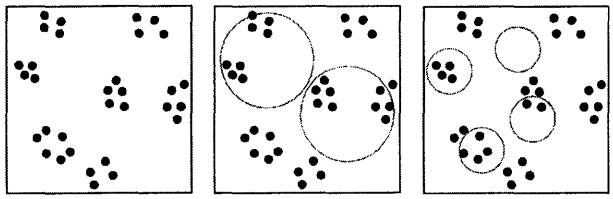

Figure 3.12 The modified quadrant count method.

The measurement was repeated multiple times and a sum similar to that for the quadrant method was observed. As with the quadrant count method, this method was repeated for progressively smaller circles. Because this method permits overlap between sampled areas, the assumption that each successive measurement is independent breaks down, and so the resulting variable is not strictly determined by a chi-squared distribution. For circles small enough that overlap is rare, however, this difference should not be substantial. Repeating the calculation using this approach produced results similar to those found using the standard quadrant count method (Figure 3.13). An average size of 18.6±3.8 nm is obtained, which is not statistically different ($p=0.01$) from the value of 14.0±3.6 obtained using the standard quadrant count method. This suggests that the observed value is not an artifact of the geometry employed, but a true characteristic length of the system.

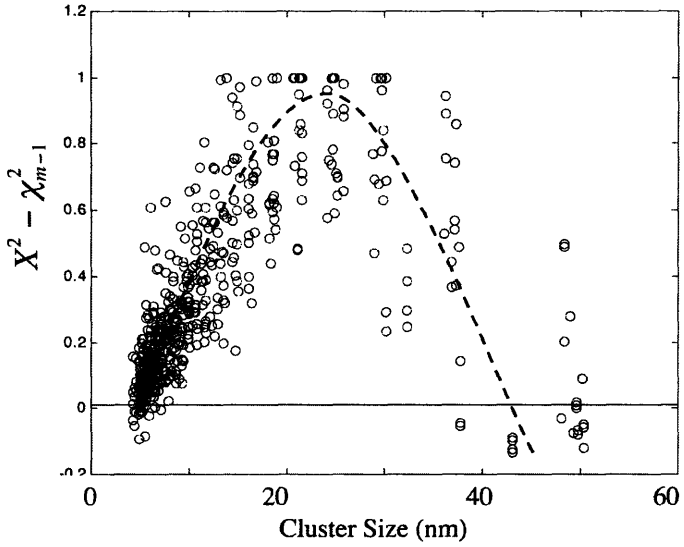

Figure 3.13 Statistical deviation from average observed number of particles for 2 wt% active polymer surfaces using the modified quadrant count method.

The characteristic length obtained by both quadrant count methods is comparable to the R_g of 18.6 nm estimated in Section 3.2.2, indicating that TEM observations and statistical analysis of clustering supports the structure predicted by Irvine et al. [10]. The presence of discrete clusters should be unique to the 2D-quasi-confined state, which provides further evidence that this polymer is confined to the bulk-water interface. Even in the presence of modest chain interpenetration, chains appear to be segregated to enough of an extent that discrete clusters are still apparent.

3.3.3 Reconstruction of Polymer Chain Trajectories

Because a relatively high fraction of PEO side chains are labeled with gold nanoparticles, it was possible to re-construct the trajectories of the backbone of gold-labeled chains. Polymer chain trajectories were formed from coordinate pair data by

linking successive nearest neighbor (n.n.) particles, subject to the constraint that no particle-particle bond could be longer than a cut-off distance chosen to be 5 nm. The average n.n. distance between particles was found to be 1.6 nm, slightly larger than the Kuhn length of PMMA (1.53 nm) [37]. In cases where more than one n.n. particle was found, the particle that ultimately produced the shortest overall contour length was used to complete the chain trajectory. Variation of the cut-off distance and the contour length restriction produced little effect on the resulting distribution of chain lengths. Example chain trajectories obtained from Figure 3.14a are shown in Figure 3.14b.

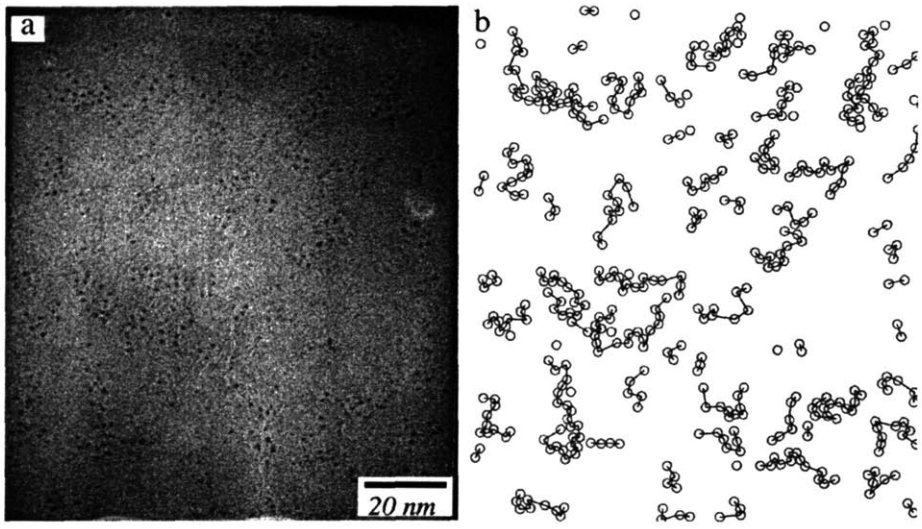

Figure 3.14 Observed images of 2D confined polymers (a) and reconstructed polymer chains (b) determined from this image.

Figure 3.15 compares the normalized distribution of chain lengths measured by gel permeation chromatography with in-line light scattering (GPC-LS) to that determined from the TEM images. The normalized GPC distribution was computed from the refractive index signal divided by the number of backbone segments. The number of backbone segments in the GPC-LS curve was taken to be the absolute molecular weight

determined by light scattering, multiplied by the weight fraction of MMA backbone segments (0.68) obtained by NMR, divided by the molecular weight of MMA (100 g/mol). The number of backbone segments for chains observed in the TEM was calculated by multiplying the number of gold particles in the chain by the factor 23, derived from the number of backbone segments per activated side chain (~19), adjusted by the approximate coupling efficiency (80%) determined from Figure 3.8. Figure 3.15 shows generally good agreement between the two distributions, with greater discrepancy observed for smaller chains (<50 segments or 2 nanoparticles) due to the increased uncertainty in chain length. The results provide additional evidence of the quasi-2D confined nature of chains at the surface, and interestingly suggest that no preferential surface localization of lower molecular weight chains occurred in this polydisperse system [38-40].

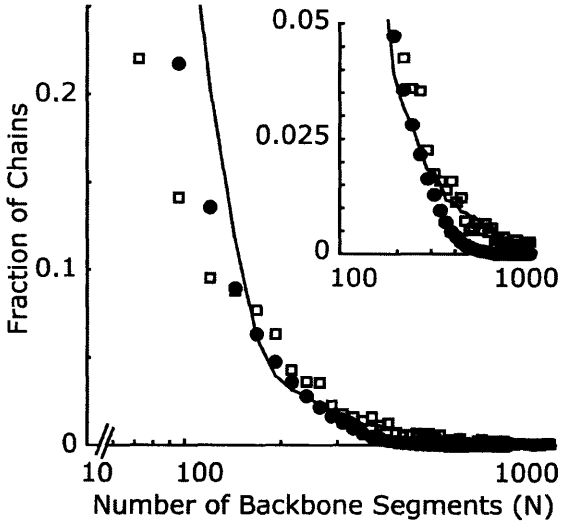

Figure 3.15 Comparison between the distributions of chain lengths determined from GPC-LS (□) and TEM (●) images. Solid line shows fitted distribution from MC simulation.

3.3.4 Scaling Behavior of 2D Confined Polydisperse Polymers

The broad molecular weight distribution of our comb polymer provided a wide range of polymer chain lengths, allowing determination of the scaling of radius of gyration with chain length by calculating R_g^2 values from the positions of the tethered nanoparticles:

$$R_g^2(k) = \frac{1}{2N_p^2} \sum_{j=1}^{N_p} \sum_{i=1}^{N_p} \left(\vec{r}_i - \vec{r}_j\right)^2 \qquad (3.7)$$

In this expression, $\vec{r}_i$ is the position vector of the ith particle and N_p is the total number of gold nanoparticles in chain k. These data gave a value for $R_g = \langle R_g^2 \rangle^{1/2}$ of 9.2 nm for the system. Figure 3.16 shows a plot of $\langle R_g^2(N) \rangle$ versus number of backbone segments $N = 23N_p$. Each data point represents at least 100 chains. An exponential fit to the data finds $\nu = 0.69 \pm 0.02$. This observed value falls between the values predicted for 2D swollen chains ($\nu = 0.75$) and 2D monodisperse polymer melts ($\nu = 0.5$).

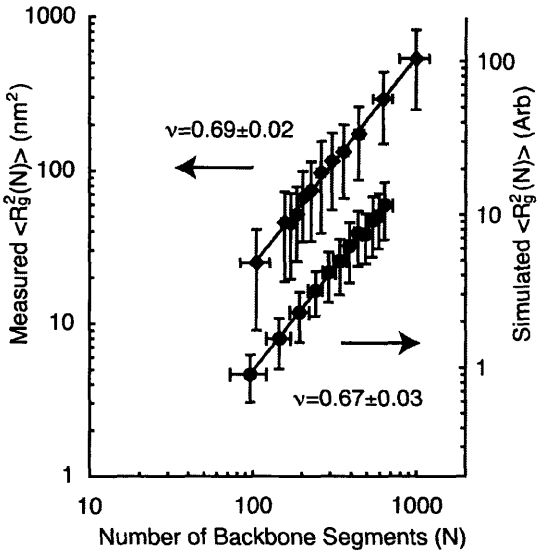

Figure 3.16 Scaling of $<R_g^2(N)>$ with number of polymer backbone segments N for observed and simulated 2D polymer chains. Solid line shows best fit.

Deviation from melt-like behavior may reflect the presence of a large fraction of short chains in our polymer (Figure 3.15), which can act as a good solvent, swelling longer chains [16]. Maier and Rädler qualitatively showed a similar effect in blends of long and short DNA chains confined in 2D [25]. Reiter and coworkers also observed an increase in ν for polydisperse systems in Monte Carlo simulations on a 2D lattice [19]. However, earlier simulations by Mansfield found that ν was independent of polydispersity over a PDI range of 1.2-1.9 [34]. Deviation from 2D melt scaling might also be observed if labeled chains are not strictly confined to 2D. Where some overlap between chains is allowed in a 2D melt, Semenov and Johner obtained $R_g^2 \sim N\ln(N)$ [20]. Alternately, our ν value might reflect behavior intermediate between swollen 2D and swollen 3D chains (ν=0.6). However, the observed close agreement between the GPC

and TEM molecular weight distributions, lack of overlapping particles and stereoimaging analysis all suggest 2D confinement of labeled chains.

3.3.5 Comparison with Monte Carlo Simulations

To compare theoretical values with our observed ν, we performed Monte Carlo simulations using the lattice model of Reiter [19] and Mansfield [34], modified such that the distribution of chain lengths could be refined to match the experimental distribution determined by GPC. When tested using distributions of lower polydispersity (Figure 3.17), this approach gave the result ν=0.56±0.04, in agreement with values reported in ref. [19].

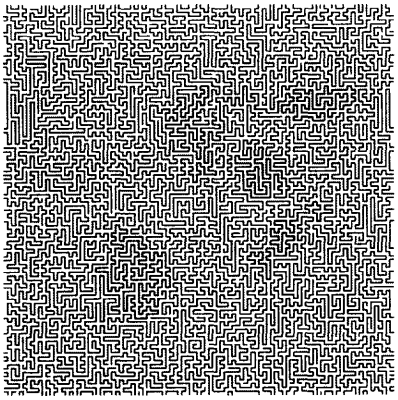

Figure 3.17 Simulated trajectories for a 2D confined system similar to ref. [19]

For a simulated system of chains with a molecular weight distribution fitted to our experimentally observed system, ν=0.67±0.03, in good agreement with the scaling exponent obtained from TEM analysis (Figure 3.11). Figure 3.10 shows the fitted MC chain length distribution (solid line). A sample MC configuration is shown in Figure 3.6c.

The MC results support the notion that polydispersity causes the observed deviation from 2D melt behavior.

3.4 Conclusions

In the work described in this chapter, the backbone conformations of amphiphilic comb copolymers were mapped at a polymer film/water interface. Using nanoparticle labeling, chain trajectories were obtained by TEM and found to be consistent with quasi-2D confinement of the comb molecules at the surface and partial swelling in two dimensions due to polydispersity. 2D Monte Carlo calculations on systems of comparable chain length distribution gave good agreement with the observed experimental scaling of R_g with chain length.

To the author's knowledge, this is the first report of the direct observation of chain conformations at a synthetic polymer film surface. The results further demonstrate that surfaces with a controlled spatial distribution of functional groups can be effectively prepared from mixtures of unmodified and functionalized amphiphilic comb molecules [10]. Such findings are of value in designing bioactive surfaces with nanometer length-scale clusters of peptides or proteins [6, 11, 12, 41]. Application of the model for estimating R_g of polydisperse polymers could be used, for example, to design surfaces with multiple length-scales of structure by blending polymers of different molecular weights and different functional groups.

Control over ligand distribution on this length scale is of importance in biology, where receptor clustering is often a prerequisite for strong cell signaling [10, 12, 42-44]. Cell adhesion, for example, requires not only that cell adhesion receptors (integrins) bind,

but also that these integrins are able to aggregate within the cell membrane to form clusters [7, 44, 45]. Surfaces that facilitate this aggregation by presenting spatially clustered ligands produce stronger cell adhesion than comparable surfaces where there is no spatial clustering [10, 11, 13]. The next chapter describes an alternate approach towards facilitating rearrangement of bound integrins through variation in tether length.

3.5 References

1. Mammen, M.; Choi, S.-K. and Whitesides, G.M. "Polyvalent interactions in biological systems: Implications for design and use of multivalent ligands and inhibitors" *Angewandte Chemie International Edition* **1998**, *37* (20): p. 2754-2794.

2. Dower, S.K.; Delisi, C.; Titus, J.A. and Segal, D.M. "Mechanism of binding of multivalent immune complexes to FC receptors" *Biochemistry* **1981**, *20*: p. 6326 - 6334.

3. Lees, W.J.; Spaltenstein, A.; Kingery-Wood, J.E. and Whitesides, G.M. "Polyacrylamides bearing pendant α-sialoside groups strongly inhibit agglutination of erythrocytes by influenza a virus: Multivalency and steric stabilization of particulate biological systems" *Journal of Medicinal Chemistry* **1994**, *37*: p. 3419-3433.

4. Mammen, M.; Dahmann, G. and Whitesides, G.M. "Effective inhibitors of hemagglutination by influenza virus synthesized from polymers having active ester groups. Insight into mechanism of inhibition" *Journal of Medicinal Chemistry* **1995**, *38*: p. 4179-4190.

5. Hauck, C.R.; Agerer, F.; Muenzner, P. and Schmitter, T. "Cellular adhesion molecules as targets for bacterial infection" *European Journal of Cell Biology* **2006**, *85* (3-4): p. 235.

6. Miyamoto, S.; Akiyama, S.K. and Yamada, K.M. "Synergistic roles for receptor occupancy and aggregation in integrin transmembrane function" *Science* **1995**, *267* (5199): p. 883-885.

7. Hynes, R.O. "Integrins: Bidirectional, allosteric signaling machines" *Cell* **2002**, *110*: p. 673-687.

8. Yauch, R.L.; Felsenfeld, D.P.; Kraeft, S.-K., et al. "Mutational evidence for control of cell adhesion through integrin diffusion/clustering, independent of ligand binding" *J. Exp. Med.* **1997**, *186*: p. 1347-1355.

9. Laplantine, E.; Maurer, P.; Vallar, L., et al. "The integrin β1 subunit cytoplasmic tail forms oligomers: A potential role in β1 integrin clustering" *Biology of the Cell* **2002**, *94* (6): p. 375-387.

10. Irvine, D.J.; Mayes, A.M. and Griffith, L.G. "Nanoscale clustering of RGD peptides at surfaces using comb polymers. 1. Synthesis and characterization of comb thin films" *Biomacromolecules* **2001**, *2*: p. 85-94.

11. Rotter; Maheshwari, G.; Brown, G., et al. "Cell adhesion and motility depend on nanoscale RGD clustering" *Journal of Cell Science* **2000**, *113*: p. 1677-1686.

12. Koo, L.Y.; Irvine, D.J.; Mayes, A.M.; Lauffenburger, D.A. and Griffith, L.G. "Co-regulation of cell adhesion by nanoscale RGD organization and mechanical stimulus" *Journal of Cell Science* **2002**, *115* (7): p. 1424-1433.

13. Danilov, Y.N. and Juliano, R.L. "$(Arg\text{-}Gly\text{-}Asp)_n$-albumin conjugates as a model substratum for integrin-mediated cell adhesion" *Experimental Cell Research* **1989**, *182*: p. 186-196.

14. Irvine, D.J.; Ruzette, A.-V.G.; Mayes, A.M. and Griffith, L.G. "Nanoscale clustering of RGD peptides at surfaces using comb polymers. 2. Surface segregation of comb polymers in polylactide" *Biomacromolecules* **2001**, *2*: p. 545-556.

15. Walton, D.G.; Soo, P.P.; Mayes, A.M., et al. "Creation of stable poly(ethylene oxide) surfaces on poly(methyl methacrylate) using blends of branched and linear polymers" *Macromolecules* **1997**, *30*: p. 6947-6956.

16. De Gennes, P.G. "Scaling concepts in polymer physics" Cornell University Press; Ithaca 1979.

17. Doi, M. "The theory of polymer dynamics" Oxford University Press; New York 1986.

18. Cloizeaux, J. and Jannink, G. "Polymers in solution" Clarendon Press; Oxford 1990.

19. Reiter, J.; Zifferer, G. and Olaj, O.F. "Monte carlo studies of polymer-chain dimensions in the melt in two dimensions" *Macromolecules* **1989**, *22*: p. 3120-3124.

20. Semenov, A.N. and Johner, A. "Theoretical notes on dense polymers in two dimensions" *European Physical Journal E* **2003**, *12*: p. 469-480.

21. Yethiraj, A. "Computer simulation study of two-dimensional polymer solutions" *Macromolecules* **2003**, *36*: p. 5854-5862.

22. Jones, R.L.; Kumar, S.K.; Ho, D.L.; Briber, R.M. and Russell, T.P. "Chain conformation in ultrathin polymer films using small-angle neutron scattering" *Macromolecules* **2001**, *34*: p. 559-567.

23. Jones, R.L.; Kumar, S.K.; Ho, D.L.; Briber, R.M. and Russell, T.P. "Chain conformation in ultrathin polymer films" *Nature* **1999**, *400*: p. 146-149.

24. Maier, B. and Rädler, J.O. "DNA on fluid membranes: A model polymer in two dimensions" *Macromolecules* **2000**, *33*: p. 7185-7194.

25. Maier, B. and Rädler, J.O. "Conformation and self-diffusion of single DNA molecules confined to two dimensions" *Physical Review Letters* **1999**, *82* (9): p. 1911-1914.

26. Wang, X. and Foltz, V.J. "Chain conformation in two-dimensional dense state" *Journal of Chemical Physics* **2004**, *121* (16): p. 8158-8162.

27. Sukhishvili, S.A.; Chen, Y.; Müller, J.D., et al. "Diffusion of a polymer 'pancake'" *Nature* **2000**, *406*: p. 146.

28. Vilanove, R. and Rondelez, F. "Scaling description of two-dimensional chain conformations in polymer monolayers" *Physical Review Letters* **1980**, *45* (18): p. 1502.

29. Gavranovic, G.T.; Deutsch, J.M. and Fuller, G.G. "Two-dimensional melts: Polymer chains at the air-water interface" *Macromolecules* **2005**, *38*: p. 6672-6679.

30. Nelson, P.H.; Hatton, T.A. and Rutledge, G.C. "General reptation and scaling of 2D athermal polymers on close-packed lattices " *J. Chem. Phys.* **1997**, *107* (4): p. 1269-1278.

31. Hainfeld, J.F. "A small gold-conjugated antibody label: Improved resolution for electron microscopy" *Science* **1987**, *236*: p. 450-453.

32. Schwartz, M.P. and Matouschek, A. "The dimensions of the protein import channels in the outer and inner mitochondrial membranes" *Proceedings of the National Academy of Science* **1999**, *96* (23): p. 13086-13090.

33. Robinson, D.G. "Methods of preparation for electron microscopy" Springer-Verlag; New York 1987.

34. Mansfield, M.L. "Monte carlo studies of polymer chain dimensions in the melt" *Journal of Chemical Physics* **1982**, *77*: p. 1554-1559.

35. Diggle, P. "Statistical analysis of spatial point patterns" Oxford University Press; London 1983.

36. Cressie, N.A.C. "Statistics for spatial data" Wiley; New York 1992.

37. Mark, J.E. "Physical properties of polmers handbook" AIP Press; Woodbury, NY 2006.

38. Hong, P.P.; Boerio, F.J. and Smith, S.D. "Effect of annealing time, film thickness, and molecular weight on surface enrichment in blends of polystyrene and deuterated polystyrene" *Macromolecules* **1994**, *27* (2): p. 596-605.

39. Hopkinson, I.; Kiff, F.T.; Richards, R.W., et al. "Investigation of surface enrichment in isotopic mixtures of poly(methy methacrylate)" *Macromolecules* **1995**, *28*: p. 627-635.

40. Schaub, T.F.; Kellogg, G.J.; Mayes, A.M., et al. "Surface modification via chain end segregation in polymer blends" *Macromolecules* **1996**, *29*: p. 3982-3990.

41. Sharma, P.; Varma, R.; Sarasij, R.C., et al. "Nanoscale organization of multiple GPI-anchored proteins in living cell membranes" *Cell* **2004**, *116*: p. 577-589.

42. Hyun, J.H.; Ma, H.W.; Zhang, Z.P.; Beebe, T.P. and Chilkoti, A. "Universal route to cell micropatterning using an amphiphilic comb polymer" *Advanced Materials* **2003**, *15* (7-8): p. 576-579.

43. Nath, N.; Hyun, J.; Ma, H. and Chilkoti, A. "Surface engineering strategies for control of protein and cell interactions" *Surface Science* **2004**, *570* (1-2): p. 98-110.

44. Bray, D.; Levin, M.D. and Morton-Firth, C.J. "Receptor clustering as a cellular mechanism to control sensitivity" *Nature* **1998**, *393*: p. 85-88.

45. Brinkerhoff, C.J. and Linderman, J.J. "Integrin dimerization and ligand organization: Key components in integrin clustering for cell adhesion" *Tissue Engineering* **2005**, *11* (5/6): p. 865-876.

Chapter 4: Effects of PEO Tether Length on Cell Attachment

4.1 Introduction

Apart from the two-dimensional spatial organization of ligands, the bioactivity of tethered ligands is also determined by the structure of the PEO brush on which they are displayed. Just as ligand clustering may enhance cell attachment by facilitating formation of focal adhesions, polymer brushes formed using PMMA-*g*-PEO can be used to modulate integrin-ligand binding, providing an additional tool for design of bioactive surfaces.

Previous research has indicated that sparsely grafted PEO surfaces do not provide substantial protein adsorption resistance [1-4]. Spacing between adjacent PEO chains must be small enough relative to the overall chain length such that adjacent chains may impinge upon one another [5]. The resulting repulsion between chains forces them to extend from the surface into solution [6, 7]. Protein resistance of these surfaces is attributed to a combination of entropically unfavorable compression and expulsion of water from the resulting PEO brush. Extending the length of the chains beyond what is needed to produce a dense brush has been demonstrated to improve overall protein resistance [3], while reduction of chain length beneath this point renders the surface susceptible to protein adsorption [4, 8].

Less is known about the overall effects of tether length on bioactivity of tethered ligands. Previous research using polyglycine tethers by Beer and coworkers has indicated that a minimum chain length is required in order for a tethered ligand to reach a binding

site within an integrin [9]. Other studies by Wong and coworkers using PEG-based lipid bilayers has indicated that extension of tether length can further enhance ligand binding by extending the spatial range over which the receptor can bind the ligand [10, 11]. In addition, because cells are able to reorganize bound ligands [12], longer tethers may facilitate formation of focal adhesions by permitting cells to reorganize bound adhesion peptides into clusters.

In addition to enhancement in signaling through ligand rearrangement, modification of brush structure may be used to modulate ligand availability. Because not all chains are used to tether ligands, PEO chains in these brushes can be divided into two types, according to function: inert chains that inhibit protein adsorption, and active chains, that tether biologically active molecules. Adjusting the length of each chain independently can be used to selectively mask or expose tethered biomolecules. Using inert chains that are short relative to the length of active chains, for example, forces the ends of longer chains to the surface [7, 13-17], potentially making compounds tethered to the ends of these chains more readily available for binding. This effect has been observed by Kim and coworkers in avidin-biotin binding in lipid monolayers [18]. Use of inert chains that are longer than active chains, by contrast, may mask active groups, reducing their bioactivity, as has been observed by Mrksich and coworkers in cell adhesion to SAM's [19].

To better understand the effects of tether length and brush structure on bioactivity, this chapter examines cell attachment and spreading to tethered adhesion peptides (PHSRN-K-GRGDSP) on PEO brush surfaces with different brush lengths and to brushes with stratified chain ends. We first examine the effects of overall tether length on cell

attachment by preparing PMMA-*g*-PEO films with PEO side chains of 10 or 22 ethylene oxide segments. Adhesion peptides were coupled to these films and cell attachment was assessed by measuring cell spreading and through immunochemical staining. Spatial organization of integrin-bound peptides was further examined using fluorescence resonance energy transfer (FRET) measurements. In addition, the effects of a bimodal length distribution of PEO chains in the brush layer was investigated by examining cell attachment and spreading on surfaces where active chains were either shorter or longer than inert chains.

4.2 Experimental Methods

4.2.1 Materials

Ethanedithiol, triisopropylsilane, Triton X-100 and N,N'-diisopropylethylamine (DIPEA) were obtained from Aldrich Chemical Co. 9-Fluorenylmethyloxycarbonyl (FMOC) protected amino acids, NovaSyn TGA resin, N-hydroxybenzotriazole (HOBt), Tris(2-carboxyethyl)phosphine (TCEP) and benzotriazole-1-yl-oxy-tris-pyrrolidino-phosphonium hexafluorophosphate (PyBOP) were purchased from NovaBiochem. Iodobeads were purchased from Pierce. $Na^{125}I$ was obtained from Perkin Elmer. All chemicals were reagent grade and used as supplied unless otherwise noted.

4.2.2 Peptide Synthesis

The PHSRN-K-GRGDSP peptide was prepared following the method of Ufret and Griffith [20]. The linear portion PHSRNGGGK(Mtt)GGRGDSPY was synthesized on

NovaSyn TGR resin using an Advanced Chem Tech 396 Ω peptide synthesizer following standard 9-fluorenylmethyloxycarbonyl (FMOC) peptide synthesis methods [21]. DIPEA was used as an activating agent. PyBOP and HOBt were used to suppress racemization. The methoxytrityl (Mtt) protecting group of the lysine was subsequently removed using 1% trifluoroacetic acid (TFA), to yield a free amine. The GGC stem was then coupled to this amine using FMOC chemistry to obtain the Y-shaped peptide PHSRNGGGK(GGC)GGRGDSPY (also referred to herein as PHSRN-K-GRGDSP). The resulting peptide was cleaved from the resin using TFA:triisopropylsilane: H_2O:ethanedithiol (92.5:2.5:2.5:2.5) and reprecipitated in cold ether several times. The peptide was then lyophilized and subsequently purified using a YMC AQ1S05 reverse phase column on a Waters Breeze HPLC system, running acetonitrile and water with 0.1% TFA as eluents (Figure 4.1).

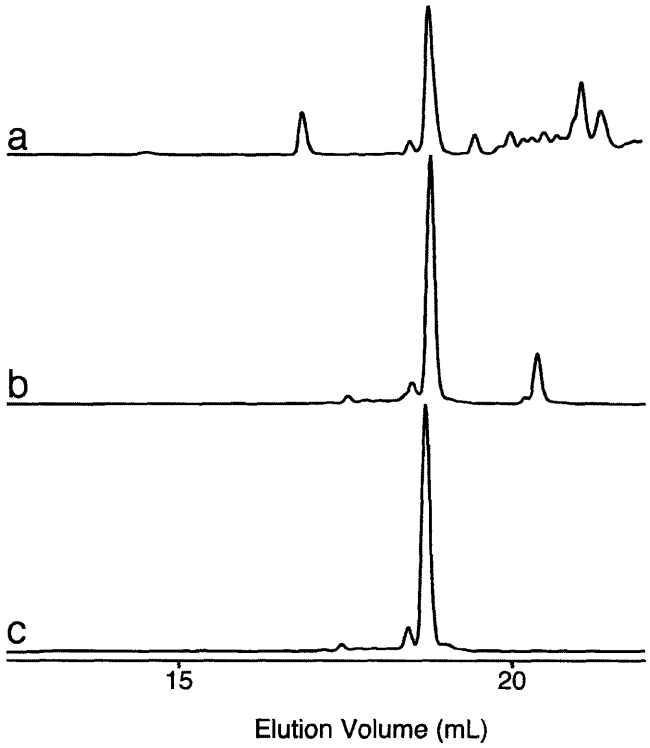

Figure 4.1 HPLC chromatograms of PHSRN-K-GRGDSP (a) Crude product (b) product following HPLC purification. The peak at ~22 minutes corresponds to a dimer that can be readily converted to a monomer using TCEP (c).

Composition was verified by mass spectrometry (Agilent). PHSRN-K-GRGDSP peptides used in radiolabeling studies were iodonated following the iodobead method [22] and purified on Sep-Pack C-18 columns (Waters).

4.2.3 Coverslip Preperation

Glass coverslips were soaked overnight in Chromerge, rinsed with deionized water, treated for 30 seconds with a 2% aqueous solution of Siliclad, rinsed again with deionized water and finally cured in an oven at 100 °C for five minutes. Surface

treatment with siliclad was verified by observing an increase in receding contact angle from 16° to 68°.

4.2.4 Spin Coating

Films of PMPI-coupled PMMA-*g*-PEO were spin coated onto the treated coverslips from 1 wt% solution in toluene. Thickness was determined by ellipsometry (Gartner) on silicon wafers similarly treated. Films were annealed at 65°C (>20° above T_g) in vacuum overnight prior to further use. Surface uniformity was verified by optical microscopy, which showed no significant defects.

4.2.5 Peptide Coupling

Peptide was coupled to the polymer by exposing the films to a PBS solution containing PHSRNGGGK(GGC)GGRGDSPY peptide and 10 μM of TCEP at pH 7.5 for two hours, to effect the coupling between the maleimide group on PMPI-activated chains and the thiol group on the GGC stem of the peptide. Peptide coupling concentrations were adjusted in the range of 1-4 μM to achieve comparable peptide densities (~2,500 peptides/μm^2) on brushes of varying active and inert chain lengths (Table 4.1). Following coupling, surfaces were rinsed twice with PBS and once with deionized water.

Table 4.1 Surface concentrations of peptides used for studies on homogeneous brushes composed entirely of active polymer, and blend brushes composed of 25 wt% active polymer with side chains of n_a EO segments and 75 wt% inert polymer having side chains of n_i EO segments.

Composition	n_a	n_i	Peptides/$10^{-3}\mu m^2$
Homogeneous			
	10	-	2.89±0.17
	22	-	2.11±0.88
Blend			
	10	22	1.77±0.46
	22	10	2.56±0.81
	10	10	2.85±0.59
	22	22	2.36±0.52

4.2.6 Determination of Surface Peptide Concentration

Surface concentration of peptide was determined using ^{125}I labeled peptides. Background arising from adsorbed, uncoupled peptide was measured from a film of PMMA-*g*-PEO not activated with PMPI. Radiolabeling measurements on polymer films of different thickness indicated that the peptide was able to react with maleimide groups buried within the film as well as those at the surface. To estimate the peptide surface coverage, total peptide concentrations were determined for several films of different thickness, and the data extrapolated to zero thickness (Figure 4.2).

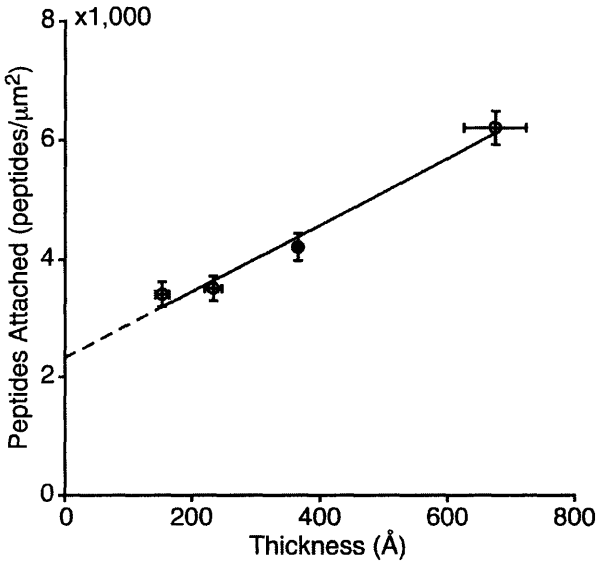

Figure 4.2 Variation in peptide density with PMMA-*g*-PEO film thickness observed by radiolabeling.

4.2.7 Substrates for FRET measurements

Alexa488 and Alexa546 chromophores used in FRET measurements were attached by reacting a 100 μM solution of the NHS ester of each chromophore with the N-terminus of PEO-tethered peptides in 0.1M sodium bicarbonate (pH 8.5) for four hours, followed by rinsing twice with PBS and once with deionized water [23]. The extent of peptide coupling was determined by observing the intensity of each chromophore in the fluorescence microscope and comparing it to standards of known concentration. Results are given in Table 4.2.

Table 4.2 Surface concentration and fraction of total peptides coupled to Alexa-488 and Alexa-546 on polymers having side chains of *n* EO segments used in FRET measurements.

Chromaphore	*n*	Molec./$10^{-3}\mu m^2$	Frac. Coupled
Alexa-488			
	10	1.20±0.15	0.41
	22	1.00±0.14	0.47
Alexa-546			
	10	0.730±0.20	0.25
	22	0.660±0.70	0.31

4.2.8 Cell Culture

All surfaces were sterilized for 20 minutes with UV light prior to use in cell culture, except surfaces for FRET experiments, which were prepared in a sterile cell culture hood. Cell culture media consisted of Modified Eagles' Medium-a supplemented with 7.5% fetal bovine serum, 1% non-essential amino acids, 1% sodium pyruvate (100 mM), 1% L-glutamine (200 mM), 1% penicillin (10,000 U/mL), 1% streptomycin (10 mg/mL) and 35 mg/ml Geneticin G418. Confluent WTNR6 fibroblast cells, passage 10-15 were detached from tissue culture plates using trypsin and suspended in media. The concentration of cells was determined using a Coulter Counter (Beckmen) and the suspension diluted to 10,000 cells per ml with media. Two ml were then added to each well of a 12-well plate, containing a polymer-coated coverslip.

4.2.9 Cell Attachment

Cells seeded on each substrate were allowed to attach for 45, 90, 135 or 180 minutes, then fixed with a 3.7% formaldehyde solution in PBS. Cell nuclei were subsequently stained for 15 minutes with 1 μg/ml Hoechst 33258 in PBS, and the surfaces then rinsed twice with PBS. Coverslips were mounted on microscope slides and imaged in a fluorescence microscope (Zeiss Axioskop). Cells were counted using ImageJ software (NIH). PMMA-*g*-PEO control substrates, to which no peptides were coupled, were included in each trial. These substrates showed no cell attachment. Additionally, control surfaces functionalized with branched peptides having the RGD site scrambled to RDG did not support cell attachment (Figure 4.3).

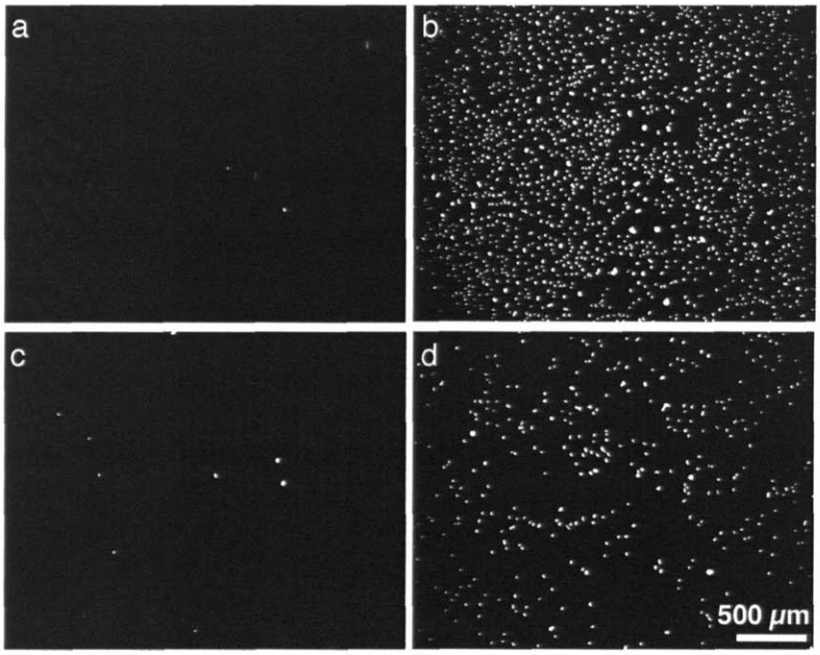

Figure 4.3 Cell attachment to unmodified PMMA-*g*-PEO_{10} (a), RGD-coupled PMMA-*g*-PEO_{10} (b), RDG-coupled PMMA-g-PEO_{10} (c) and glass (d), 24-hours post-seeding in serum containing media.

4.2.10 Cell Spreading

Cells were allowed to attach for 30 minutes, and then washed with PBS supplemented with calcium and magnesium. Fresh media was added and the surfaces were returned to the incubator. Samples were taken at thirty minute intervals and fixed with 3.7% formaldehyde solution in PBS. To determine cell spreading area, cell membranes were stained with 0.5% DiI for 15 minutes in PBS at 36°C and the surfaces then rinsed twice with PBS. Coverslips were mounted on microscope slides and imaged in a fluorescence microscope (Zeiss Axioskop). Images were acquired as 16-bit grayscale TIFF's, and imported into ImageJ software (NIH). The threshold level was adjusted such that only the cell membranes were selected. Dust particles, air bubbles and other debris were manually deselected. Finally, the "Analyze particles" script was run to identify individual cells and measure their area (Figure 4.4).

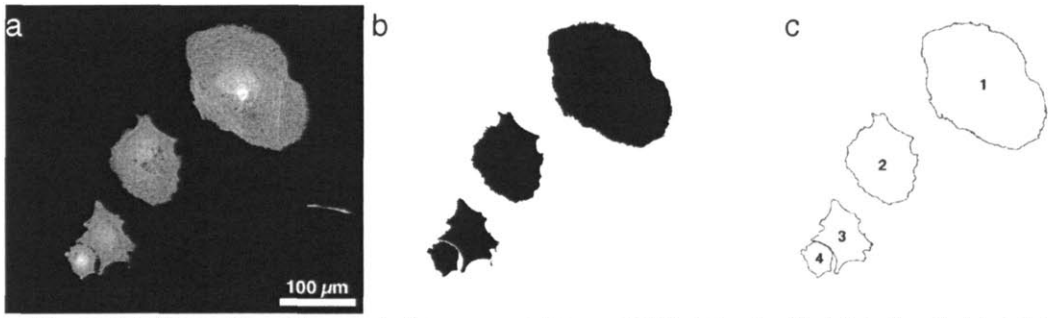

Figure 4.4 Measuring cell area. A fluorescence image of DiI stained cells (a) is thresholded (b) and then analyzed using ImageJ (c).

4.2.11 Immunostaining

Cells were incubated in serum containing media on polymer substrates for 45, 90 or 135 min as described in the *Cell Culture* section above. Adherent cells were fixed with 3.7% formaldehyde in PBS, dried with acetone, permeabilized with 0.1% Triton X-100 in PBS and washed with PBS. Cells were then treated with 50 μg/ml phalloidin-TRITC to stain for actin fibers and a 1:25 dilution of anti-vinculin-FITC conjugate for 40 minutes at room temperature, followed by two additional PBS washes. Coverslips were mounted on microscope slides and imaged with a fluorescence microscope (Zeiss Axioskop).

4.2.12 FRET measurements

FRET measurements were performed on a Zeiss Axioskop equipped with an AxioCam HR digital camera. The FRET filter set consisted of a dichroic mirror (Chroma 505DCLP), FITC excitation filter (Chroma D470/40) and a rhodamine emission filter (Chroma HQ610/75). Spectral bleed-through was corrected for following the method outlined by Gordon et al. [24] by subtracting images obtained using a FITC (Zeiss Filter Set 09) or rhodamine (Zeiss Filter Set 15) filter set, each scaled by an empirically determined bleed-through constant using equation 4.1 below:

$$F^c = F_f - D_f \frac{F_d}{D_d} - A_f \frac{F_a}{A_a} - C_f \qquad (4.1)$$

Variables used in this equation are defined in Table 4.3.

Table 4.3 Variables used in equation 4.1

Symbol	Filter Set	Fluorochromes	Meaning
F_f	FRET	Donor and Acceptor	Raw FRET signal of sample
D_f	Donor	Donor and Acceptor	Donor fluorescence from sample
A_f	Acceptor	Donor and Acceptor	Acceptor fluorescence from sample
F_d	FRET	Donor	Apparent FRET intensity when only donor is present
D_d	Donor	Donor	Donor fluorescence when only the donor is present
F_a	FRET	Acceptor	Apparent FRET intensity when only acceptor is present
A_a	Acceptor	Acceptor	Donor fluorescence when only the acceptor is present
C_f	FRET	None	Cell autofluorescence correction constant

Adapted from Gordon et al. [24]

Contributions to the FRET signal from cell autofluorescence were corrected for by subtracting mean cell intensity measured using the FRET filter from cells on substrates with no chromaphores. The distance (r) between chromaphores was estimated from [24]:

$$E = \frac{R_0^6}{R_0^6 + r^6} \tag{4.2}$$

where E is the resonance transfer energy, determined by multiplying the observed FRET intensity by an empirically determined transfer constant, and R_0 is the Förster radius for Alexa488/Alexa546 (5.5 nm) [25] Negative controls on which there were no chromaphores did not show significant FRET (Figures 4.5 and 4.6).

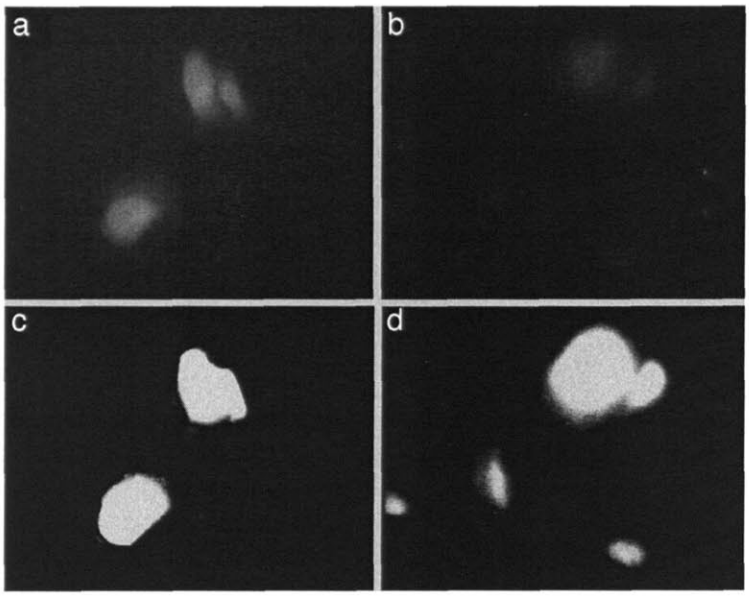

Figure 4.5 Images of cells on surfaces containing both chromaphores (a) and control surfaces containing no chromaphores (b) showing little FRET on surfaces with no chromaphores. Cell areas are shown in C and D based on cell autofluorescence using a DAPI filter (contrast enhanced to show cell area).

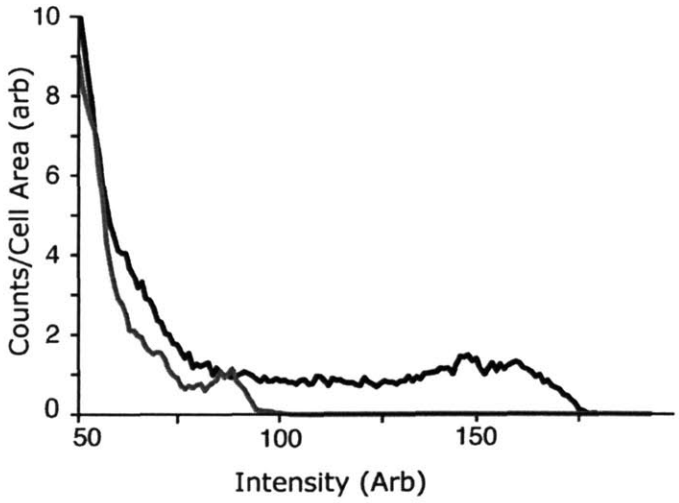

Figure 4.6 Histograms of pixel intensity, normalized for cell for surfaces containing both chromaphores (black) and control surfaces containing no chromaphores (gray).

4.3 Results and Discussion

4.3.1 Cell Attachment to Homogeneous, Monomodal Brushes

To examine effects of PEO tether length on cell attachment behaviors, cell spreading and fluorescence resonance energy transfer (FRET) studies were performed to compare the attachment of fibroblasts on peptide-presenting PMMA-*g*-PEO surfaces of different PEO side chain length. Comb copolymers with 10 and 22 EO units per side chain, corresponding to contour lengths of 6.5 nm and 13 nm, respectively, were synthesized and cast into films. A fraction of the PEO side chains was functionalized with the branched peptide PHSRN-K-GRGDSP. We found that when the film thickness was systematically varied, the amount of peptide covalently bound to the film increased with increasing film thickness (Figure 4.2). The increase in peptide concentration with thickness is attributed to diffusion of peptides into the hydrated film and binding to maleimide groups within the film. To estimate the density of peptides available for cell interactions at the film surface, these data were extrapolated to zero film thickness.

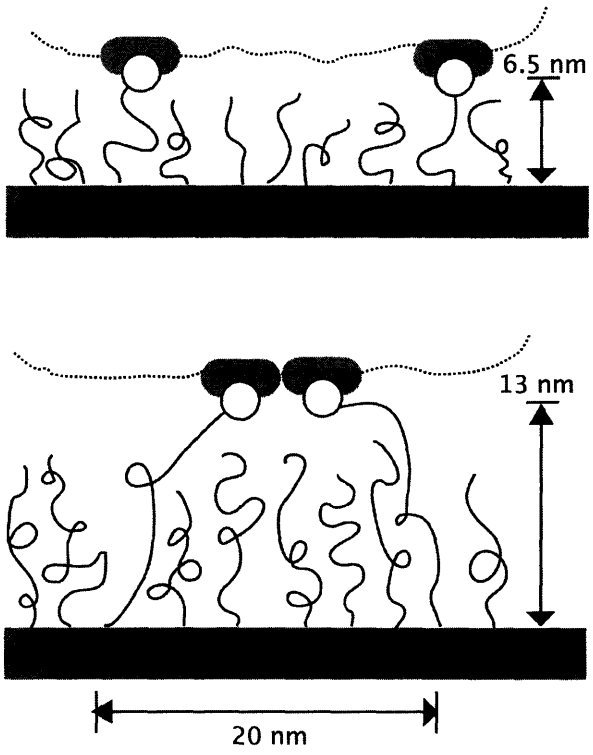

Figure 4.7 Schematic illustration of integrins interacting with PHSRN-K-GRGDSP peptide-coupled amphiphilic comb surfaces with 10-mer (top) and 22-mer (bottom) PEO side chains.

Reaction concentrations were then varied to achieve surface peptide densities of ~2,500 peptides/μm^2 (Figure 4.7), corresponding to an average equilibrium spacing between peptides of ~20 nm. While the spacing between adjacent integrins in various types of functional clusters (e.g. focal contacts and focal adhesions) is not precisely known, the chosen average peptide spacing of 20 nm is about twice the dimension of an integrin head [26-28]. At this peptide density, integrins bound to peptides attached by 10-mer (3 nm) PEO tethers will likely be constrained from forming close-neighbor aggregates (on average), even if they displace their tethers by the fully extended tether

length. Integrins bound to peptides on 22-mer (7 nm) tethers, by contrast, should be able to extend their tethers to form close-neighbor associations.

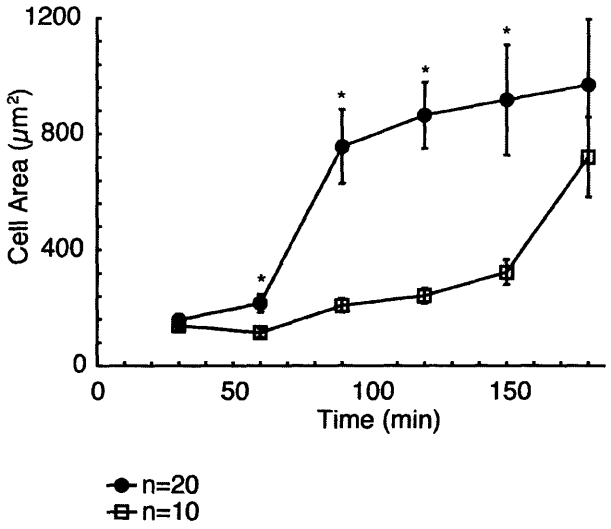

Figure 4.8 Cell spread area on PHSRN-K-GRGDSP-coupled surfaces of PMMA-*g*-PEO with 10-mer (squares) and 22-mer (circles) PEO side chains. * $p<0.01$

Figure 4.8 shows a comparative time course of cell spreading on surfaces made from PMMA-*g*-PEO_{10} and PMMA-*g*-PEO_{22}. The evolution of intracellular organization of actin and vinculin during spreading is shown in Figure 4.9. On both substrates, little evidence of cell spreading, actin stress fibers, or focal adhesions is seen at times less than one hour. Cells plated on substrates presenting peptides bound by the more extensible 22-mer PEO tethers form focal adhesions and begin to spread within 90 minutes after plating, while those bound to the 10-mer tethers remain predominantly rounded. By 150 minutes after plating, however, cells binding to both surfaces show similar degrees of spreading and similar organization of acting and vinculin. We attribute the faster

spreading on longer tether substrates to the increased ability of cells on these substrates to aggregate integrins by displacing adhesive ligands from their average ~20 nm spacing to create local clusters [29, 30]. Longer tether substrates to the increased ability of cells to locally reorganize peptides on surfaces bearing longer tethers [29, 30].

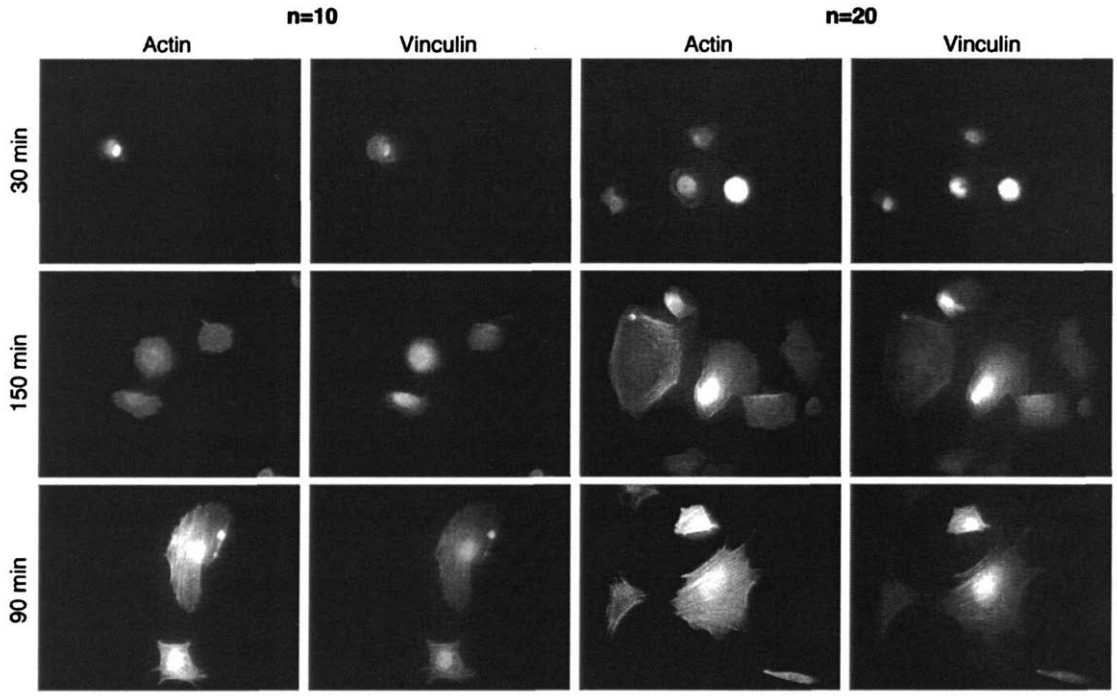

Figure 4.9 Actin and vinculin staining of cells adhering to PHSRN-K-GRGDSP coupled to surfaces of PMMA-*g*-PEO with 10-mer (left) and 22-mer (right) PEO side chains at different incubation time points.

In studies of fibroblast spreading on fibronectin, Dubin-Thaler and co-workers reported that the lag time for initiation of cell spreading decreased with increasing surface fibronectin density, and suggested that spreading initiation might be viewed as a cellular "phase change" that occurred after the cell crossed a threshold of integrin signaling [31].

Integrin signaling requires integrin clustering [30], hence, initiation of spreading may require formation of a threshold quantity of integrin clusters. For substrates coated with fibronection by adsorption at low and moderate densities, molecules are distributed stochastically on the surface and thus some molecules intrinsically are clustered. The probability of finding a suitable cluster within a given area of the surface increases with increasing fibronectin density. During adhesion (and spreading) cells sample the surface, forming and breaking integrin-matrix bonds dynamically. Because many more binding and unbinding events are required to find a threshold quantity of statistically clustered ligands on a sparsely-coated surface, reaching the threshold for the quantity of clustered, bound integrins required to initiate spreading is expected to take longer [32, 33]. In our studies, the average surface density of adhesion peptide is the same on PEO_{10} and PEO_{22} surfaces, but due to the greater mobility of PEO_{22} tethers, we expect that the PEO_{22} surfaces present a greater number of functional adhesion peptide clusters, because bound integrins can move tethered peptides sufficient lateral distances to allow integrin aggregates to form.

To more directly address the possibility of cell-induced movement of tethered peptides, FRET measurements were conducted on surfaces in which PEO-tethered peptides were randomly labeled with Alexa-488 or Alexa-546. For the surface density of peptides used (~2,500 total peptides/μm^2), donor- and acceptor-labeled peptides are separated by more than 20 nm on both comb surfaces. This distance is more than three times the Förster radius for this chromophore pair, and therefore little FRET is observed on either surface in the absence of cells. When fibroblasts attach, a dramatic increase in FRET is observed. Figure 4.10 shows bright field images and maps of average

chromophore pair separation calculated from FRET data obtained from each comb surface after 3 hours of incubation. Bright field images of the two surfaces show adherent cells with similar morphologies and spread areas (some rounded cells are also observed on PEO_{10} surfaces). Donor-acceptor separations calculated based on FRET, however, show a substantial difference in cells with similar morphologies, with cells adhering to peptides bound by long tethers showing a smaller separation between bound ligands. A mean separation of 15.6±1.4 nm was observed for chromophores on PMMA-*g*-PEO_{22}, while a separation 17.5±1.3 nm was found for PMMA-*g*-PEO_{10} (sample size: 30 cells per surface; statistically significant at $p=0.05$). Peptides tethered by longer PEO chains thus appear to be more readily repositioned laterally to accommodate receptor clustering.

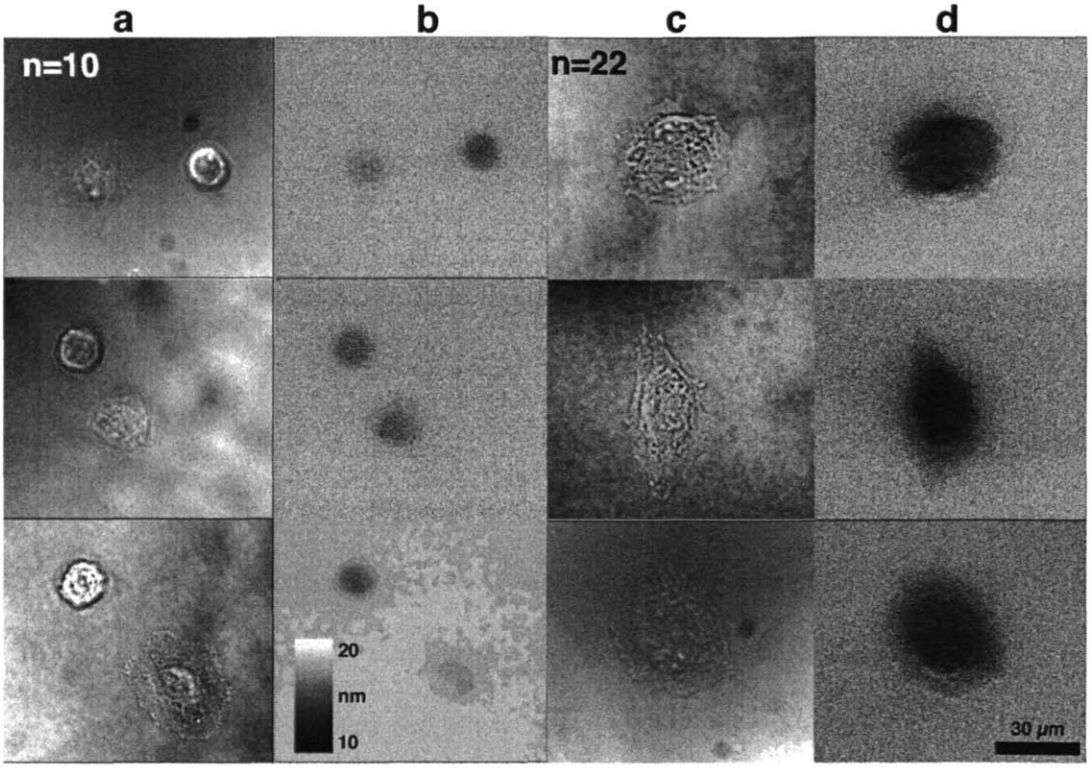

Figure 4.10 Bright field images (a, c) and ligand spacing calculated from FRET measurements (b, d) for PHSRN-K-GRGDSP coupled to PMMA-*g*-PEO polymers with 10-mer (a, b) and 22-mer (c, d) PEO side chains.

The observed FRET intensity might alternatively be explained by micron-scale deformation of the polymer film. Cells can exert significant traction forces on their substrate, and cell-induced deformation has been reported for hydrogel substrates [34]. However, two observations suggest that micron-scale cell-induced deformation of the PMMA-*g*-PEO film substrates does not occur in our systems. First, fluorescence depletion rings around cells that would indicate micron-scale rearrangement of the polymer are absent. Second, when cells are removed from the films using trypsin, the resulting substrates show uniform fluorescence intensity, suggesting that no permanent deformation occurred. Both observations support the premise that the observed FRET increase in the presence of cells was due to rearrangement of peptide bound integrins.

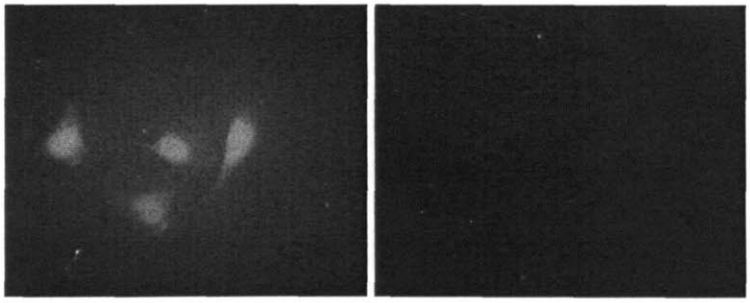

Figure 4.11 FRET images obtained in the presence of cells (left) and of a surface where cells have been removed using trypsin (right).

We note that the average ligand spacing where we observe these effects, 20 nm, is significantly smaller than the 58 nm spacing reported by Cavalcanti-Adam et al. to affect

cytoskeletal organization of fibroblasts when single RGD ligands are presented at precise spacings [35]. We used a different RGD peptide, a different substrate, and a different cell line, and imaged cells within the first 3 hrs rather than after 24 hrs, as was done in that study. These factors and others could contribute to the difference in ligand spacing found to induce cell response.

4.3.2 Cell Attachment to and Spreading on Blend and Bimodal Brushes

To examine the effects of tether length distribution on ligand accessibility, cell attachment and spreading assays were performed on surfaces composed of blends of 25% PMPI-activated PMMA-*g*-PEO of a given PEO chain length (n_a), blended with inert PMMA-*g*-PEO of PEO chain length n_i. Surfaces with both longer active than inert chains and longer inert than active chains were examined. To control for variation in brush structure associated with blending active and inert polymer, blends of components of identical length (10 or 22 EO segments) were also examined.

Figure 4.12 compares cell attachment (a) and spreading (b) on each of the four comb blend surfaces as a function of incubation time. Control blends, for which the active chains were of equal length to inert chains, showed good cell attachment, with an overall increase in cell number and spreading over time. Bimodal brushes in which inert chains are longer than active chains, by contrast, showed little cell attachment and poor spreading, even after three hours. This indicates that longer inert chains effectively masked active groups attached to shorter chains, making these surfaces non-adhesive to cells. These findings are consistent with previous studies that found substantial inhibition

of cell adhesion when adhesion peptides were attached to short chains in a bimodal polymer brush [19, 36].

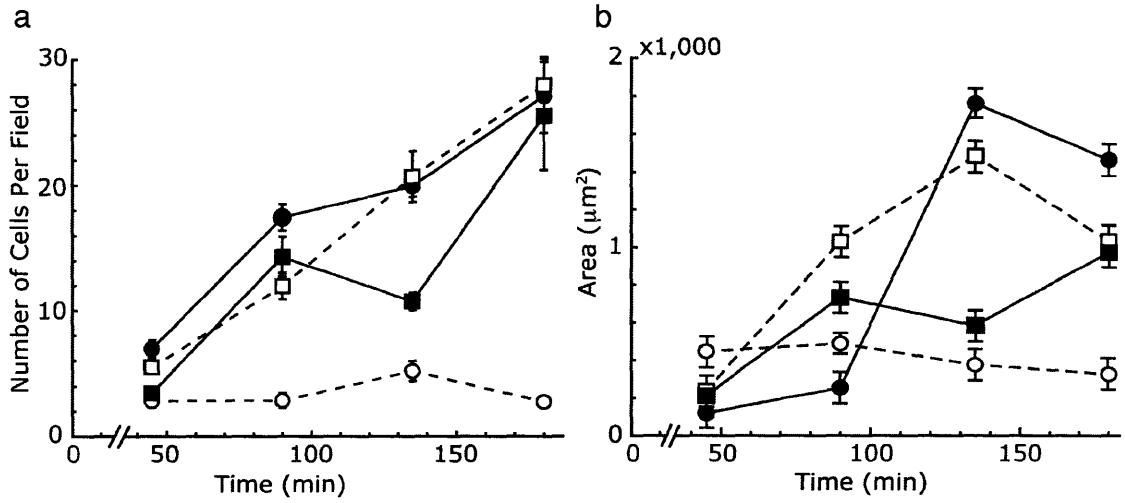

Figure 4.12 (a) Cell attachment and (b) spreading on surfaces made from 25 wt% PMPI-coupled comb blended with unmodified comb. PEO side chain lengths of active and inert combs varied. Closed squares: n_a=22 blended with n_i=22. Closed Circles n_a=10, n_i=10. Open squares: n_a=22, n_i=10. Open Circles: n_a=10, n_i=22.

Bimodal brushes in which active groups were tethered to 22-mer PEO chains, by contrast, show cell attachment and spreading comparable to that of a monomodal brush with the same active chain length (Figure 4.12). No improvement in cell attachment is observed, beyond the previously noted difference between 10- and 22-mers found for a monomodal brush (Figure 4.12a). As seen in Figure 4.12b blends with n_a=22 active chains show a dramatic increase in cell spreading around 130 minutes, while the monomodal n_a=10 brush shows comparable spreading only after three hours of incubation time. For the bimodal blend, stratification of chain ends to the top of the brush caused by a difference of ten EO units appears insufficient to produce an observable

enhancement in cell attachment or spreading from a monomodal brush of equivalent active EO chain length. Our data are in disagreement with the simulation results of Chen and Dormidontova [37], who found enhanced receptor-ligand binding on a bimodal brush with ligands attached to long tethers. The discrepancy between simulation and experiment may reflect the different range of tether lengths studied.

.

4.4 Conclusions

This study demonstrated that increasing the length of PEO tethers used to attach RGD adhesion peptides to a polymer brush increases the rate of cell spreading and permits formation of focal adhesions at shorter incubation times. FRET measurements suggest that the observed enhancement in cell adhesion kinetics is most likely due to the added mobility afforded by longer tethers, which facilitates nanoscale rearrangement of surface-bound peptides and promotes integrin clustering. Hence, the use of long tethers (i.e., whose extended length permits lateral ligand overlap) appears an effective strategy to promote the formation of integrin clusters.

Bimodal brushes composed of short active chains and long inert chains showed a dramatic decrease in cell attachment and spreading, consistent with the screening of adhesion peptides by the longer inert chains. Such a structure may be of value in designing targeted drug-delivery vehicles with surface-tethered functional groups selectively masked to reduce toxicity or prolong lifetime *in vivo* [18, 38]. By contrast, ligand accessibility does not appear to be enhanced by a bimodal brush with shorter inert chains. For this case, adhesive properties were similar to those of a monomodal brush of

long polymer tethers, suggesting that a bimodal brush affords little advantage in the chain length regime investigated.

4.5 References

1. Prime, K.L. and Whitesides, G.M. "Self-assembled organic monolayers: Model systems for studying adsorption of proteins at surfaces." *Science*, **1991**, 252(5009): p. 1164-1167.
2. Ostuni, E.; Chapman, R.G.; Holmlin, R.E.; Takayama, S. and Whitesides, G.M. "A survey of structure-property relationships of surfaces that resist the adsorption of protein." *Langmuir*, **2001**, 17: p. 5605-5620.
3. Zhu, B.; Eurell, T.; Gunawan, R. and Leckband, D. "Chain-length dependence of the protein and cell resistance of oligo(ethylene glycol)-terminated self-assembled monolayers on gold." *J Biomed Mater Res*, **2001**(56): p. 406-416.
4. Unsworth, L.D.; Sheardown, H. and Brash, J.L. "Protein resistance of surfaces prepared by sorption of end-thiolated poly(ethylene glycol) to gold: Effect of surface chain density." *Langmuir*, **2005**, 21: p. 1036-1041.
5. Singh, N.; Cui, X.; Boland, T. and Husson, S.M. "The role of independently variable grafting density and layer thickness of polymer nanolayers on peptide adsorption and cell adhesion." *Biomaterials*, **2007**, 28(5): p. 763.
6. de Gennes, P.G. "Conformations of polymers attached to an interface." *Macromolecules*, **1980**, 13: p. 1069-1075.
7. Milner, S.T.; Witten, T.A. and Cates, M.E. "Theory of the grafted polymer brush." *Macromolecules*, **1988**, 21: p. 2610-2619.

8. Malmsten, M.; Emoto, K. and Van Alstine, J.M. "Effect of chain density on inhibition of protein adsorption by poly(ethylene glycol) based coatings." *Journal of Colloid and Interface Science*, **1998**, 202(2): p. 507-517.

9. Beer, J.H.; Springer, K.T. and Coller, B.S. "Immobilized arg-gly-asp (RGD) peptides of varying lengths as structural probes of the platelet glycoprotein iib/iiia receptor." *Blood*, **1992**, 79(1): p. 117-128.

10. Wong, J.Y.; Kuhl, T.L.; Israelachvili, J.N.; Mullah, N. and Zalipsky, S. "Direct measurement of a tethered ligand-receptor interaction potential." *Science*, **1997**, 275: p. 820-822.

11. Jeppesen, C., Wong, J.Y., Kuhl, T.L., *et al.* "Impact of polymer tether length on multiple ligand-receptor bond formation." *Science*, **2001**, 293: p. 465-468.

12. Griffith, L.G. and Lopina, S. "Microdistribution of substratum-bound ligands affects cell function: Hepatocyte spreading on PEO-tethered galactose." *Biomaterials*, **1998**, 19(11-12): p. 979.

13. Milner, S.T.; Witten, T.A. and Cates, M.E. "Effects of polydispersity in the end-grafted polymer brush." *Macromolecules*, **1989**, 22: p. 853-861.

14. Lai, P.Y. and Zhulina, E.B. "Structure of a bidisperse polymer brush: Monte carlo simulation and self-consistent field results." *Macromolecules*, **1992**, 25(20): p. 5201-5207.

15. Dan, N. and Tirrell, M. "Effects of bimodal molecular weight distribution on the polymer brush." *Macromolecules*, **1993**, 26: p. 6467-6473.

16. Kent, M.S.; Factor, B.J.; Satija, S.; Gallagher, P. and Smith, G.S. "Structure of bimodal polymer brushes in a good solvent by neutron reflectivity." *Macromolecules*, **1996**, 29: p. 2843-2849.

17. Levicky, R.; Koneripalli, N.; Tirrell, M. and Satija, S.K. "Stratification in bidisperse polymer brushes from neutron reflectivity." *Macromolecules*, **1998**, 31(8): p. 2616-2621.

18. Kim, D.H.; Klibanov, A.L. and Needham, D. "The influence of tiered layers of surface-grafted poly(ethylene glycol) on receptor-ligand-mediated adhesion between phospholipid monolayer-stabilized microbubbles and coated glass beads." *Langmuir*, **2000**, 16(6): p. 2808-2817.

19. Mrksich, M. "A surface chemistry approach to studying cell adhesion." *Chem. Soci. Rev.*, **2000**, 29: p. 267-273.

20. Ufret, M.L. and Griffith, L.G. *in preparation.*

21. Chan, W.C. and White, P.D. "FMOC solid phase peptide synthesis." Oxford University Press; Oxford 2000.

22. Markwell, M.A.K. "A new solid-state reagent to iodinate proteins: Conditions for the efficient labeling of antiserum." *Anal. Biochem.*, **1982**, 125: p. 427-432.

23. Hermanson, G.T. "Bioconjugate techniques." Academic Press; San Diego 1996.

24. Gordon, G.W.; Berry, G.; Liang, X.H.; Levine, B. and Herman, B. "Quantitative fluorescence resonance energy transfer measurements using fluorescence microscopy." *Biophysical Journal*, **1998**, 74: p. 2702-2713.

25. Lakowicz, J.R. "Principles of fluorescence spectroscopy." Kluwer Acacdemic; New York 1999.

26. Hynes, R.O. "Integrins: Bidirectional, allosteric signaling machines." *Cell*, **2002**, 110: p. 673-687.

27. Puklin-Faucher, E.; Gao, M.; Schulten, K. and Vogel, V. "How the headpiece hinge angle is opened: New insights into the dynamics of integrin activation." *J. Cell Biol.*, **2006**, 175(2): p. 349-360.

28. Iwasaki, K., Mitsuoka, K., Fujiyoshi, Y., *et al.* "Electron tomography reveals diverse conformations of integrin $\alpha_{iib}\beta_3$ in the active state." *Journal of Structural Biology*, **2005**, 150(3): p. 259-267.

29. Galbraith, C.G.; Yamada, K.M. and Galbraith, J.A. "Polymerizing actin fibers position integrins primed to probe for adhesion sites." *Science*, **2007**, 315(5814): p. 992-995.

30. Miyamoto, S.; Akiyama, S.K. and Yamada, K.M. "Synergistic roles for receptor occupancy and aggregation in integrin transmembrane function." *Science*, **1995**, 267(5199): p. 883-885.

31. Dubin-Thaler, B.J.; Giannone, G.; Dobereiner, H.-G. and Sheetz, M.P. "Nanometer analysis of cell spreading on matrix-coated surfaces reveals two distinct cell states and steps." *Biophysical Journal*, **2004**, 86(3): p. 1794-1806.

32. Brinkerhoff, C.J. and Linderman, J.J. "Integrin dimerization and ligand organization: Key components in integrin clustering for cell adhesion." *Tissue Engineering*, **2005**, 11(5/6): p. 865-876.

33. Irvine, D.J.; Hue, K.-A.; Mayes, A.M. and Griffith, L.G. "Simulations of cell-surface integrin binding to nanoscale-clustered adhesion ligands." *Biophysical Journal*, **2002**, 82: p. 120-132.

34. Kong, H.J.; Polte, T.R.; Alsberg, E. and Mooney, D.J. "FRET measurements of cell-traction forces and nano-scale clustering of adhesion ligands varied by substrate stiffness." *Proceedings of the National Academy of Science*, **2005**, 102(12): p. 4300-4305.

35. Cavalcanti-Adam, E.A.; Volberg, T.; Micoulet, A., *et al.* "Cell spreading and focal adhesion dynamics are regulated by spacing of integrin ligands." *Biophysical Journal*, **2007**: biophysj.106.089730.

36. Dori, Y.; Bianco–Peled, H.; Satija, S.K., *et al.* "Ligand accessibility as means to control cell response to bioactive bilayer membranes." *Langmuir*, **2000**, 50: p. 75-81.

37. Chen, C.-C. and Dormidontova, E.E. "Architectural and structural optimization of the protective polymer layer for enhanced targeting." *Langmuir*, **2005**, 21: p. 5605-5615.

38. Lee, J.H.; Lee, H.B. and Andrade, J.D. "Blood compatibility of polyethylene oxide surfaces." *Progress in Polymer Science*, **1995**, 20(6): p. 1043.

Chapter 5: Summary and Outlook

This thesis examined methods of using amphiphilic graft copolymers to control the presentation and accessibility of surface bound ligands with the object of enhancing cell-surface interactions. Two specific means of controlling presentation were investigated: using backbone molecular weight to generate 2D clusters of ligands, and using PEO side chains to control ligand availability. Both means of control were investigated using a variety of techniques, beginning with polymer synthesis, followed by chemical and structural characterization and finally through evaluation of cell-surface interactions. Where applicable, numerical simulations were employed to better understand experimental observations.

Clustering was investigated by preparing thin films of PMMA-*g*-PEO, composed of blends of inert and active polymers. The active polymers adjacent to the water interface were decorated with gold nanoparticles, thereby tracing the trajectory of the quasi-2D chain backbones. Examination of gold-decorated films in the TEM revealed the presence of clusters of gold particles, providing the first direct observation of ligand clustering in these systems [1]. This finding was confirmed through statistical analysis of the particle distributions.

One interesting observation arising from these experiments was the broad distribution in cluster size. By correlating chain lengths determined by light scattering, chain trajectories determined from TEM images and Monte Carlo simulations, Chapter 3

demonstrated that the broad distribution in cluster size arises from polydispersity of the underlying polymer. This polydispersity also leads to unusual scaling behavior. Based on reconstructed chain trajectories and Monte Carlo simulations it was demonstrated that the radius of gyration for chains in this system scales as $R_g \sim N^{\nu}$ with $\nu=0.69\pm0.02$. This is larger than the theoretically expected value of $\nu=0.5$ for a 2D polymer melt [2-4], which is attributed by swelling of long chains by short chains owing to the large polydispersity.

There are several potential applications of these findings. Engineering polymers with a specific distribution of molecular weights, for example, can be used to control the nanometer lengths scale organization of systems with several different tethered functional groups. Two or more different functional groups can be introduced using orthogonal coupling chemistry [5, 6]. Comb activated with PMPI can be blended with comb activated with NHS, for example. Exposing surfaces made from this blend to amine-containing molecules will result in coupling only to the NHS groups. A thiol-bearing second molecule could then be coupled to the remaining PMPI groups through a subsequent solution coupling [7]. Organization of clusters on this surface will be dictated by the relative molecular weights of the active polymers used. Discrete, non-interpenetrating clusters of each molecule will be generated by blending monodisperse polymers. Where there is a substantial difference in molecular weights, by contrast, a greater degree of interpenetration between clusters can be expected, where larger molecular weight chains will be swollen by the smaller chains [1, 3]. Cluster size in these circumstances will still be dictated by the molecular weight of the backbone, permitting creation of a surface with two (or more) length scales of structure. This may be of value

in producing synthetic surfaces that more closely mimic not only the chemical functionality, but also the spatial organization of proteins.

This general approach to creating nanoscale clusters discussed in Chapter 3 requires only an amphiphilic graft copolymer, and is not limited to PMMA-*g*-PEO. Applying alternate chemistries for the backbone and side chain could also be used to produce more uniform cluster sizes [8]. For example, PEO can be grafted onto a number of different hydrophobic backbones such as polyesters [9], polyolefins [10], and poly(amino acids) [11] each of which can be synthesized to have a low polydispersity. Further adaptations could be made to any similar system where the polymer backbone is confined at equilibrium in two dimensions, as is realized with lipid bilayers . Though this study focused specifically on cell adhesion, this method could be employed in numerous other applications. Because of the importance of multivalent interactions in biological systems [12], similar approaches could be used in other applications such as inhibition of viral infection [13], production of more effective antibodies [14, 15], and development of improved biosensors.

Synthetic methods for producing amphiphilic graft copolymers are discussed in Chapter 2. The broad range of cluster sizes, observed in Chapter 3 indicates that it would be desirable to modify these synthetic methods to produce such a narrow molecular weight distribution. This would require several changes in the chemistry employed. PEO macromonomer would need to be entirely monofunctional [16-18]. This could be accomplished through alternative synthetic routes, such as anionic polymerization [19-21]. Additional improvements might be realized through use of a protecting group on the terminal hydroxyl end to prevent side reactions that might lead to formation of cross-

links. Once monofunctional macromonomer was available, controlled polymerization techniques could be employed to produce more nearly monodisperse polymers [22].

Chapter 4 investigated the effects of tether length on cell adhesion. Several observations were made. Cell attachment is enhanced when tethers are long, relative to the size of an integrin. FRET measurements indicate that this is due not only to their greater ability to access the binding pocket of an integrin [23], but also due to increased opportunities for integrins to reorganize bound ligands into clusters. Application of this design parameter could be of use in any number of biological problems in which spatial organization of bound ligands is important.

Bimodal brushes did not have an observable effect on bioactivity. This finding implies that it is possible to decouple design of the underlying protein resistant brush from design of the polymer tethers used to anchor biomolecules. There are several practical implications of this finding. For instance, this suggests that protein resistance could be obtained using an entirely different length of PEO chain than that used for tethering, permitting use of a less expensive polymer to form the underbrush. In addition, use of two graft copolymers with different chain lengths could also relieve the restraint that the polymer used for tethering be protein resistant. Provided that there is sufficient intermixing between the two graft copolymers, only the underbrush polymer need be protein resistant. This could facilitate use of longer tethers by extending the range of useful compositions of copolymers used as tethers.

Chapter 4 also demonstrated that it is possible to mask tethered active groups by using inert chains of greater length. This provides a means of deliberately masking tethered bioactive groups. This could be used, for example, to shield tethered toxic

molecules that were necessary to introduce some specific chemical function. Other applications where it might be desirable to mask chemical function include drug delivery (Figure 5.1). In these instances, drug molecules could be tethered using a biodegradable spacer, such that they would be masked from the cell until release and would leave an intact protein resistant brush behind. Alternately, the longer inert chains used to mask these drug groups could be tethered, such that following a designated incubation period the inert chains would release from the brush, leaving the surface-bound drug molecules exposed and biologically active. These approaches are applicable not just to graft-copolymer systems, but to any system that uses a PEO brush in which PEO chains serve both to resist protein adsorption and to anchor bioactive polymers.

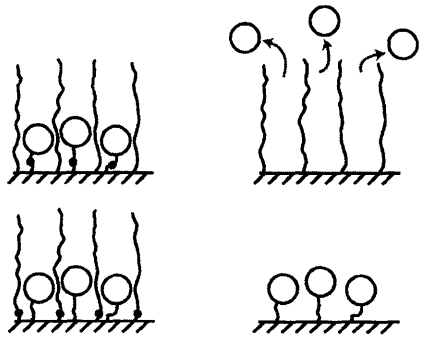

Figure 5.1 Release of a tethered drug masked by long polymer chains (top) and un-masking of tethered drugs (bottom) using biodegradable linkers (grey).

Both control over cluster size through backbone molecular weight and control over ligand accessibility through side chain length have broader applications apart from creating 2D cell-interactive surfaces. Amphiphilic graft copolymers can be incorporated as components in multi-scale systems, for example, by preparing micro-scale polymer building blocks that could then be mechanically assembled into larger scale structures [24-26]. These design principles could also be adapted to fabricate larger self-assembling

systems. Incorporation of comb polymer into the synthesis of micro- or nano- particles could be used to produce nanometer-length scale clusters of biomolecules. Colloidal self-assembly methods could then be used to assemble these particles into crystals suitable for fabrication of tissue scaffolds [27]. The resulting materials would possess biologically relevant structures on multiple length-scales, as determined both by colloid size and polymer architecture.

5.2 References

1. Kuhlman, W.A.; Olivetti, E.A.; Griffith, L.G. and Mayes, A.M. "Chain conformations at the surface of a polydisperse amphiphilic comb copolymer film" *Macromolecules* **2006**, *39* (15): p. 5122-5126.
2. Cloizeaux, J. and Jannink, G. "Polymers in solution" Clarendon Press; Oxford 1990.
3. De Gennes, P.G. "Scaling concepts in polymer physics" Cornell University Press; Ithaca 1979.
4. Yethiraj, A. "Computer simulation study of two-dimensional polymer solutions" *Macromolecules* **2003**, *36*: p. 5854-5862.
5. Roberts, M.J.; Bentley, M.D. and Harris, J.M. "Chemistry for peptide and protein pegylation" *Advanced Drug Delivery Reviews* **2002**, *54*: p. 459-476.
6. Veronese, F.M. "Peptide and protein pegylation: A review of problems and solutions" *Biomaterials* **2001**, *22*: p. 405-417.
7. Richardson, L. and Griffith, L.G. "In preparation" **2007**.
8. Velichkova, R.S. and Christova, D.C. "Amphiphilic polymers from macromonomers and telechelics" *Progress in Polymer Science* **1995**, *20* (5): p. 819-887.
9. Taniguchi, I.; Kuhlman, W.A.; Mayes, A.M. and Griffith, L.G. "Functional modification of biodegradable polyesters through a chemoselective approach: Application to biomaterial surfaces" *Polymer International* **2006**, *55*: p. 1385-1397.

10. Lu, Y.; Chen, S.; Hu, Y. and Chung, T.C. "Synthesis of graft copolymer polyethylene-graft-poly(ethylene oxide) by a new anionic graft-from polymerization" *Polymer International* **2004**, *53* (12): p. 1963-1967.

11. Winblade, N.D.; Nikolic, I.D.; Hoffman, A.S. and Hubbell, J.A. "Blocking adhesion to cell and tissue surfaces by the chemisorption of a poly-L-lysine-graft-(poly(ethylene glycol); phenylboronic acid) copolymer" *Biomacromolecules* **2000**, *1* (4): p. 523-533.

12. Mammen, M.; Choi, S.-K. and Whitesides, G.M. "Polyvalent interactions in biological systems: Implications for design and use of multivalent ligands and inhibitors" *Angewandte Chemie International Edition* **1998**, *37* (20): p. 2754-2794.

13. Gargano, J.M.; Ngo, T.; Kim, J.Y.; Acheson, D.W.K. and Lees, W.J. "Multivalent inhibition of ab5 toxins" *J. Am. Chem. Soc.* **2001**, *123* (51): p. 12909-12910.

14. Oda, M.; Sato-Nakamura, N. and Azuma, T. "Molecular characterization of monovalent and multivalent hapten-protein conjugates for analysis of the antigen-antibody interaction" *Analytical Biochemistry* **2004**, *333* (2): p. 365-371.

15. Dower, S.K.; Delisi, C.; Titus, J.A. and Segal, D.M. "Mechanism of binding of multivalent immune complexes to FC receptors" *Biochemistry* **1981**, *20*: p. 6326 - 6334.

16. Yagci, Y. and Ito, K. "Macromolecular architecture based on anionically prepared poly(ethylene oxide) macromonomers" *Macromolecular Symposia* **2005**, *226* (1): p. 87-96.

17. Ali, M.M. and Stover, H.D.H. "Well-defined amphiphilic thermosensitive copolymers based on poly(ethylene glycol monomethacrylate) and methyl methacrylate prepared by atom transfer radical polymerization" *Macromolecules* **2004**, *37*: p. 5219-5227.

18. Taniguchi, I.; Kuhlman, W.A.; Griffith, L.G. and Mayes, A.M. "Macromonomer purification strategy for well-defined polymer amphiphiles incorporating poly(ethylene glycol) monomethacrylate" *Macromol. Rapid Commun.* **2006**, *27*: p. 631 – 636.

19. Masson, P.; Beinert, G.; Franta, E. and Rempp, P. "Synthesis of poly(ethylene oxide) macromers" *Polymer Bulletin* **1982**, *7* (1).

20. Ito, K.; Hashimura, K.; Itsuno, S. and Yamada, E. "Poly(ethylene oxide) macromonomers. 8. Preparation and polymerization of w-hydroxypoly(ethylene oxide) macromonomers" *Macromolecules* **1991**, *24* (14): p. 3977-3981.

21. Ito, K.; Tsuchida, H.; Hayashi, A., et al. "Reactivity of poly(ethylene oxide) macromonomers in radical copolymerization" *Polymer Journal* **1985**, *17* (7): p. 827-839.

22. Hawker, C.J.; Mecerreyes, D.; Elce, E., et al. ""Living" Free radical polymerization of macromonomers: Preparation of well defined graft copolymers" *Macromolecular Chemistry and Physics* **1997**, *198* (1): p. 155-166.

23. Beer, J.H.; Springer, K.T. and Coller, B.S. "Immobilized Arg-Gly-Asp (RGD) peptides of varying lengths as structural probes of the platelet glycoprotein ii_b/iii_a receptor" *Blood* **1992**, *79* (1): p. 117-128.

24. Griffith, L.G. and Swartz, M.A. "Capturing complex 3D tissue physiology in vitro" *Nature Reviews Molecular Cell Biology* **2006**, *7*: p. 211-224.

25. Muschler, G.F.; Nakamoto, C. and Griffith, L.G. "Engineering principles of clinical cell-based tissue engineering" *J Bone Joint Surg Am* **2004**, *86* (7): p. 1541-1558.

26. Banerjee, P.; Irvine, D.J.; Mayes, A.M. and Griffith, L.G. "Polymer latexes for cell-resistant and cell-interactive surfaces" *J. Biomed Mater Res* **2000**, *50*: p. 331-339.

27. Finne-Wistrand, A. and Albertsson, A.-C. "The use of polymer design in resorbable colloids" *Annual Review of Materials Research* **2006**, *36*: p. 369-395.

Appendix A: Sample MC Code

```
% This code implements a 2D lattice simulation of polymer chains
% that can be adjusted to fit a specified molecular weight distribution.

% For Matlab/Octave



%---------------------------------InitConfig

function [Next,Prev]=InitConfig(n);

% Generates an initial configuration with f

% Prev and Next are 2D arrays.
% Each array element contains the location of the next segment
% {1..4} = {n,w,s,e} or 0 {end}

% This particular example makes n chains of all the same length

Prev=3*[zeros(1,n);ones(n,n-1)'];
Next=[ones(n,n-1)';zeros(1,n)];


%---------------------------------WRAP

function x=wrap(x,n);

%Apply Periodic B.C.

            x=mod(x,n);
            if x==0
                        x=n;
            end;


%---------------------------------PlotDense

function PlotDense(Next,Prev);
% Plots a 2D system described by Next and Prev

% Make a new figure and frame our plot:
figure;
hold off;
plot([1 1 size(Next,1) size(Next,1) 1],[1 size(Next,1) size(Next,1) 1 1],'.r');
hold on;
axis off;

% Draw lines connecting each segment.
% Some lines are drawn twice

for i=1:size(Next,1)
      for j=1:size(Next,1)
            switch Next(i,j)
            case 1
                  plot([i,i+1],[j,j]);
            case 2
                  plot([i,i],[j,j-1]);
            case 3
                  plot([i,i-1],[j,j]);
            case 4
```

```
                plot([i,i],[j,j+1]);
            otherwise
                %plot(i,j,'or');
            end;
            switch Prev(i,j)
            case 1
                plot([i,i+1],[j,j]);
            case 2
                plot([i,i],[j,j-1]);
            case 3
                plot([i,i-1],[j,j]);
            case 4
                plot([i,i],[j,j+1]);
            otherwise
                %plot(i,j,'om');
            end;
        end;
end;
axis equal;



%-----------------------------------MCSTEP

function
[Next,Prev,LastPr,AcceptedSteps]=MCStep(Next,Prev,LastPr,AcceptedSteps)

% Performs one MC Step

% Based on:
% Reiter, J.; Zifferer, G. and Olaj, O.F. Macromolecules 1989, 22: 3120-3124.
% Mansfield, M.L. Journal of Chemical Physics 1982, 77: p. 1554-1559.

% Next, Prev are 2D arrays listing how nodes are connected
%            {1..4} = {n,w,s,e} or 0 {end}

% LastPr is the last calculated P for determining whether ot reject a step
% AcceptedSteps is a counter to track only *accepted* MC steps

n=size(Next,1); % The size of our 2D array.

global ScalConst;    % Scaling constant to reject MC steps.

% Find a random chain end
EndX=ceil(rand*n);
EndY=ceil(rand*n);

while not(or(Next(EndX,EndY)==0,Prev(EndX,EndY)==0))
        EndX=ceil(rand*n);
        EndY=ceil(rand*n);
end;

[cnt,SCRATCH]=CalcProb(Next,Prev);
LastNext = Next;
LastPrev = Prev;

%Now find a segment to attack (hint: not your previous link...)
% First, figure out who is attached to you:
NearNabX=EndX;  % For the an isolated point, there is no n.n., so... use self.
NearNabY=EndY;
if Next(EndX,EndY)==0
        NextIsEnd=1;
        switch Prev(EndX,EndY)
        case 1
                NearNabX=EndX+1;
```

```
                NearNabY=EndY;
        case 2
                NearNabX=EndX;
                NearNabY=EndY-1;
        case 3
                NearNabX=EndX-1;
                NearNabY=EndY;
        case 4
                NearNabX=EndX;
                NearNabY=EndY+1;
        end;
else
        NextIsEnd=0;
        switch Next(EndX,EndY)
        case 1
                NearNabX=EndX+1;
                NearNabY=EndY;
        case 2
                NearNabX=EndX;
                NearNabY=EndY-1;
        case 3
                NearNabX=EndX-1;
                NearNabY=EndY;
        case 4
                NearNabX=EndX;
                NearNabY=EndY+1;
        end;
end;
NearNabX=wrap(NearNabX,n);
NearNabY=wrap(NearNabY,n);



ToAttackX=NearNabX;
ToAttackY=NearNabY;

while and(ToAttackX==NearNabX,ToAttackY==NearNabY)
        Direction =ceil(rand*4);
        switch Direction
        case 1
                ToAttackX=EndX+1;
                ToAttackY=EndY;
        case 2
                ToAttackX=EndX;
                ToAttackY=EndY-1;
        case 3
                ToAttackX=EndX-1;
                ToAttackY=EndY;
        case 4
                ToAttackX=EndX;
                ToAttackY=EndY+1;
        end;
end;

ToAttackX=wrap(ToAttackX,n);
ToAttackY=wrap(ToAttackY,n);

% Join the chains
                if Next(EndX,EndY)==0;
                        Next(EndX,EndY)=Direction;
                        NextToPrev=1;
                else
                        Prev(EndX,EndY)=Direction;
                        NextToPrev=-1;
                end;
```

```
%Are we attacking an end?
if or(Next(ToAttackX,ToAttackY)==0,Prev(ToAttackX,ToAttackY)==0)
      AttackedAnEnd=1;
      % We're attacking an end.
            if Next(ToAttackX,ToAttackY)==0
                  NextToPrev=NextToPrev+1;
                  Next(ToAttackX,ToAttackY)=mod(Direction+2,4);
                  if Next(ToAttackX,ToAttackY) ==0
                        Next(ToAttackX,ToAttackY) =4;
                  end;
            else
                  NextToPrev=NextToPrev-1;
                  Prev(ToAttackX,ToAttackY)=mod(Direction+2,4);
                  if Prev(ToAttackX,ToAttackY) ==0
                        Prev(ToAttackX,ToAttackY) =4;
                  end;
            end;
      else  %An end is attacking a middle
            %Choose which direction to join in
                  AttackedAnEnd=0;
                  FrontOrBack = rand>0.5;
                  TmpX=ToAttackX;
                  TmpY=ToAttackY;
                  if FrontOrBack
                        switch Prev(ToAttackX,ToAttackY)
                        case 1
                              TmpX=wrap(ToAttackX+1,n);
                        case 2
                              TmpY=wrap(ToAttackY-1,n);
                        case 3
                              TmpX=wrap(ToAttackX-1,n);
                        case 4
                              TmpY=wrap(ToAttackY+1,n);
                        end;
                        Next(TmpX,TmpY)=0;
                        NextToPrev=NextToPrev-1;
                        Prev(ToAttackX,ToAttackY)=mod(Direction+2,4);
                        if Prev(ToAttackX,ToAttackY) ==0
                              Prev(ToAttackX,ToAttackY) =4;
                        end;
                  else
                        switch Next(ToAttackX,ToAttackY)
                        case 1
                              TmpX=wrap(ToAttackX+1,n);
                        case 2
                              TmpY=wrap(ToAttackY-1,n);
                        case 3
                              TmpX=wrap(ToAttackX-1,n);
                        case 4
                              TmpY=wrap(ToAttackY+1,n);
                        end;
                        Prev(TmpX,TmpY)=0;
                        NextToPrev=NextToPrev+1;
                        Next(ToAttackX,ToAttackY)=mod(Direction+2,4);
                        if Next(ToAttackX,ToAttackY) ==0
                              Next(ToAttackX,ToAttackY) =4;
                        end;
                  end;
end;

            %Check to see if a chain has switched directions:
            if NextToPrev ==-2
                        TMP=Prev(ToAttackX,ToAttackY);
                        Prev(ToAttackX,ToAttackY)=Next(ToAttackX,ToAttackY);
                        Next(ToAttackX,ToAttackY) = TMP;
```

```
                while Prev(ToAttackX,ToAttackY)~=0
                        switch Prev(ToAttackX,ToAttackY)
                        case 1
                                ToAttackX=ToAttackX+1;
                        case 2
                                ToAttackY=ToAttackY-1;
                        case 3
                                ToAttackX=ToAttackX-1;
                        case 4
                                ToAttackY=ToAttackY+1;
                        otherwise
                                fprintf('CHAIN ERROR -- check init config!')
                        end;
                        ToAttackX=wrap(ToAttackX,n);
                        ToAttackY=wrap(ToAttackY,n);
                        TMP=Prev(ToAttackX,ToAttackY);
                        Prev(ToAttackX,ToAttackY)=Next(ToAttackX,ToAttackY);
                        Next(ToAttackX,ToAttackY) = TMP;
                end;
        elseif NextToPrev == 2
                        TMP=Next(ToAttackX,ToAttackY);
                        Next(ToAttackX,ToAttackY)=Prev(ToAttackX,ToAttackY);
                        Prev(ToAttackX,ToAttackY) = TMP;
                while Next(ToAttackX,ToAttackY)~=0
                        switch Next(ToAttackX,ToAttackY)
                        case 1
                                ToAttackX=ToAttackX+1;
                        case 2
                                ToAttackY=ToAttackY-1;
                        case 3
                                ToAttackX=ToAttackX-1;
                        case 4
                                ToAttackY=ToAttackY+1;
                        otherwise
                                fprintf('CHAIN ERROR -- check init config!')
                        end;
                        ToAttackX=wrap(ToAttackX,n);
                        ToAttackY=wrap(ToAttackY,n);

   TMP=Next(ToAttackX,ToAttackY);
                        Next(ToAttackX,ToAttackY)=Prev(ToAttackX,ToAttackY);
                        Prev(ToAttackX,ToAttackY) = TMP;
                end;
        end;

   %Now break the chain elsewhere!
   %First: figure out how long it is.
   ArbStartX=ToAttackX;
   ArbStartY=ToAttackY;
ItsALoop=0;
   k=0;
   while and(Prev(ToAttackX,ToAttackY)~=0,ItsALoop==0)
        switch Prev(ToAttackX,ToAttackY)
        case 1
                ToAttackX=ToAttackX+1;
        case 2
                ToAttackY=ToAttackY-1;
        case 3
                ToAttackX=ToAttackX-1;
        case 4
                ToAttackY=ToAttackY+1;
        end;
        ToAttackX=wrap(ToAttackX,n);
        ToAttackY=wrap(ToAttackY,n);
        k=k+1;
```

```
            ItsALoop = and(ToAttackX==ArbStartX,ToAttackY==ArbStartY);
      end;

%We're at the start of the chain. Now find the other end:
if ItsALoop==0;
    k=0;
      while and(Next(ToAttackX,ToAttackY)~=0,k<30)
            switch Next(ToAttackX,ToAttackY)
            case 1
                  ToAttackX=ToAttackX+1;
            case 2
                  ToAttackY=ToAttackY-1;
            case 3
                  ToAttackX=ToAttackX-1;
            case 4
                  ToAttackY=ToAttackY+1;
            otherwise
                  fprintf('DANGER');
            end;
            ToAttackX=wrap(ToAttackX,n);
            ToAttackY=wrap(ToAttackY,n);
            k=k+1;
      end;
end;
% Post: k= length of chain.
if k==0
      k=1;
end;
if    or(AttackedAnEnd==1,ItsALoop==1)
      BreakAt = ceil(rand*k);
      for l=1:BreakAt
            tPrevX=ToAttackX;
            tPrevY=ToAttackY;
            switch Prev(ToAttackX,ToAttackY)
            case 1
                  ToAttackX=ToAttackX+1;
            case 2
                  ToAttackY=ToAttackY-1;
            case 3
                  ToAttackX=ToAttackX-1;
            case 4
                  ToAttackY=ToAttackY+1;
            end;
            ToAttackX=wrap(ToAttackX,n);
            ToAttackY=wrap(ToAttackY,n);
      end;
      Next(ToAttackX,ToAttackY)=0;
      Prev(tPrevX,tPrevY)=0;
end;

Accepted=1;
[count,TmpPr]=CalcProb(Next,Prev);
if cnt~=count
      Next = LastNext;
      Prev = LastPrev;
    Accepted=0;
else
    if not(or(TmpPr<LastPr,exp(-TmpPr/ScalConst)>rand))
        Next = LastNext;
        Prev = LastPrev;
        Accepted=0;
    else
        LastPr=TmpPr;
    end;
end;
```

```
AcceptedSteps=AcceptedSteps+Accepted;


% ----------------------------------------CalcProb
function [count,Pr]=CalcProb(Next,Prev)

% Calculates the SSE difference between the simulated and desired MWD

% Bins = global variable containing the bins of the MWD histogram
% TrueDist = distribution being fit (GPC/LS)

n=size(Next,1);

% Create table of chain lengths

ChainList=[];

for k=1:n
       for l=1:n
              if Next(k,l)==0
             ThisLength=1;
                     x=k;
                     y=l;
                     while Prev(x,y)~=0
                            switch Prev(x,y)
                            case 1
                                   x=x+1;
                            case 2
                     y=y-1;
                            case 3
                                   x=x-1;
                            case 4
                                   y=y+1;
                            end;
                            x=wrap(x,n);
                            y=wrap(y,n);
                ThisLength=ThisLength+1;
                     end;
             ChainList=[ChainList,ThisLength];
              end;
       end;
end;

count=size(ChainList,2);

ThisDist= hist(log(ChainList),Bins)';
ThisDist=ThisDist./max(ThisDist)

Pr=sum((ThisDist-TrueDist).^2);
```

```
%-------------------------Sample Run Code

% Generate Initial Config: (50x50 matrix for example)
[Next,Prev]=InitConfig(50);

LastPr=inf;

% Initially, use a large ScalConst to accept all steps
global ScalConst;
ScalConst = 10;

for j=1:10000
    AcceptedSteps=0;
    % Conduct 20,000 steps at each ScalConst (~T)
    while AcceptedSteps < 20000
        for l=1:200
       [Next,Prev,LastPr,AcceptedSteps]=MCStep(Next,Prev,LastPr,AcceptedSteps);
        end;
    end;
    ScalConst = ScalConst/2;
end;

PlotDense(Next,Prev);
```